Faculté des Sciences Appliquées
Département d'Architecture, Géologie, Environnement et Constructions
Jean-Marc FRANSSEN, professeur - Thibaut FOHN, ingénieur de recherche
Liège, le 6 Mars 2013

FIDESC4: Fire behaviour of steel members with class 4 cross sections under axial compression and axial compression with eccentricity

Report of the experimental tests performed at the University of Liège

Table des matières

1. Design, preparation and achievement of the experimental tests

1.1. Introduction

One of the main objectives of the project is the creation of a full range of experimental evidence about the fire behaviour of steel members with welded or hot-rolled class 4 cross sections (I and H shape) by carrying out a number of fire tests. The load capacity of these sections is not directly affected by the yield strength of the steel, but by local and global deformations of the compressed areas of the cross-section reached choosing the appropriate cross-sectional shape, beam load form and force.

In these two work packages (WP4 & WP5) dedicated to I-columns with slender cross-sections subjected to axial compression and to combined axial compression and bending at elevated temperature, 8 experimental tests have been carried out with 6 columns with welded constant and variable cross-sections and 2 constant hot-rolled columns.

The fire tests consist in applying a mechanical load until reaching the load ratio (percentage of the cold failure load) for the steel members and then heating the latter at least until mechanical failure. The column is heated along its whole length. This procedure is the same for the 8 tests of these WP's. These tests are designed so that the failure is induced by a global buckling along weak or strong axis eventually combined with local buckling of sections walls. There is no lateral restraint installed along the weak axis.

The manufacturers of the steel profiles are Lindab (Luxembourg) for the welded specimens and the hot-rolled specimens were provided by Desmo (Czech Republic).

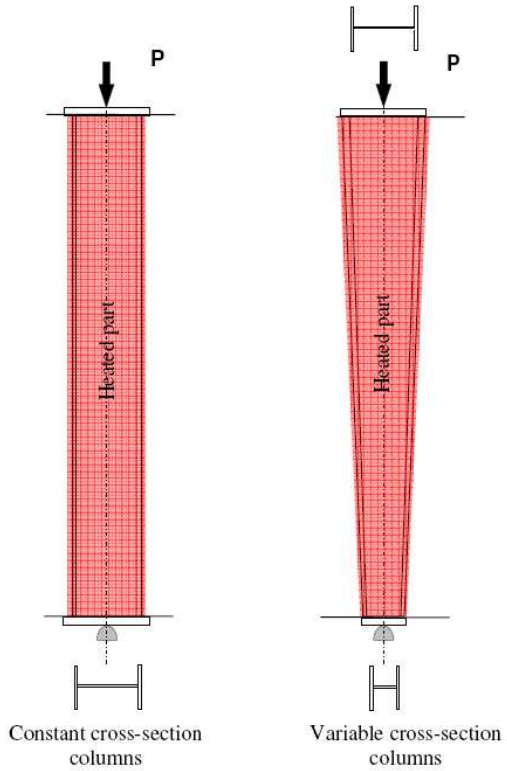

Figure 1 : Global design of the fire tests

1.2. Description of the samples

a) Test No 1

The specimen of the test No 1 is a column with a constant hot-rolled cross-section **IPE240A**. The profile is a class 4 in pure compression so that the failure can be induced by a global buckling along weak axis combined with local buckling of sections walls.

Non-dimensional slenderness of this cross-section is λ_p= *0,245* along the strong axis and λ_p= *1,255*along the weak axis. There is no lateral restraint installed along the weak axis.

An eccentricity of 5 mm is provided to the applied load in the direction of the weak axis in order to control the failure mode. For this test, the eccentricity of the load and of the support are arranged in such a way us to produce a small uniform bending moment distribution ($\psi = 1$).

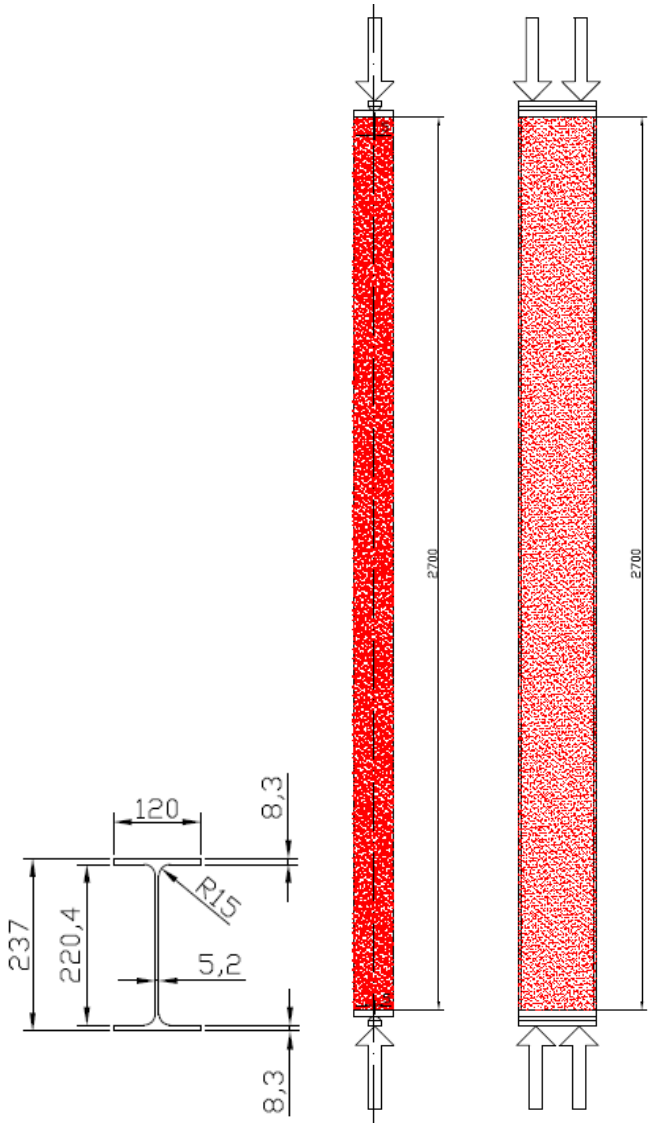

Figure 2 : Test No 1 - Cross-section designed for the test (left) and global design of the test (right)

b) Test No 2 – Test No 3

The columns of the two second tests have the same constant welded cross-section shown in figure 3 consisting of Class 4 web and Class 4 flanges. The third column is just to be loaded at a higher load ratio than the second one. The failure temperatures will be thus different.

Non-dimensional slenderness of the cross-section is λ_p= *0,164* along the strong axis and λ_p= *0,995* along the weak axis. There is no lateral restraint put along the weak axis.

An eccentricity of 5 mm. is provided to the applied load in the direction of the weak axis in order to control the failure mode. For this test the eccentricity of the load and of the support are arranged in such a way us to produce a small uniform bending moment distribution ($\psi = 1$).

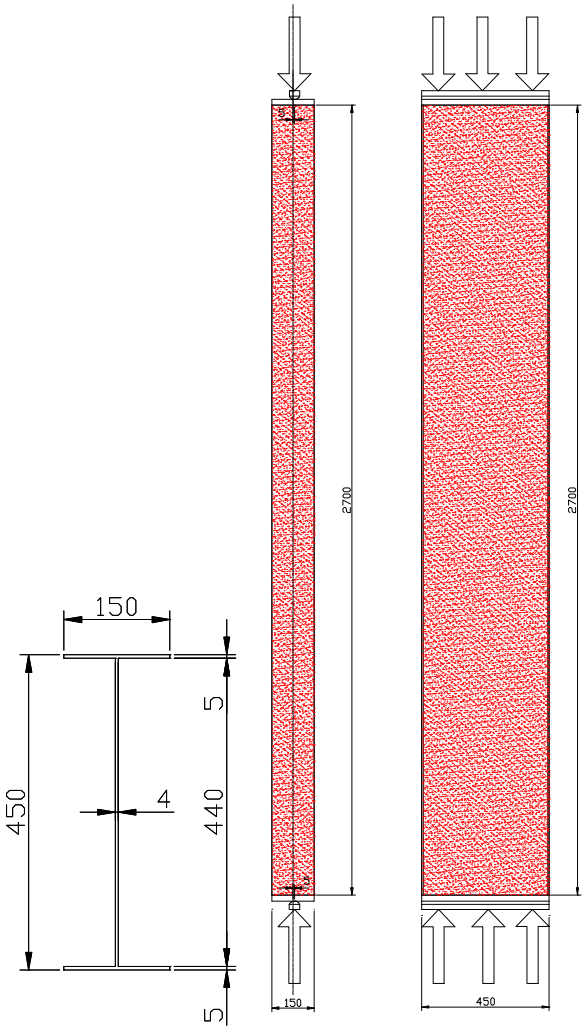

Figure 3 : Test No 2 and 3 - Cross-section designed for the test (left) and global design of the test (right)

c) Test No 4

The fourth test will be carried out with a different cross-section consisting of variable welded cross-section. The non-constant cross-section shown in Figure 4 below consists of Class 4 web and Class 4 flanges.

Non-dimensional slenderness of the cross-section is $\lambda_p = 0{,}267$ along the strong axis and $\lambda_p = 1{,}029$ along the weak axis.

The load is applied with an eccentricity of 6 mm. in the direction of the strong axis. For this test the eccentricity of the load and of the support are arranged in such a way us to produce a uniform bending moment distribution ($\psi = 1$).

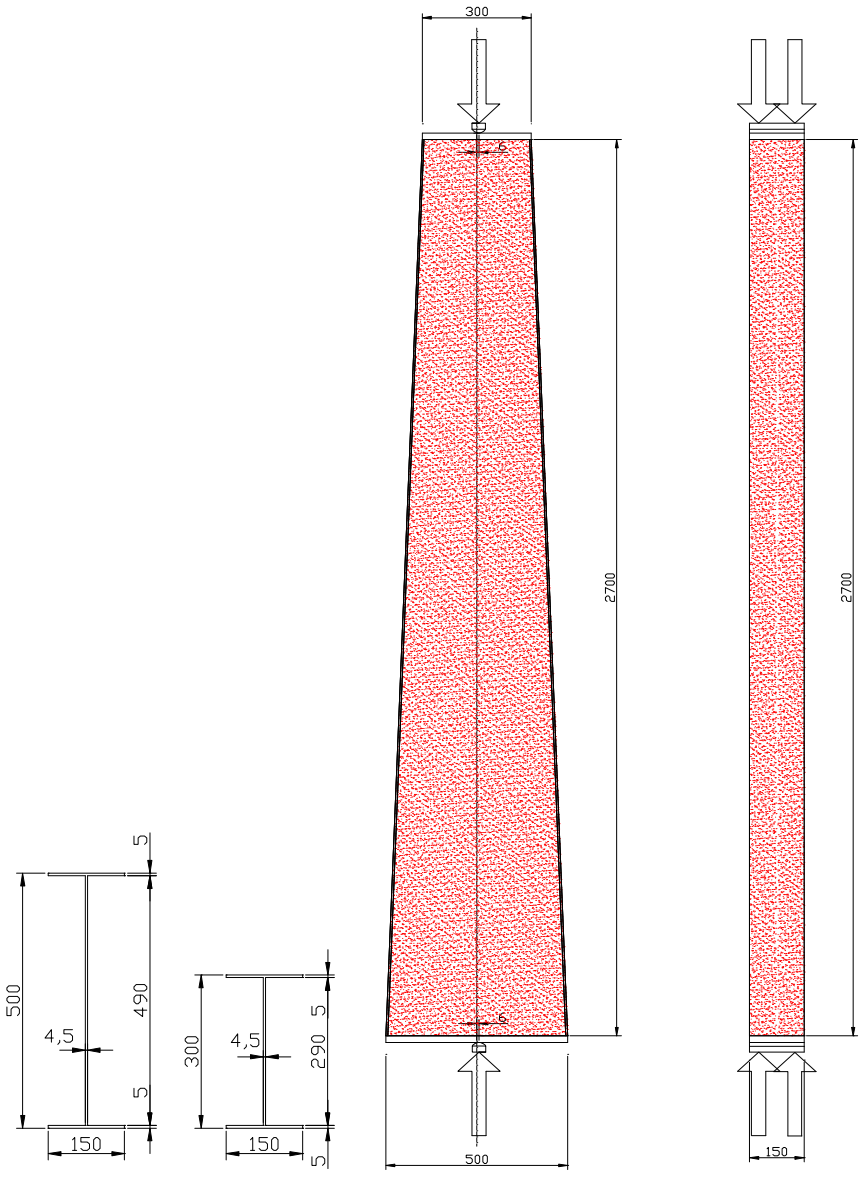

Figure 4 : Test No 4 - Cross-section designed for the test (left) and global design of the test (right)

d) Test No 5

The column with constant welded cross-section shown in Figure 5 consists of Class 4 web and Class 4 flanges. Non-dimensional slenderness of the cross-section is $\lambda_p = 0{,}212$ along the strong axis and $\lambda_p = 0{,}991$ along the weak axis.

The load is applied with an eccentricity of 71 mm. in the direction of the **strong axis**. For this test the eccentricity of the load and of the support are arranged in such a way us to produce a uniform bending moment distribution ($\psi = 1$).

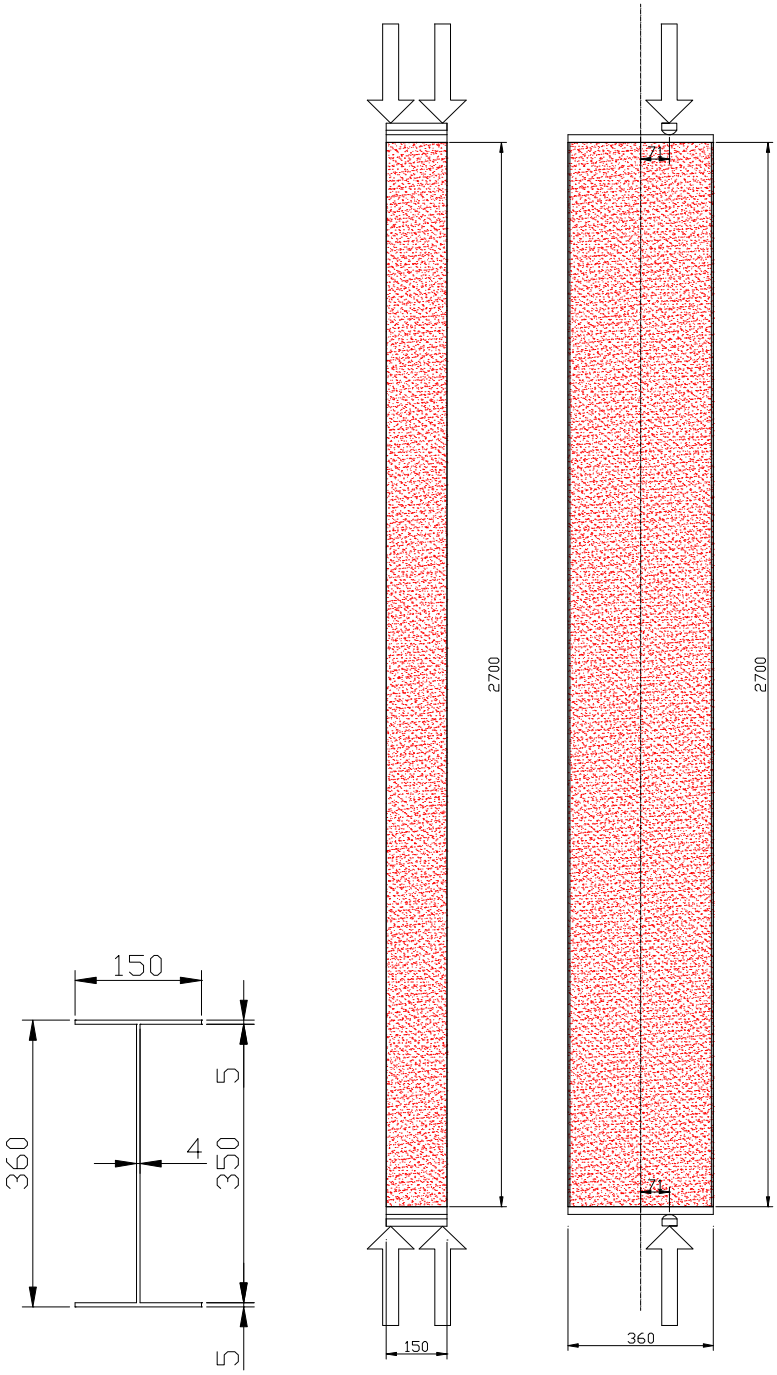

Figure 5 : Test No 5 - Cross-section designed for the test (left) and global design of the test (right)

e) Test No 6

The same column geometry and test set-up as the test No 5 is to be used. The eccentricity of the applied load is larger. Indeed the load is applied with an eccentricity of 177,5 mm. in the direction of the **strong axis**.

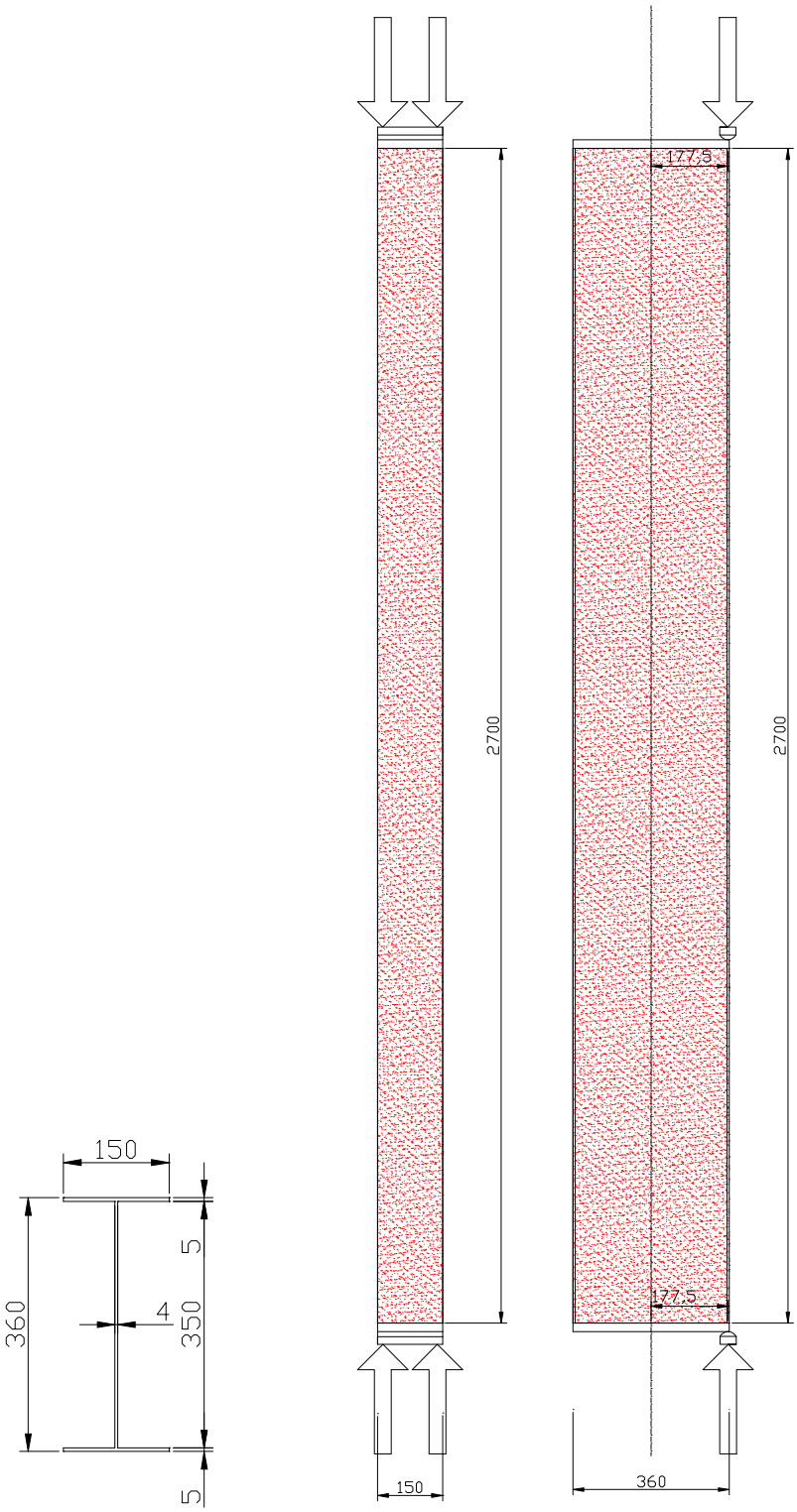

Figure 6 : Test No 6 - Cross-section designed for the test (left) and global design of the test (right)

f) Test No 7

The cross-section consists of a HE340AA with Class 3 web in pure compression and Class 4 flanges in pure bending y-y and pure compression. In pure bending z-z the flanges are class 3. Non-dimensional slenderness of the cross-section is $\lambda_p = 0{,}256$ along the strong axis and $\lambda_p = 0{,}478$ along the weak axis.

The load is applied with an eccentricity of 100 mm. in the direction of the **strong axis** at the top of the column and without eccentricity at the other extremity. For this test the eccentricity of the load and of the support are arranged in such a way us to produce a triangular bending moment distribution ($\psi = 0$).

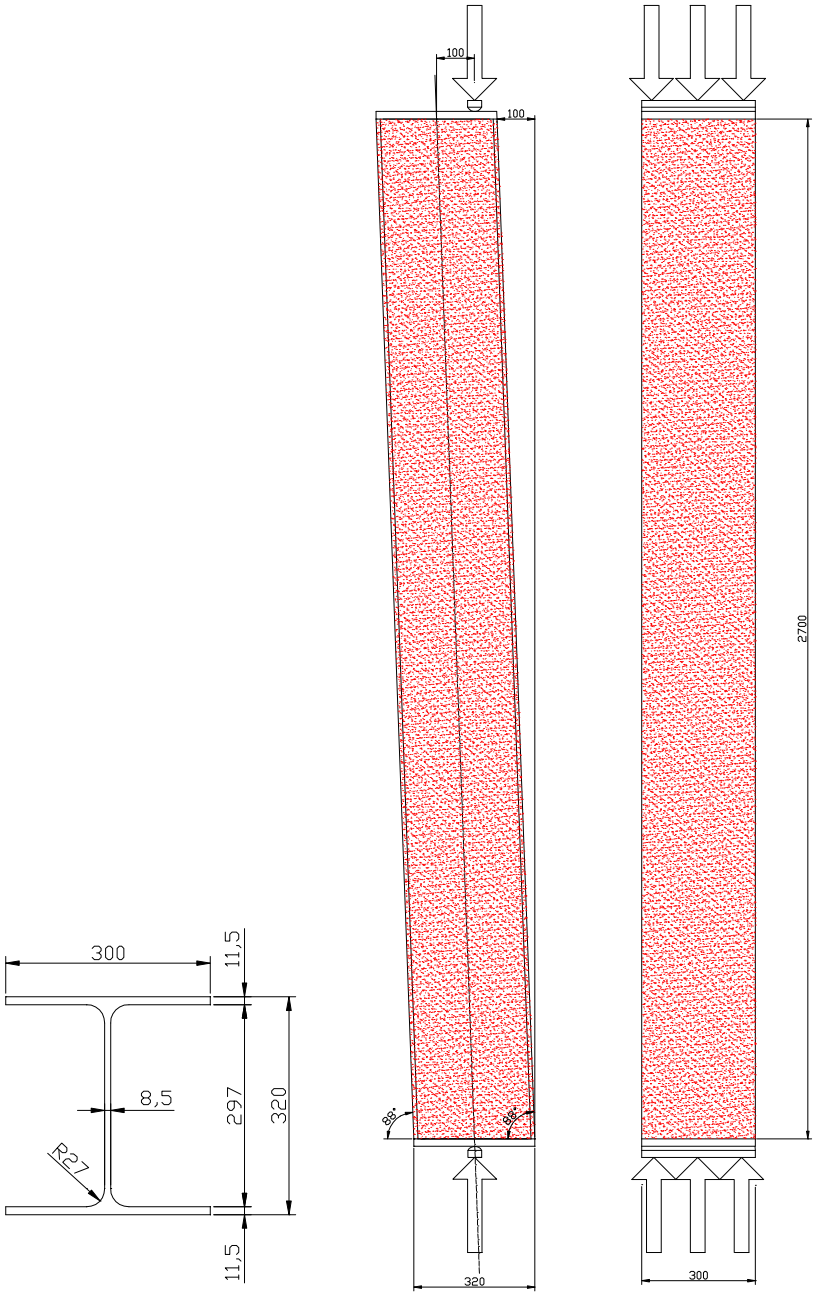

Figure 7 : Test No 7 - Cross-section designed for the test (left) and global design of the test (right)

g) Test No 8

This cross-section shown in Figure 8 consists of Class 4 web and Class 4 flanges. Non-dimensional slenderness of the cross-section is $\lambda_p = 0{,}164$ along the strong axis and $\lambda_p = 0{,}995$ along the weak axis.

The load is applied with an eccentricity of 150 mm. in the direction of the **strong axis** at the larger base of the steel member and without eccentricity at the other base.

For this test the eccentricity of the load and of the support are arranged in such a way us to produce a triangular bending moment distribution ($\psi = 0$).

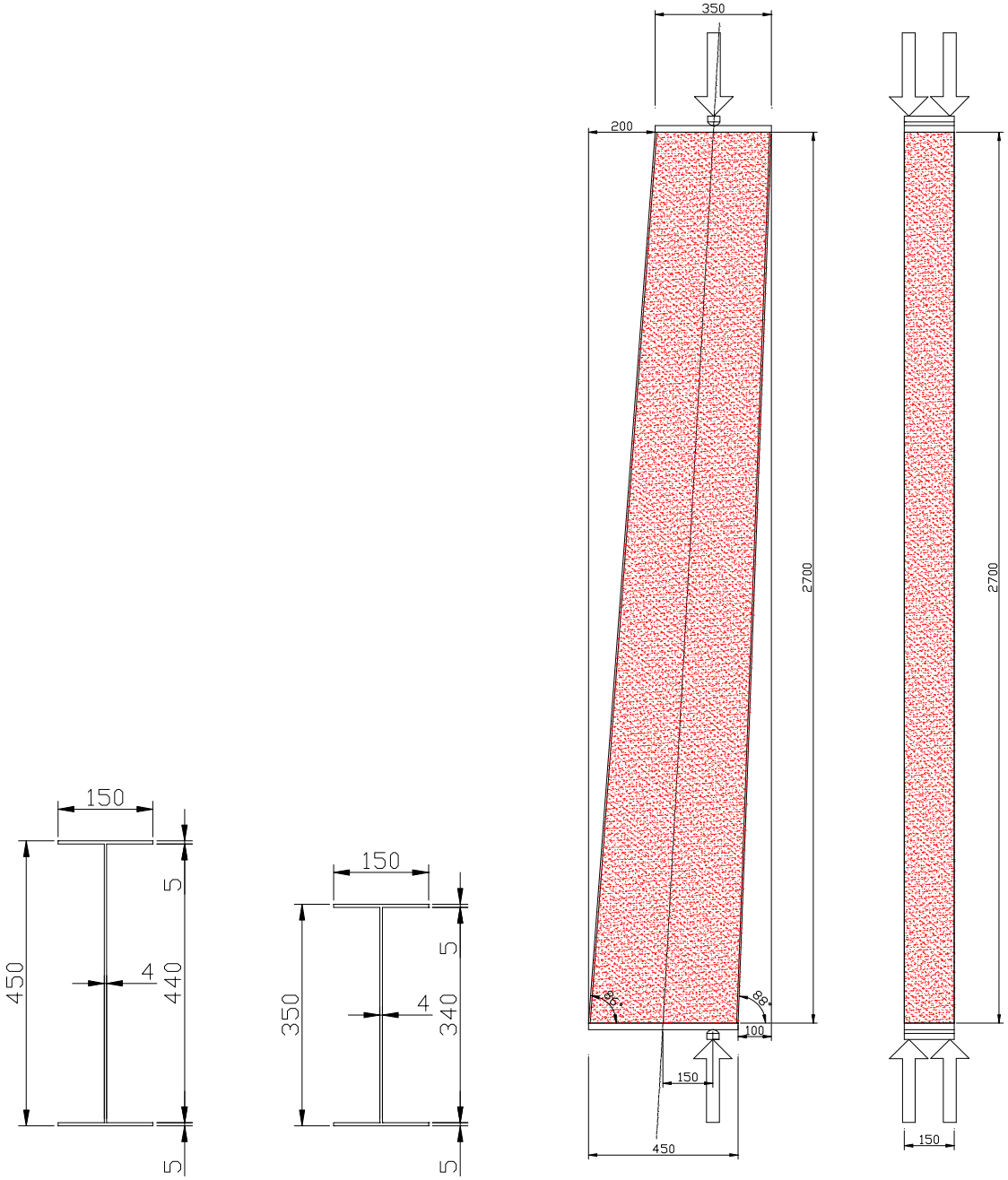

Figure 8 : Test No 8 - Cross-section designed for the test (left) and global design of the test (right)

1.3. Measuring of the imperfections of the columns

The measuring of the global and local imperfections of the 8 specimens was performed manually. The methodology was to put a straight aluminum bar (with the same length than the specimen) along the web and along the both flanges of the column. Once the rule placed, we measure the distance between the bottom of the ruler and the web (or the flange) of the column each 10 centimeters length. Finally we obtain a profile of the imperfections along the web and the flanges of each column.

The reference for these profiles is the bottom of the ruler; so by deducing the distance between the ruler and the web (or flange) measured at the two extremities of the specimen from all the other measured distances, we can draw the profiles presented in the schemes here below for each column with an imperfection equal to zero at the extremities. By this way, we suppose that the two points of reference for the measurements are the two extremities of the column. Thanks to these data providing the profile of the imperfections along the column, we can deduce the global imperfection of the column and also the local imperfections observed around the global one. The following graphs show these profiles.

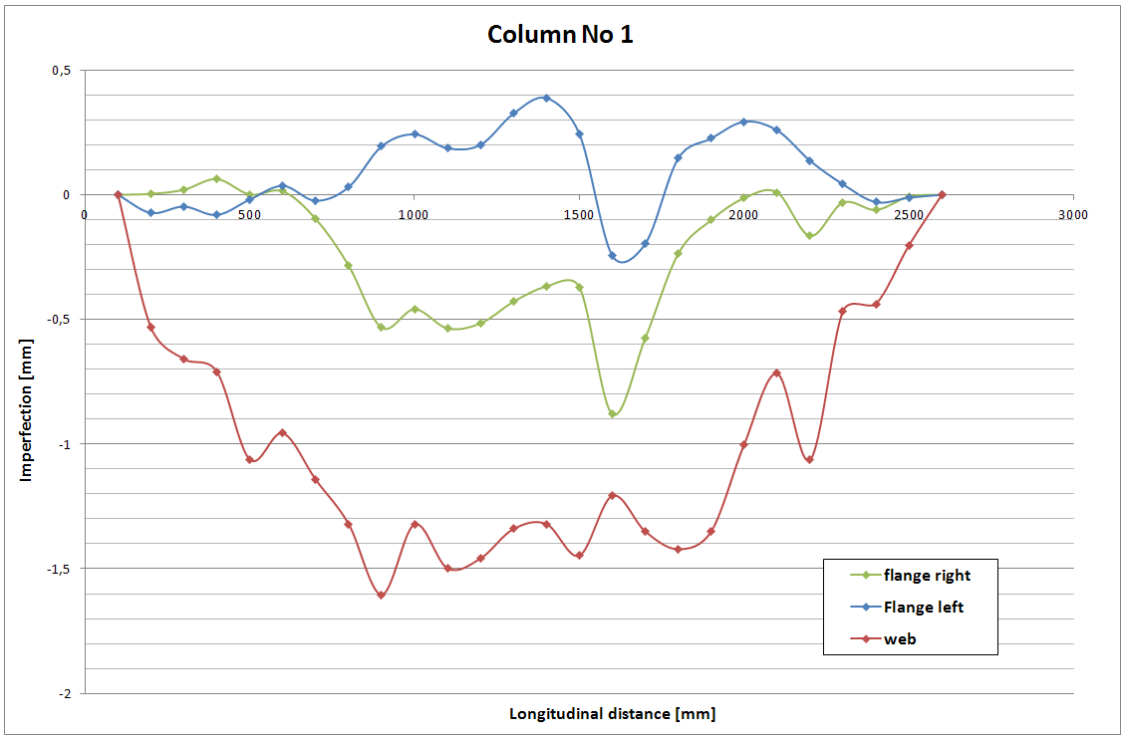

Figure 9 : Column No 1 - Profile of the amplitude of the imperfections along the web and the both flanges

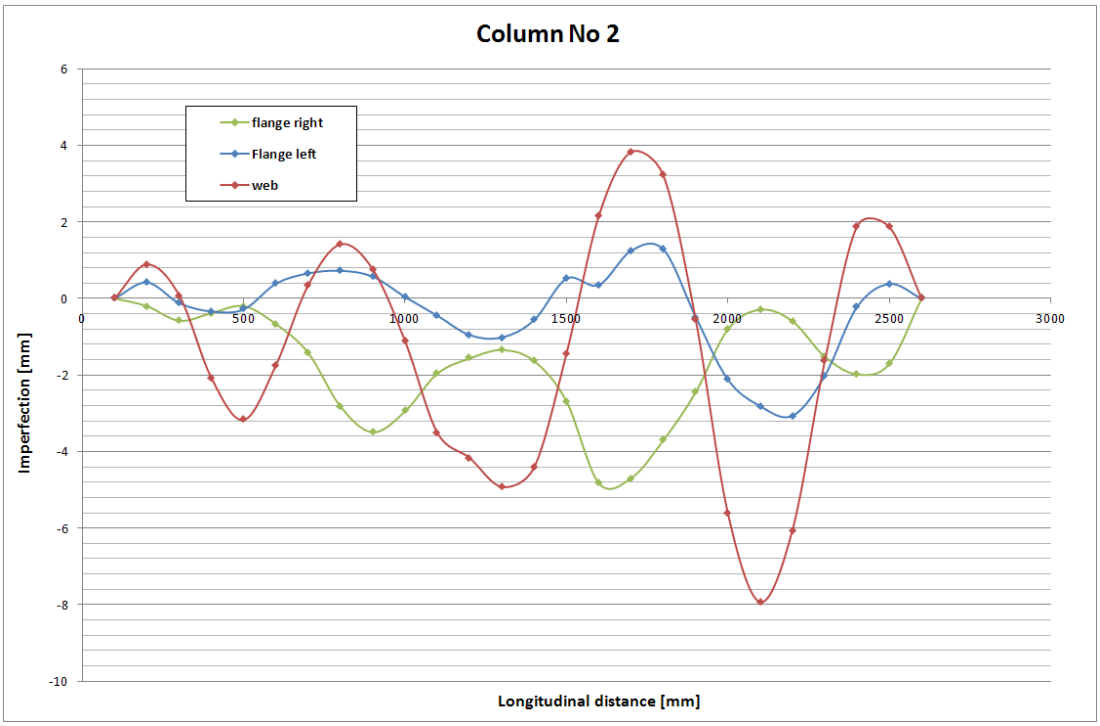

Figure 10 : Column No 2 - Profile of the amplitude of the imperfections along the web and the both flanges

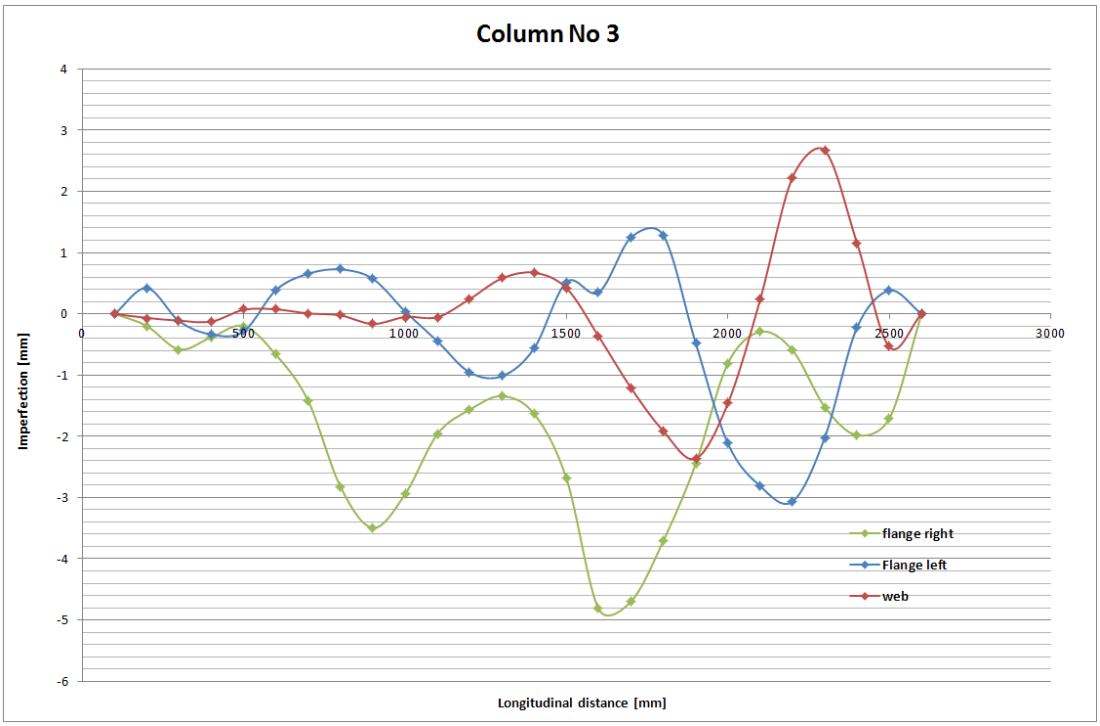

Figure 11 : Column No 3 - Profile of the amplitude of the imperfections along the web and the both flanges

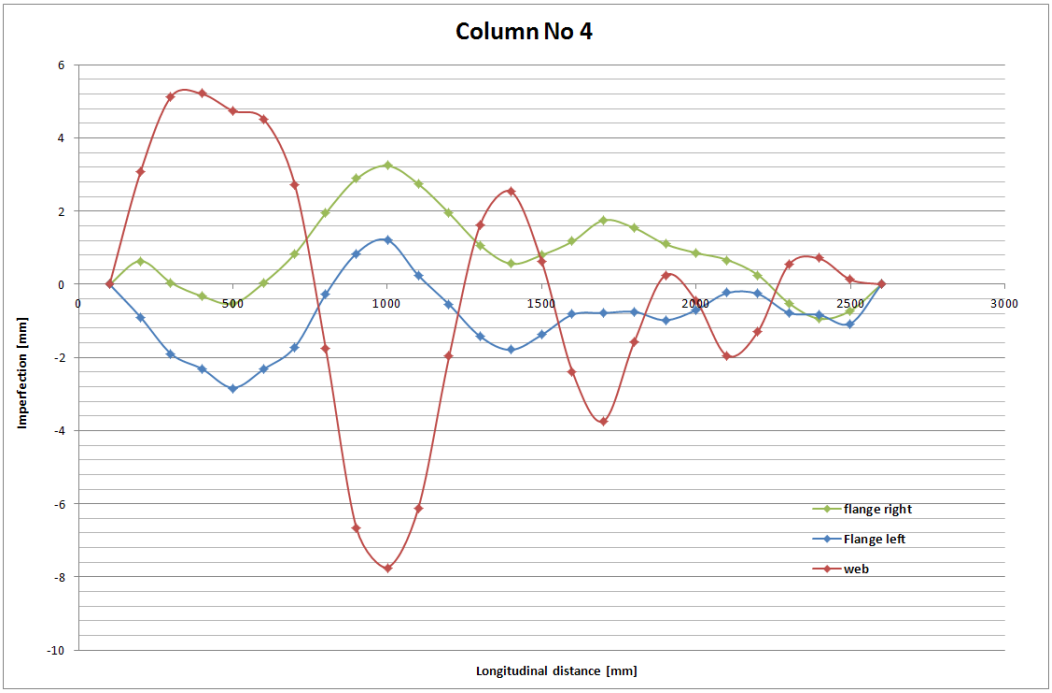

Figure 12 : Column No 4 - Profile of the amplitude of the imperfections along the web and the both flanges

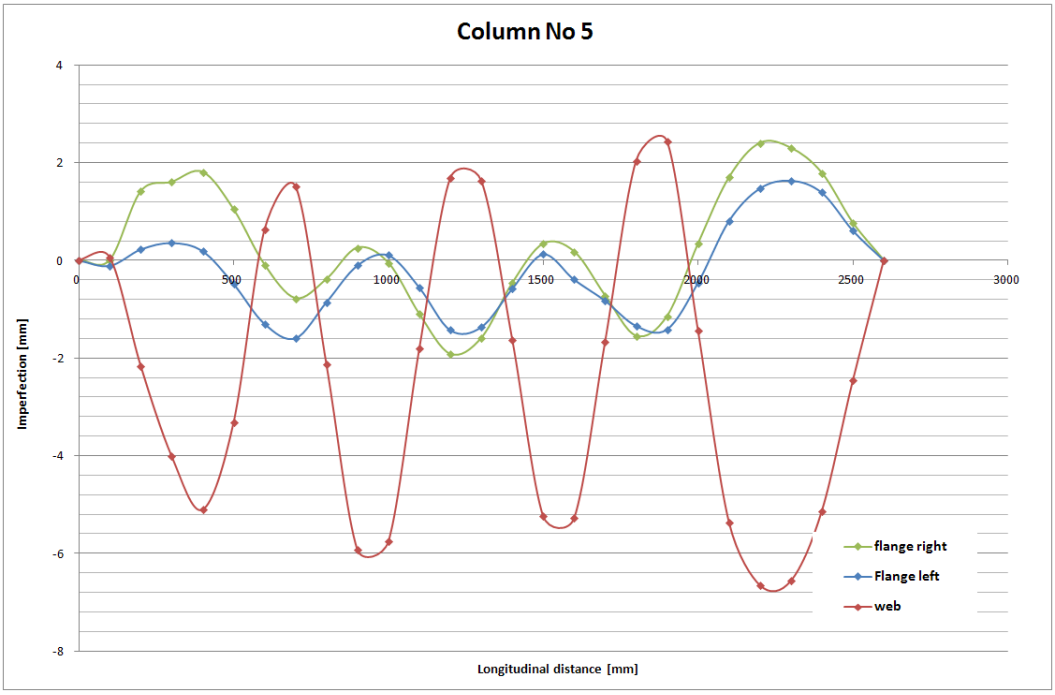

Figure 13 : Column No 5 - Profile of the amplitude of the imperfections along the web and the both flanges

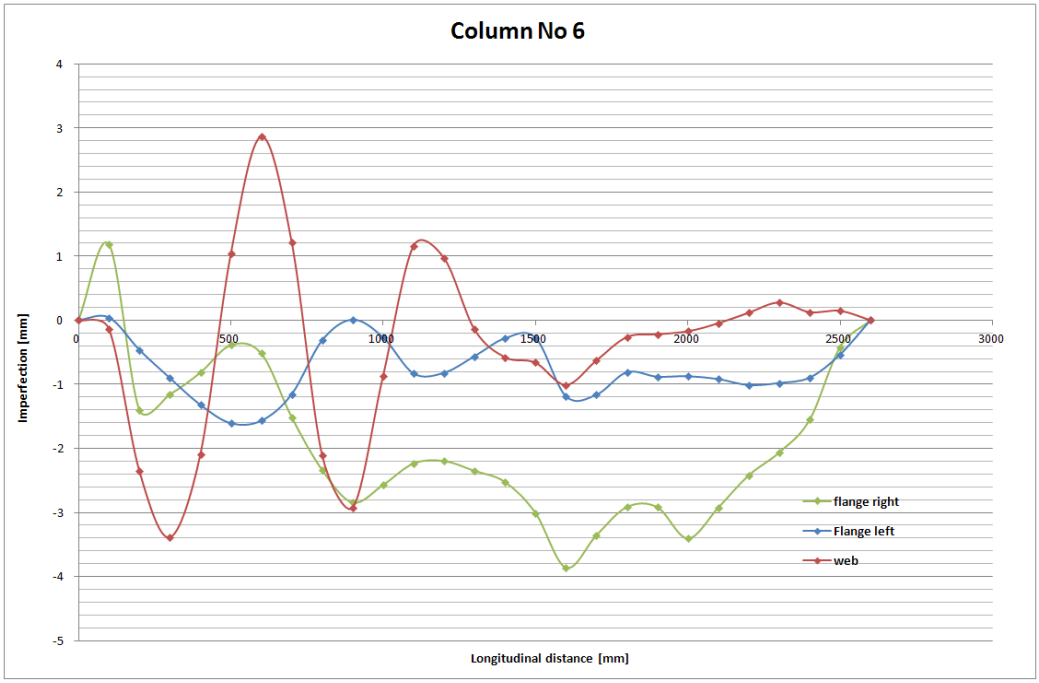

Figure 14 : Column No 6 - Profile of the amplitude of the imperfections along the web and the both flanges

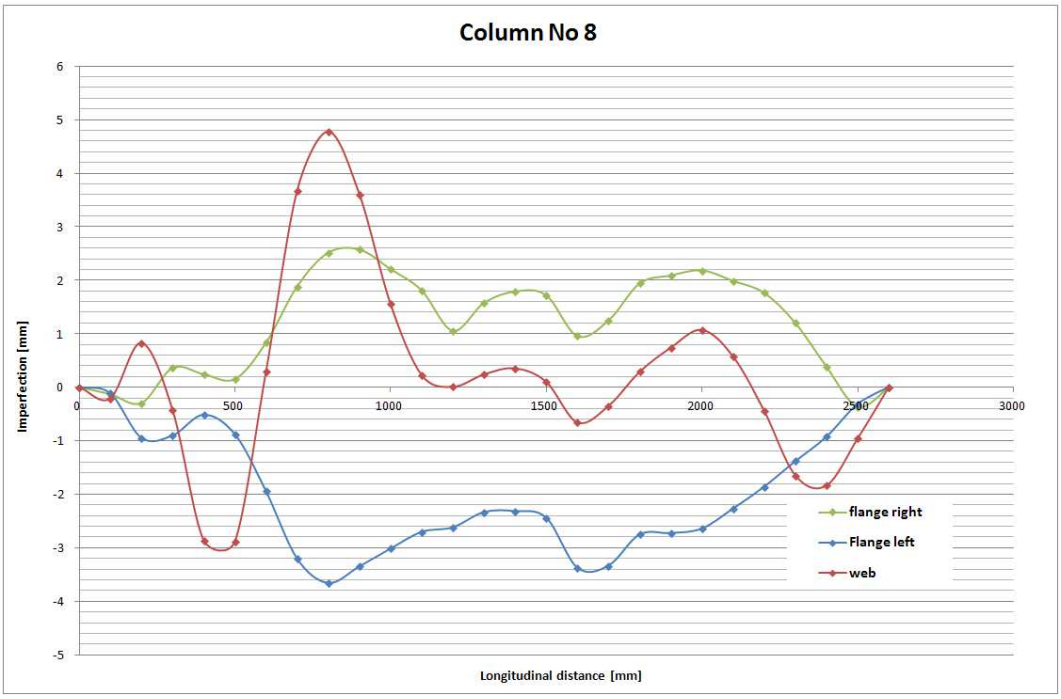

Figure 15 : Column No 8 - Profile of the amplitude of the imperfections along the web and the both flanges

1.4. Test methodology and equipment's

1.4.1. Test methodology

The methodology of the fire tests is summarized in this section in order to describe the mechanical and the fire loading being used, to present the support conditions and the testing frame for the experimental tests in the laboratory of the University of Liège.

The fire tests consist in applying a mechanical load until reaching the load ratio (percentage of the cold failure load selected to reach a temperature of at least 450°C in the column) for the steel members and then heating the latter at least until mechanical failure. The column is heated electrically along its whole length using flexible ceramic pad heaters. This procedure is the same for the eight tests of the project.

1.4.2. Loading equipment

The tested columns are placed in the steel frame of the laboratory. This one is made up of a steel frame with jacks to apply the mechanical load on the tested column pushing up the lower beam of the frame. The steel frame has been prepared because it was necessary to make some holes in the steel profiles madding up the frame to fix the pinned supports located at the extremities of the specimens. Some bolts Φ20 will be used to fix the specimen to the pinned support and also to fix the pinned supports to the steel testing frame.

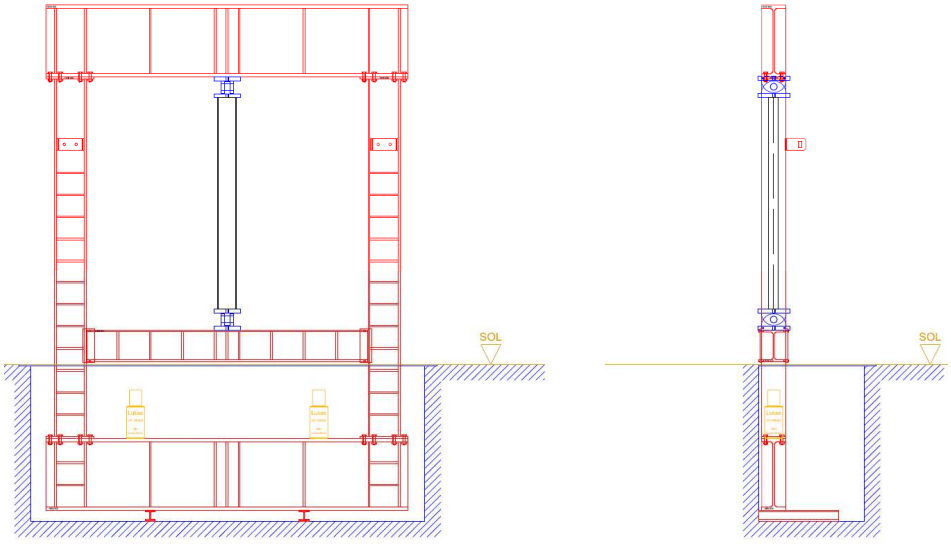

Figure 16 : Testing frame for the experimental tests

Figure 17 : Testing frame for the experimental tests with the equipped column

The extremities of the columns are fixed using pinned supports which enable the rotation in only one direction, see Figure 18. This kind of supports permits to control the failure mode.

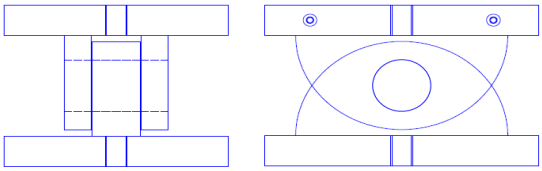

Figure 18 : Pinned supports

In addition, this support cannot overreach the temperature of 200°C. But the columns (and thus its end-plates) will be heated until a maximum of 650°C. So a thermal disconnection between the steel end-plate of the tested columns and the steel pinned support is installed. A layer of 35mm of thickness of the material Promatect-H that allows ensuring sufficient compression strength in its heated state for the most critical of our experimental tests and that provides a lambda value at 650°C of around 0.235W/m*K measured with hotwire system is placed between the end-plates and the pinned-supports, see details in Figure 19.

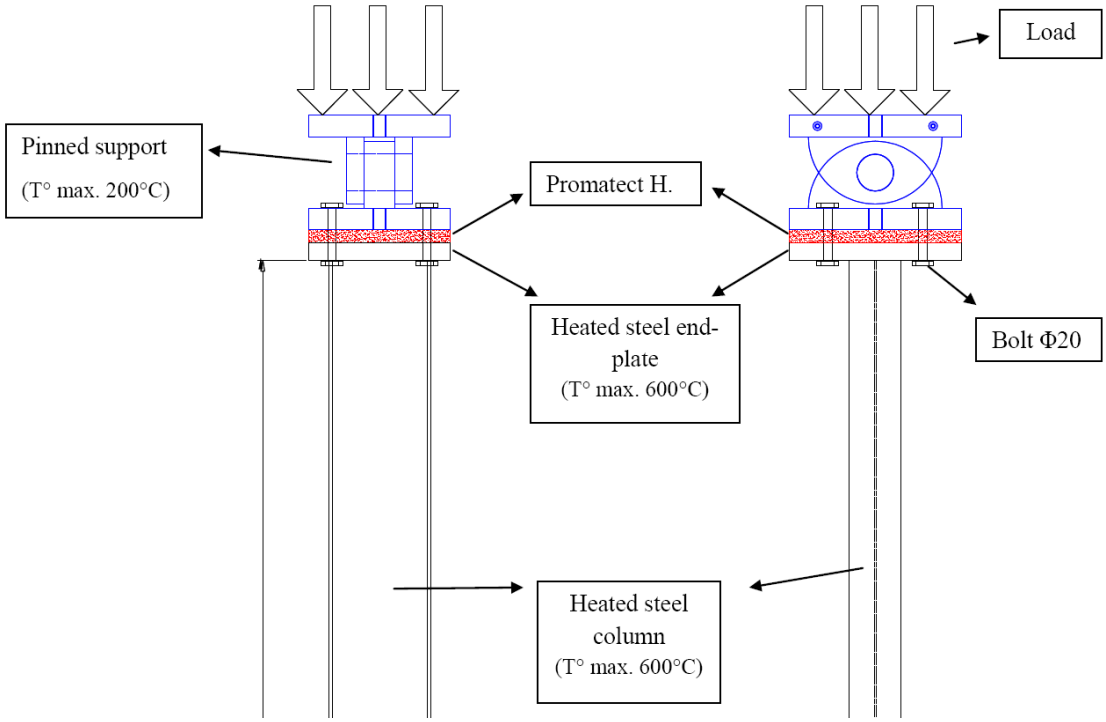

Figure 19: Layout of the insulating and resistant material Promatect H

Figure 20 : Pinned support with thermal disconnection

1.4.3. Heating equipment

The columns are heated using electrical elements; more precisely, flexible ceramic pad heaters are placed along the profile providing a uniform increase of the temperature in the profile. The planning heating velocity is around 5°C/min. The heating equipment's have been ordered from the supplier Stork Technical Service STS. The different components of the heating equipment's are briefly described in this section.

a) Mannings 65kVA power unit with 6 temperature controllers

Figure 21 : Mannings 65kVA power unit with 6 temperature controllers

This unit provides a 60 volts supply for powering various types of low voltage heating elements. The unit consists of an air natural 3 phase transformer, switching is by contactors. The output channels are controlled by means of energy regulators and 6 temperature controllers, provision is made for connection to external control from any compatible programmer/control unit. Each channel has its own auto/manual switch so any channel can be operated either automatically, via an external compatible programmer unit, or manually by means of the internal energy regulator and temperature controller.

b) Six Channel Automatic P256 Programmer/Controller

Figure 22 : Six channel Automatic P256 Programmer/Controller

The Mannings 6 channel Automatic P256 Programmer/Controller has been developed to be used in conjunction with Mannings' heat treatment Transformer Units to provide automatic temperature process control of up to six Transformer Unit output channels. Each control channel can either be operated for manual temperature control of the work piece, or in automatic mode. In automatic mode, the channel controller will ensure that the control zone temperature closely follows the temperature rise, hold and fall and hold period parameters programmed by the operator.

By means of microprocessor controlled programming, LCD display and push button operation, programming and operation of the unit are kept simple and user friendly. The LCD display provides visual indication of the running heat treatment program status and control zone output. In addition, individual control zone neon's indicate when a control zone contactor is energized.

c) Manning flexible ceramic pad heating elements

Figure 23 : Ceramic pad heating elements

Mannings ceramic pad heating elements are constructed from high grade sintered alumina ceramic beads, Nickel-Chrome core wire and Nickel cold tail wire. The construction allows the heating element to be flexible and provides high heat transfer efficiency. In order to be able to heat all the 8 different columns of the experimental tests, two sizes of the ceramic pad heating elements were used: 610 x 85mm and 1220 x 45mm.

1.4.4. Measuring equipment

a) Temperatures

The temperatures have been recorded during the whole duration of each test and at several positions along the web and the flanges of the columns by means of thermocouples.

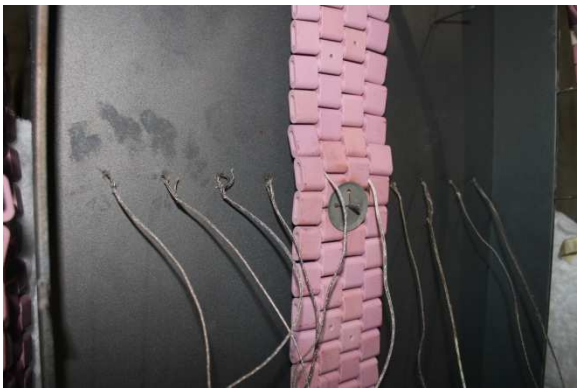

Figure 24 : Thermocouples

We are able to calculate the mean temperature in the steel of the column and we get the exact temperatures at several positions in order to observe the temperatures distribution and gradients induced along the column by the pad heaters. For each test, depending on the geometry of the column, the location of the thermocouples has been slightly adapted.

b) Displacements

Several displacements have been measured by means of displacement transducers. The vertical global extension of the whole column subjected to the fire and to the load is obtained by the mean of the displacements measured by two displacement transducers located at the bottom face of the lower beam of the testing frame. The global deflections at mid-span of the column in the direction of the strong axis and of the weak axis are also measured by means of displacements transducers, cf. Figure 25. Precisely, the transversal displacement in the direction of the weak axis is measured at the middle of the width of the web whereas the transversal displacement in the direction of the strong axis is measured at the middle of the width of the flange.

Figure 25 : Displacement transducer

Moreover, a visual examination was conducted to observe the local displacements of section walls once the insulation surrounding the column was removed.

1.5. Modeling of the tests: Preliminary numerical simulations to select the loading and the heating process and values

Some preliminary numerical simulations were performed with the software SAFIR before the ordering of the equipment's and of the specimens in order to select the loading and the heating process and values for the experimental tests.

1.5.1. Main assumptions

The columns were meshed using rectangular shell elements in order to take into account the local instabilities in section walls and were heated at a velocity of 13°C/min.

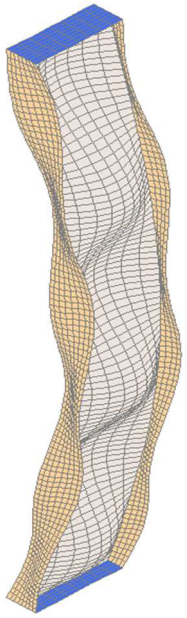

The initial local and global imperfections considered for all the tests were:

- Web = h/200 (sinusoïdal shape)
- Flange = (b/2)/50 (sinusoïdal shape)
- Global = L/500 (half sinusoïdal shape)

The support conditions used for the numerical simulation have been chosen in order to represent in the best way the real end conditions of the experimental tests (see Figure 26).

A particular case has also been studied to take into account the fact that the lower beam of the testing frame could rotate in the plan of the frame modifying the support condition at the lower end of the column. Only one node is blocked in the vertical direction at the bottom base.

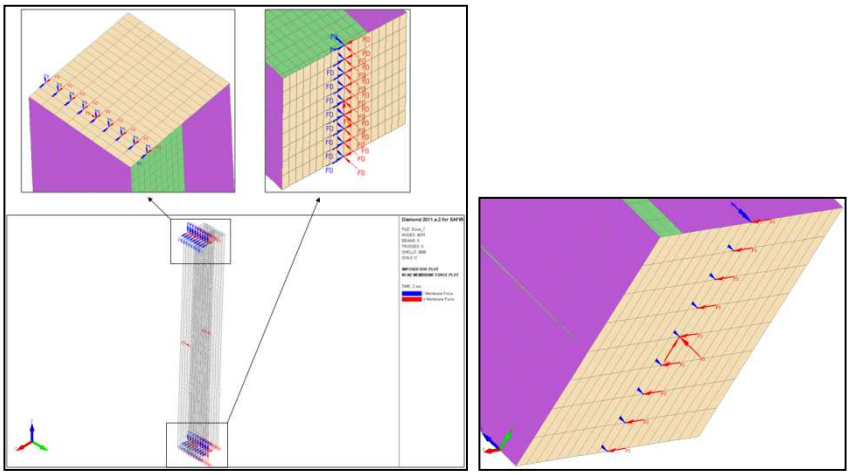

Figure 26 : Numerical model, support conditions; general case (left) – particular case (right)

1.5.2. Results of the simulations and selection of the load and temperature values

By these numerical simulations, we established the relation between the applied load and the critical temperature of the column for each test of the experimental program that allow us to select the values of the applied load as a function of the temperature and to predict the failure mode. We obtained the expected vertical and transversal displacements.

- Test No 1

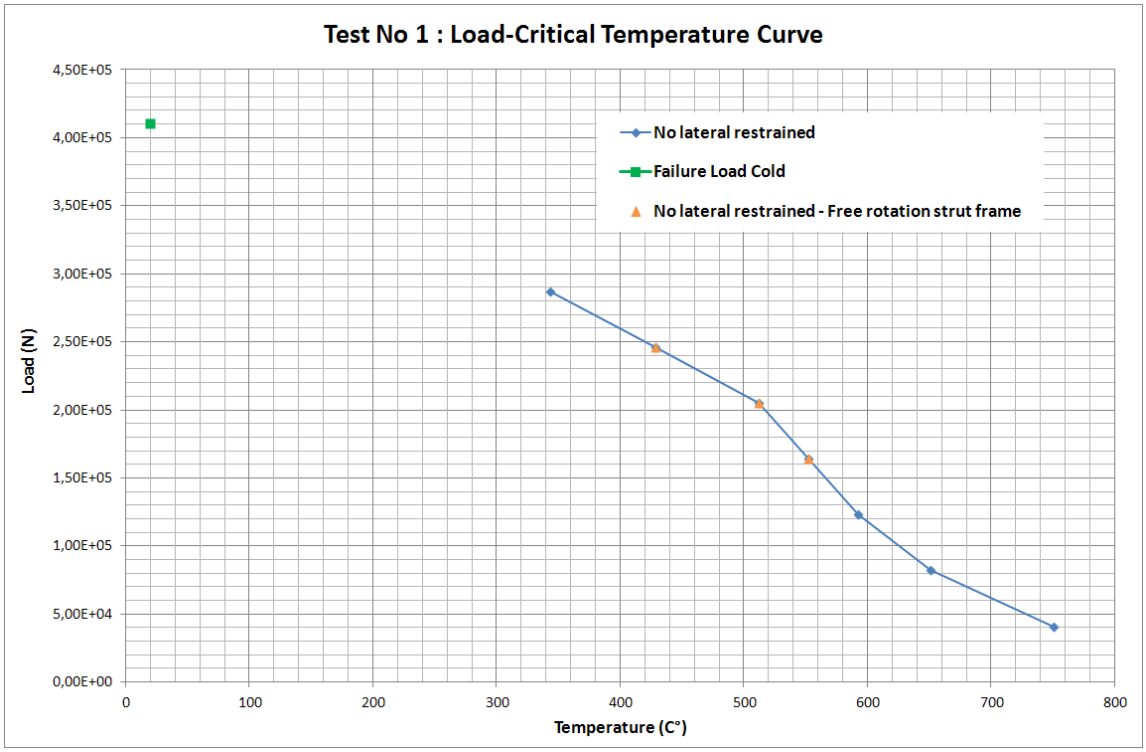

Figure 27 : Relation between Load and Critical Temperature of the Test No 1

- Test No 2 and test No 3

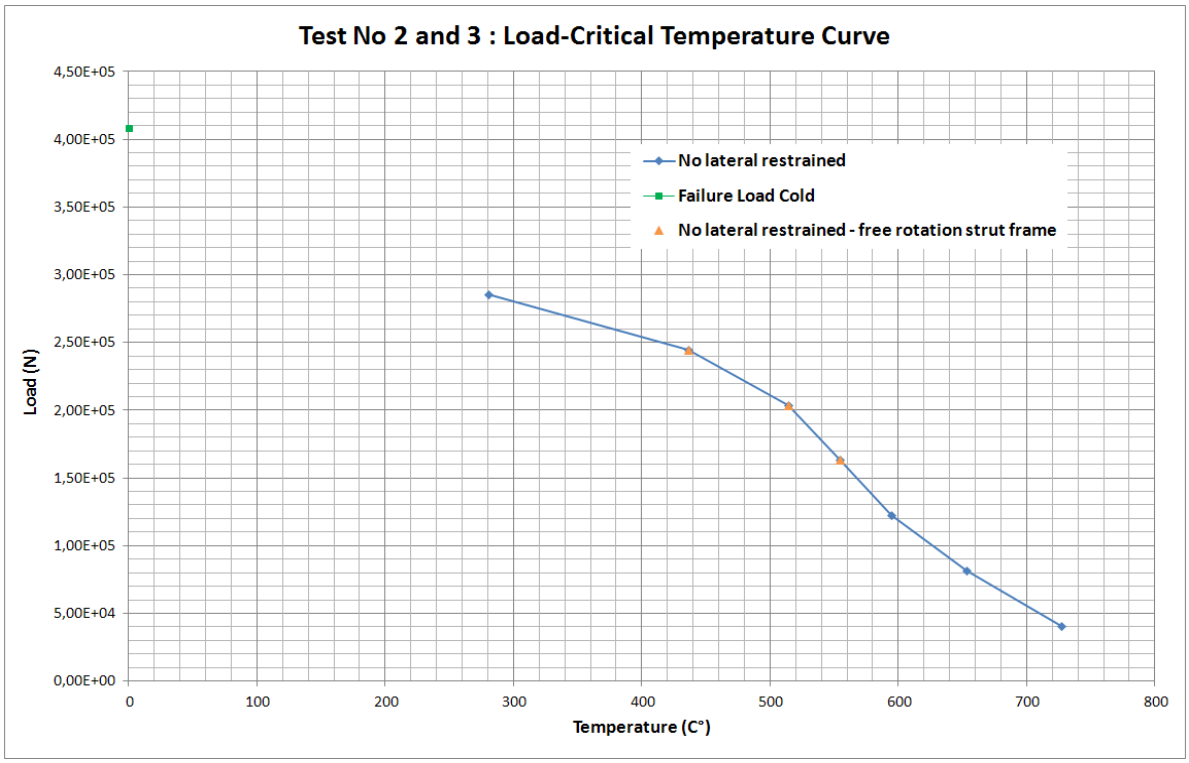

Figure 28 : Relation between Load and Critical Temperature of the Test No 2 and No 3

- Test No 4

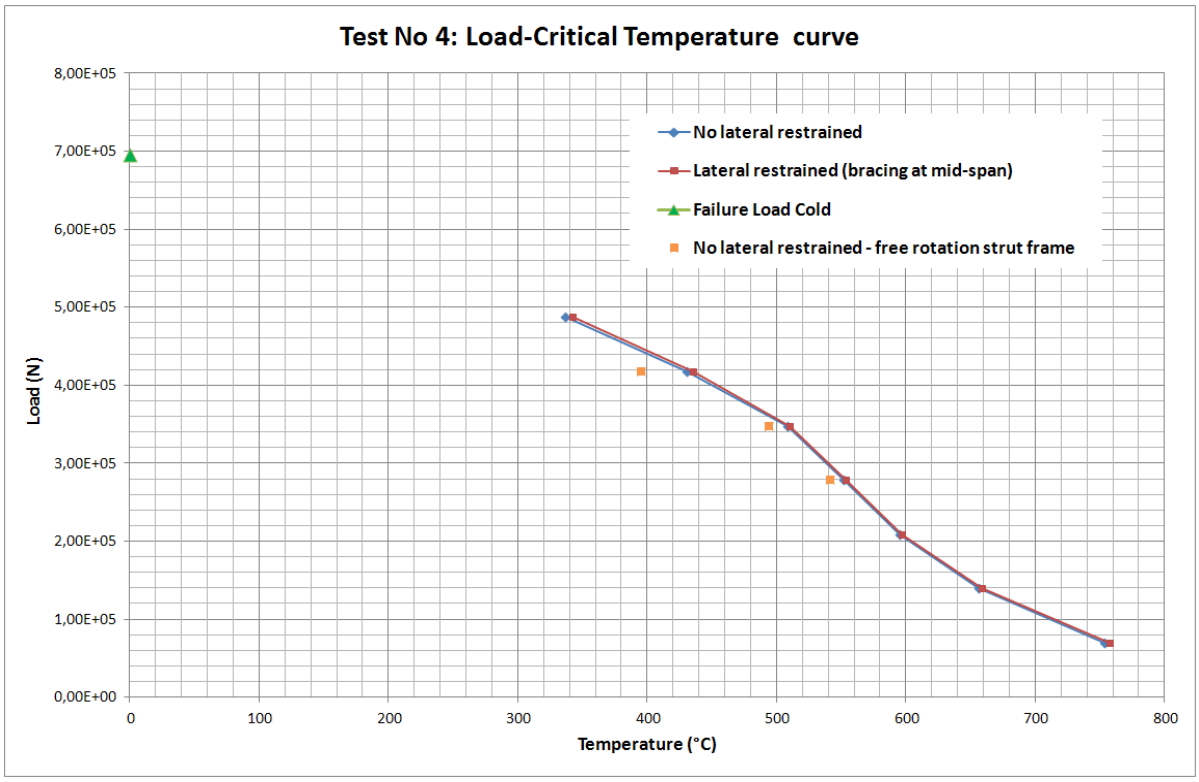

Figure 29 : Relation between Load and Critical Temperature of the Test No 4

- Test No 5

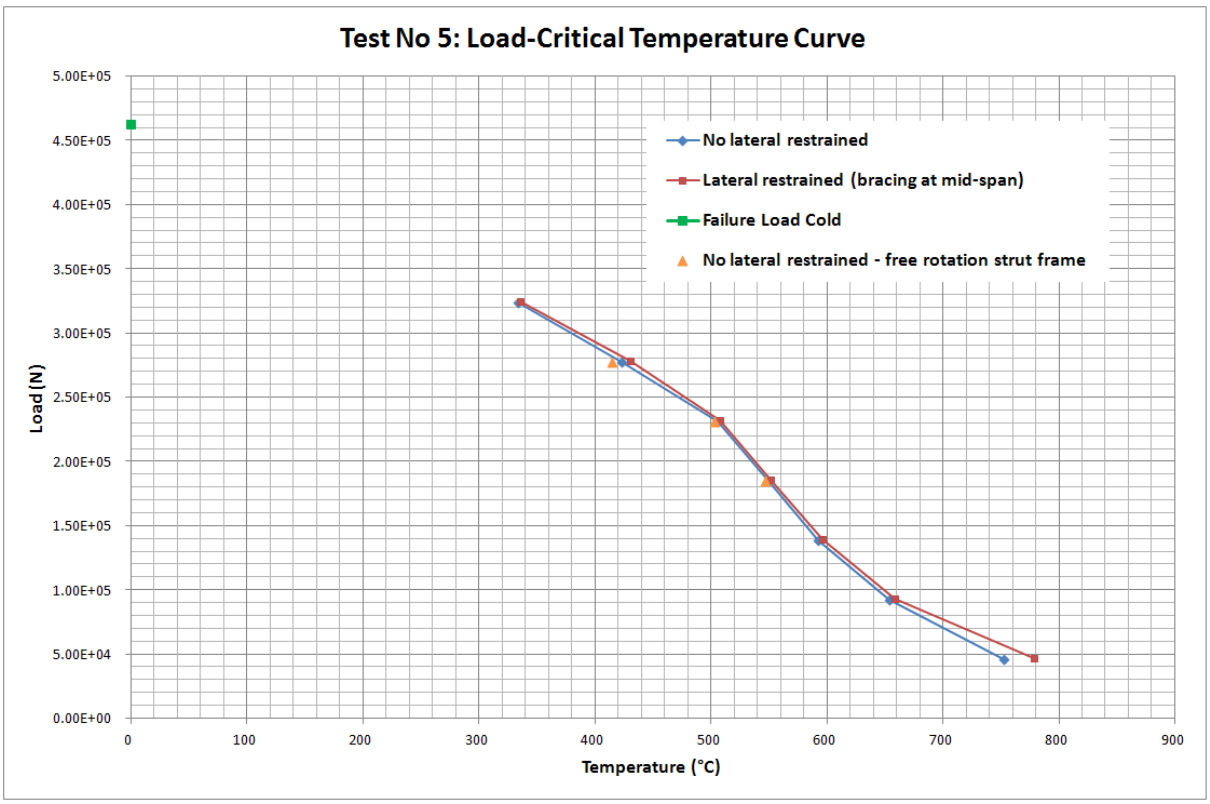

Figure 30 : Relation between Load and Critical Temperature of the Test No 5

- Test No 6

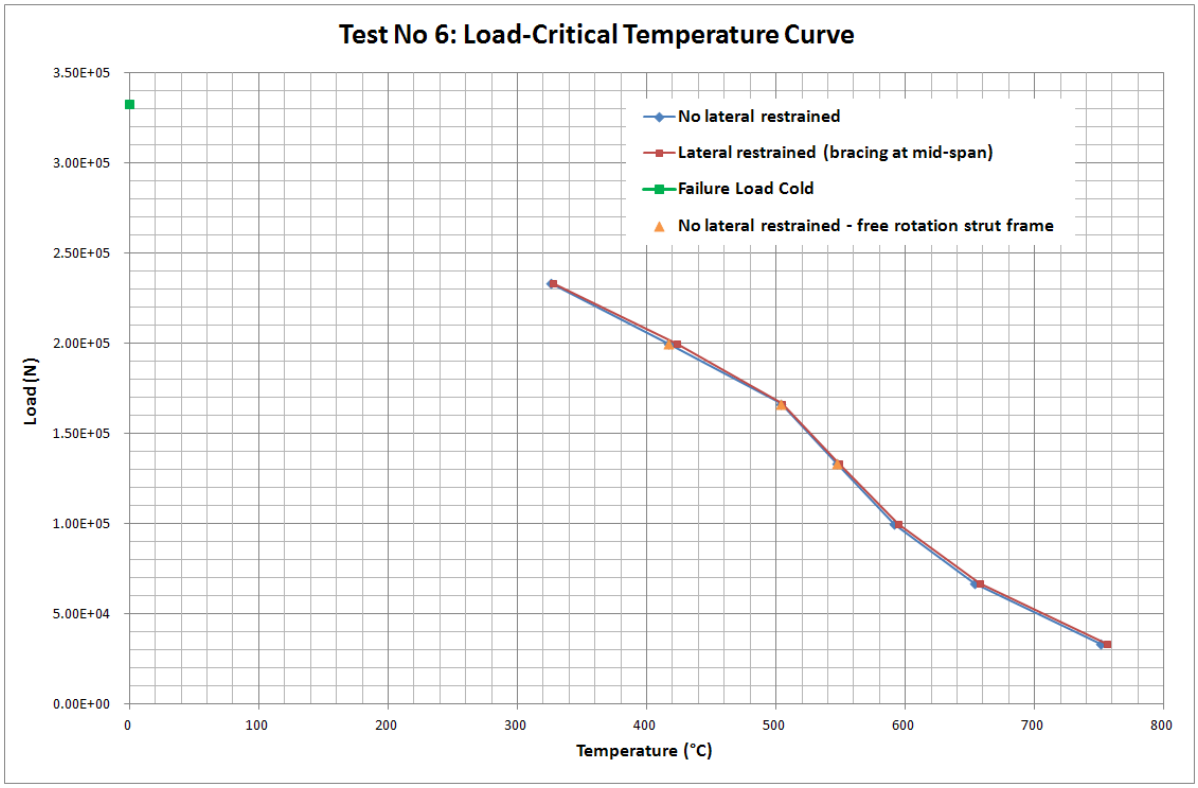

Figure 31 : Relation between Load and Critical Temperature of the Test No 6

- Test No 7

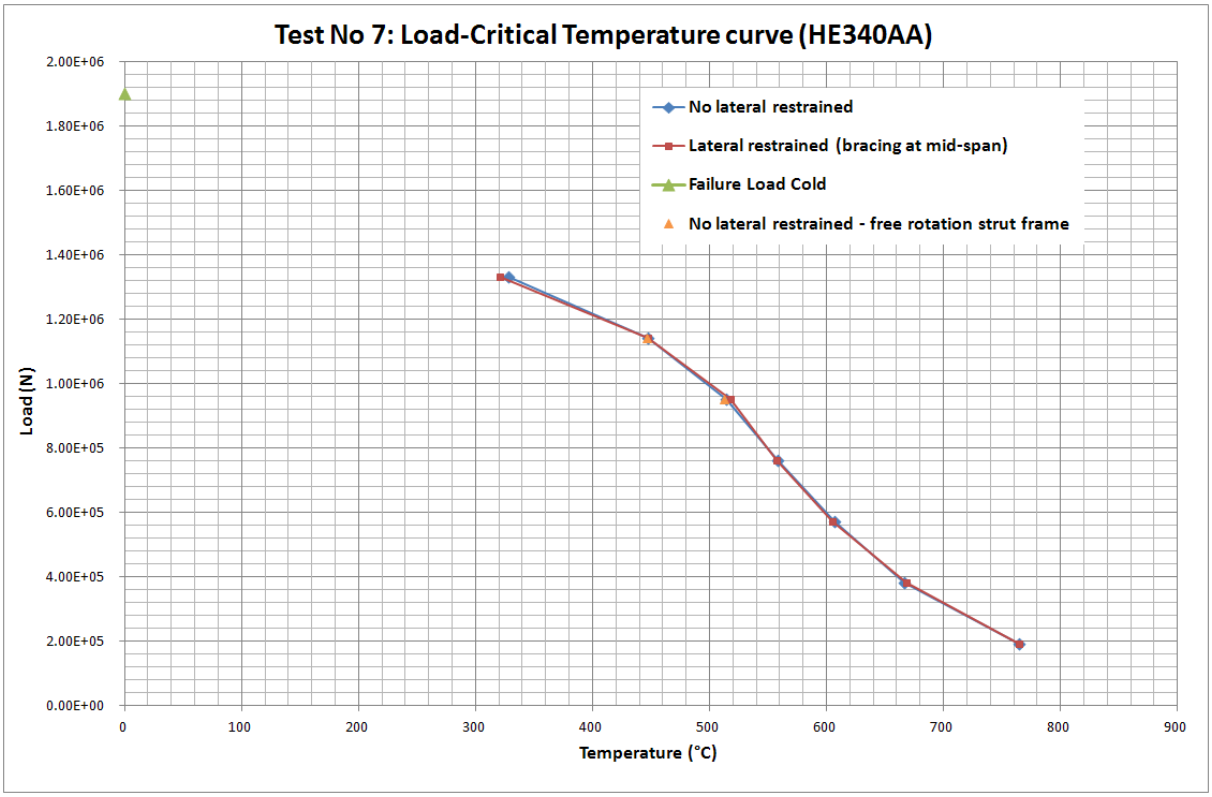

Figure 32: Relation between Load and Critical Temperature of the Test No 7

- Test No 8

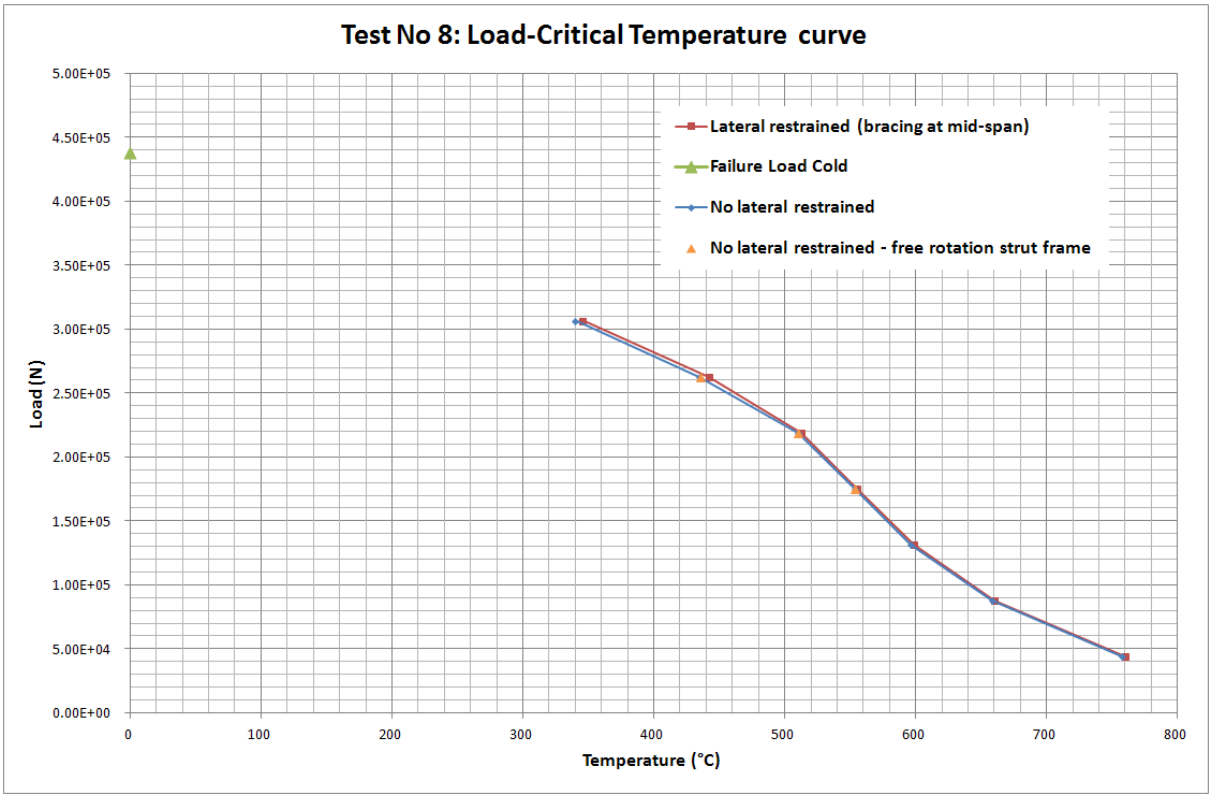

Figure 33 : Relation between Load and Critical Temperature of the Test No 8

1.6. Progress and results of the experiments

As the arrangement of the pad heating elements depends on the geometry of the column, it is slightly different between the eight tests and the layout of these pads is presented for each test.

After connecting all sensing devices (thermocouples, displacement transducers) to the measuring equipment, after connection the heating pads and controlling thermocouples to the transformer, and after putting the insulating materials, the column was ready for the experiment and the test can be launched.

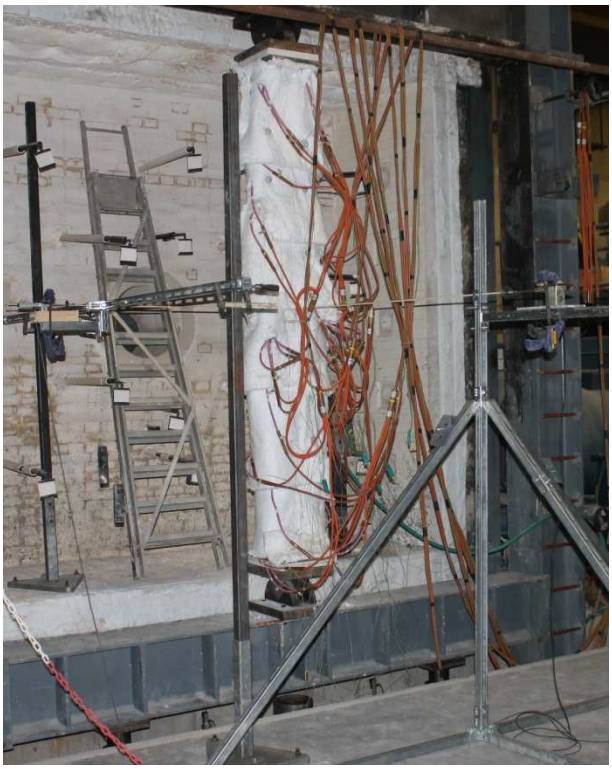

Figure 34 : Equipped column with all sensing devices, pad heating's and insulation

Some blank tests have been performed before launching the real experimental tests in order to master the heating and loading methodologies and equipment's.

The load is applied on the column with two jacks pushing up the lower beam of the testing frame; it is the usual way we apply the load in the vertical furnace of the laboratory of Liege and this method is thus well known and mastered.

The blank tests aimed essentially to observe the temperature provision provided by the ceramic heating pads and then the distribution of the temperature into the steel columns. Indeed, it was a new heating method for our laboratory.

1.6.1. Blank test: column No 3

Lindab provided two times the set of the welded columns to be tested by the ULg in this project. The first set was provided without certificate and samples to realize the material tests for the steel of the columns. All the columns were thus re-produced a second time. We kept the column of test No 3 of this first set to perform preliminary heating tests.

Heating preliminary tests

Some preliminary tests were performed to study the heating of the steel by using the heating pads.

The first test was done putting the heating pads against the steel web of the column. Moreover we decide to impose a velocity of heating of 100°C/h using the automatic mode available with our equipment's that allows giving a temperature profile which will be followed the most closely by the activation of the heating pads on the basis of information from the thermocouple, displayed on the measuring device.

In automatic mode, the channel controller will ensure that the control zone temperature closely follows the temperature rise (in this case 100°C/h), hold and fall and hold period parameters programmed by the operator.

We decided to record the temperature at three different positions below and around the heating pad to study the variation of the temperatures of the steel; one thermocouple was put directly below the heating pad (i.e. between the pad and the steel), one thermocouple at 1cm from the pad, and a last one just at the middle distance between two resistances, see Figure 35.

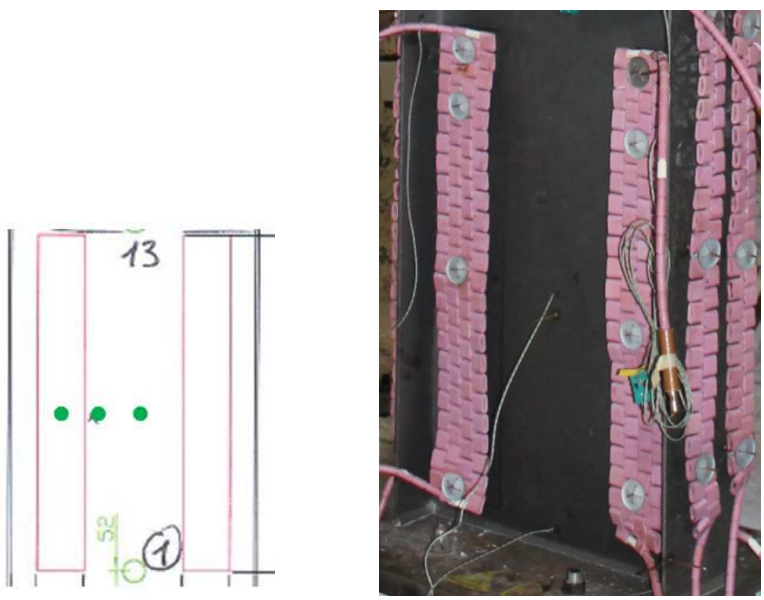

Figure 35 : Location of the thermocouples along the height of the web of the column below and between two resistances (the pads were put directly against the steel)

The temperature distribution obtained with this setup is presented in the Figure 36.

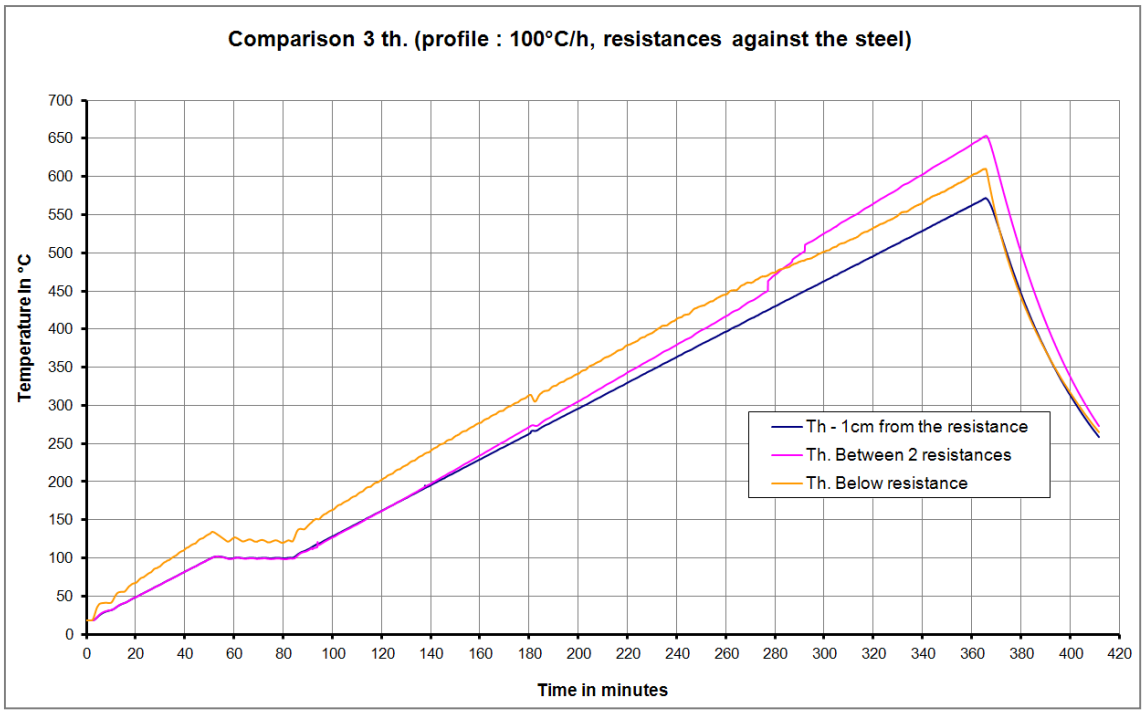

Figure 36 : Temperature comparison between the 3 thermocouples

The biggest variation of the temperatures observed between these 3 thermocouples is presented in the Figure 37.

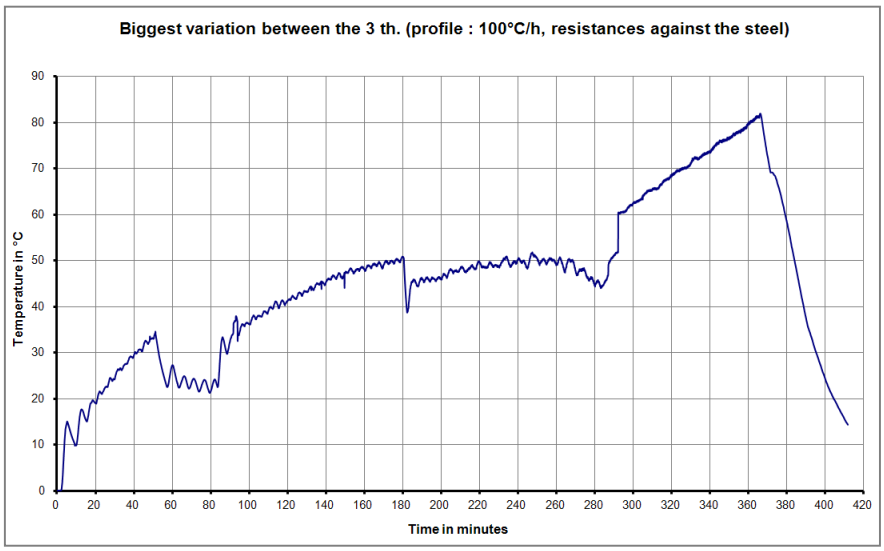

Figure 37 : Biggest variation between the temperatures from the 3 thermocouples

A significant temperature gradient is observed with maximum amplitude of 80°C while the maximum distance between the thermocouple is only 13 cm. These results is not very convincing because the objective is to reach the most uniform temperature along the whole column.

A second test have been performed putting in this case the resistance at a distance of 25mm from the surface of the steel of the web of the column in order to use the convection and also the radiation from the resistances to heat the steel column. The thermocouples were located at the same positions than in the previous test.

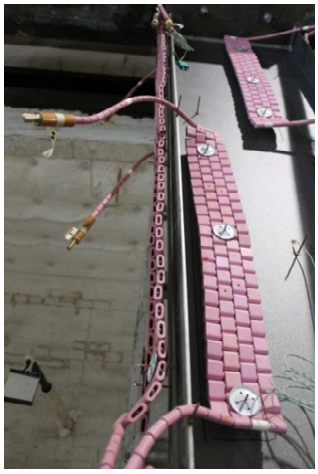

Figure 38 : Positioning of the resistance (25mm from the surface of the steel)

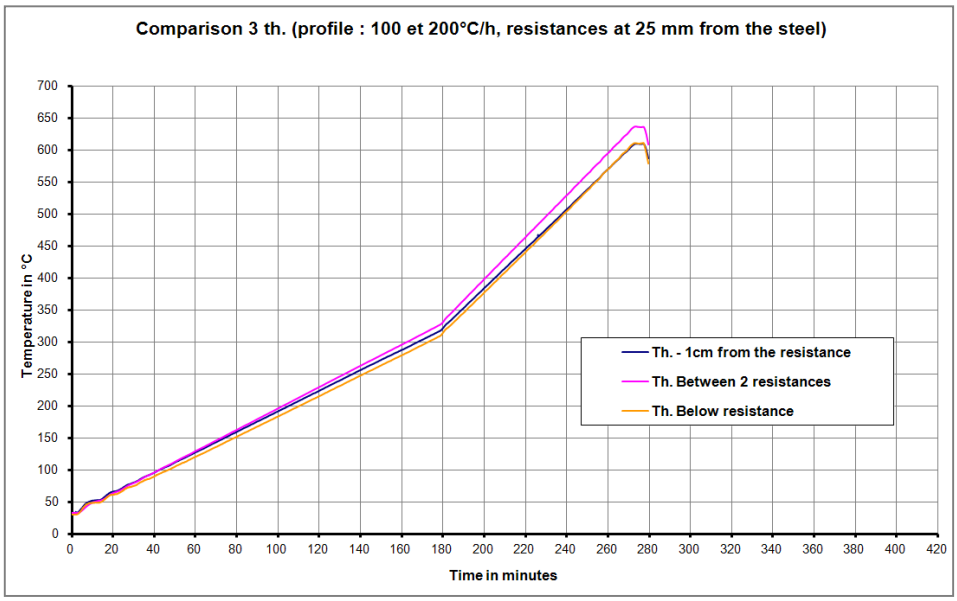

Figure 39 : Temperature comparison between the 3 thermocouples with the resistances at 25mm from the steel

The biggest variation of the temperatures observed between these 3 thermocouples is presented in the Figure 40. We can observe than the gradient is largely smaller than in the previous case with the resistance put against the steel (gradient max. 29°C).

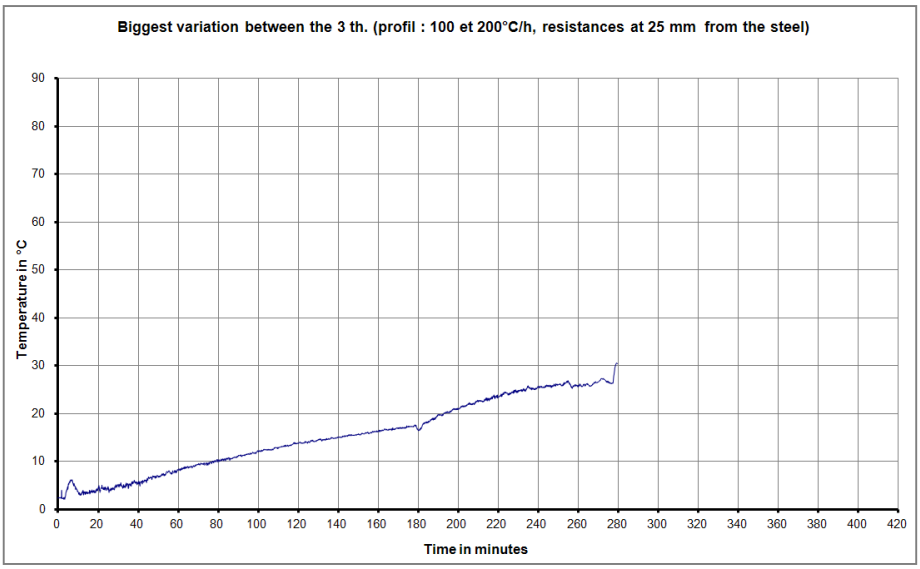

Figure 40 : Biggest variation between the temperatures of the thermocouples

Finally the column of the blank test was tested as in the real experimental test. The column has been firstly loaded and then heated with a velocity of 400°C/h until mechanical failure.

The used Mannings 6 channel Automatic Programmer/Controller has been developed to provide automatic temperature process control of up to six Transformer Unit output channels.

Each control channel can either be operated for manual temperature control of the workpiece, or in automatic mode. In automatic mode, the channel controller will ensure that the control zone temperature closely follows the temperature rise, hold and fall and hold period parameters programmed by the operator.

To improve the uniformity of the heating of the whole column, the column was divided in 6 control zones gathering a certain number of resistances. Each zone is managed by a channel control and the temperature rise imposed to all the zones are the same (constant velocity of 400°C/h).

The cold failure load, the selected value of the applied load and the failure temperature computed with SAFIR software are given in the table here below with the main dimensions of the column No 3.

Sizes [mm]	h	t_w	b	t_f	H
	450	4	150	5	2700

Results	Cold failure load [KN]	Load applied for the test [KN]	Experimental Failure temperature [°C]	Failure temperature (SAFIR) [°C] ***Before the test***
	408	204	**345**	420

The definition of the six control zones is given in the Figure 41 with the location of the thermocouples using for the control zone temperatures in the automatic mode (encircled number of the thermocouple).

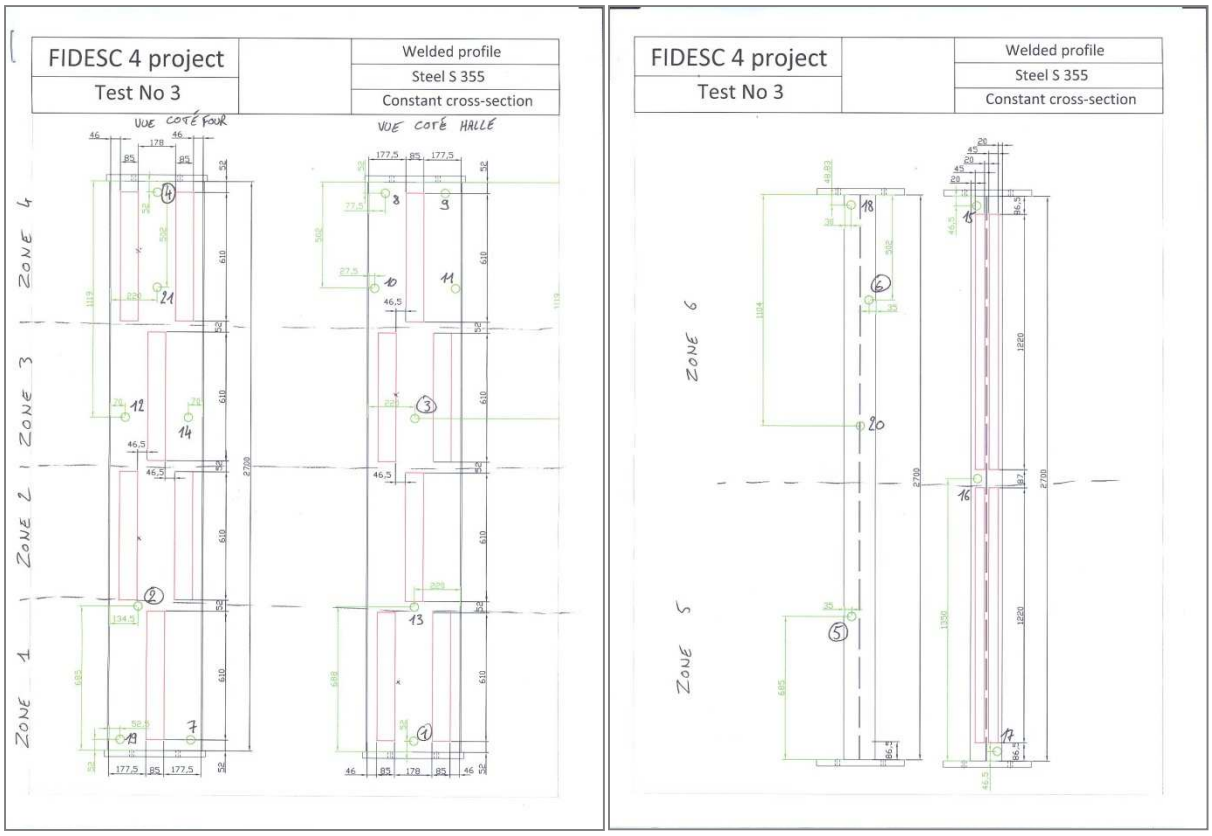

Figure 41 : Definition of the 6 control zones for the thermocouples

The temperature profiles given by the 6 control thermocouples are presented in the Figure 42.

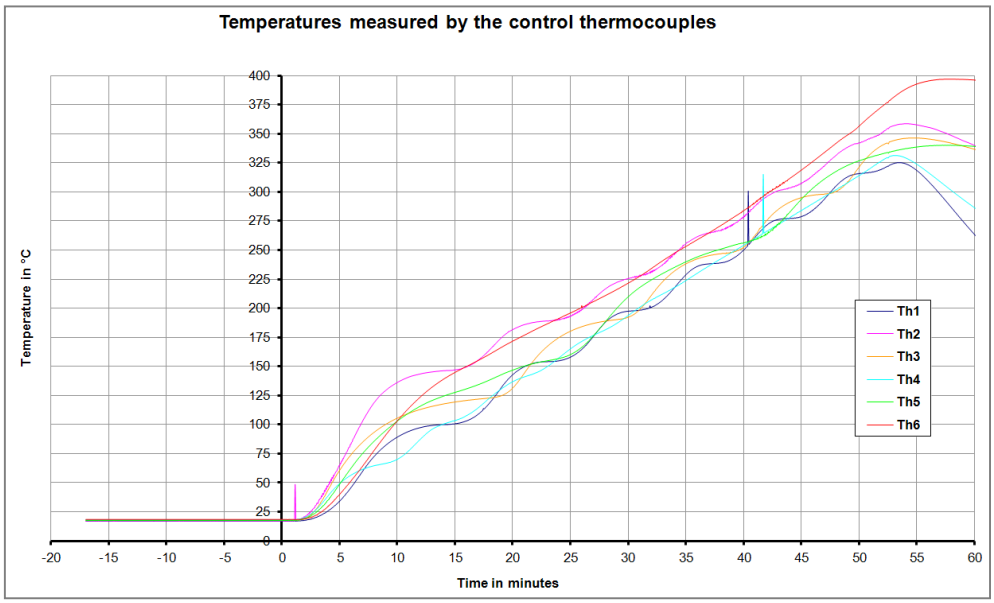

Figure 42 : Profile of the temperatures obtained for the 6 control thermocouples

The mechanical failure occurred at a temperature of 345°C (mean temperature between the 6 temperatures of the control thermocouples). The failure occurred earlier than the failure temperature calculated with SAFIR because the fixation of one of the control thermocouples broke down and the temperature recorded by this thermocouple was lower than the real temperature of the steel in the zone. So the global failure was induced by an excessive heating of the resistances of the zone No 1.

However we can observe that the automatic mode was successful because the temperature of the 6 zones followed well the instruction (temperature rise of 400°C/h) imposed by the automatic controller.

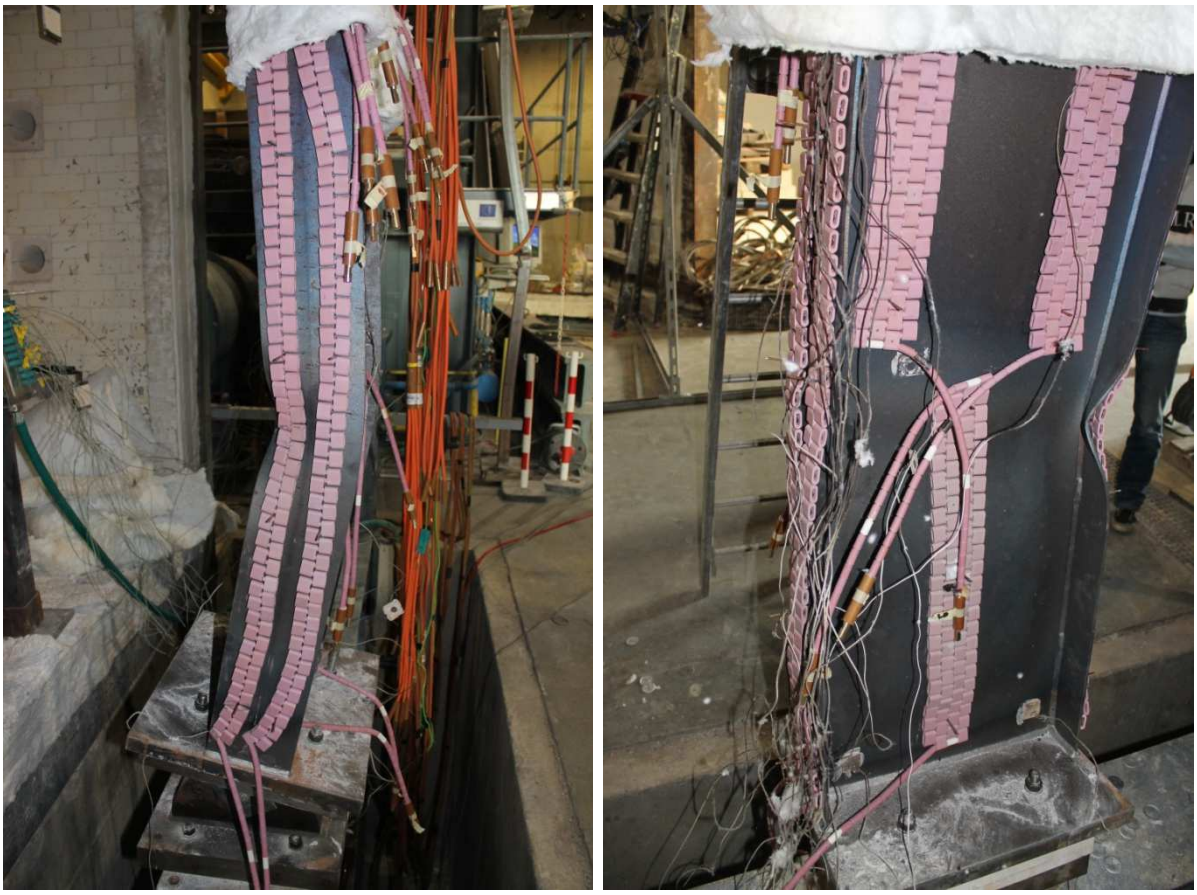

Figure 43 : Failure mode for the blank test of the column No 3

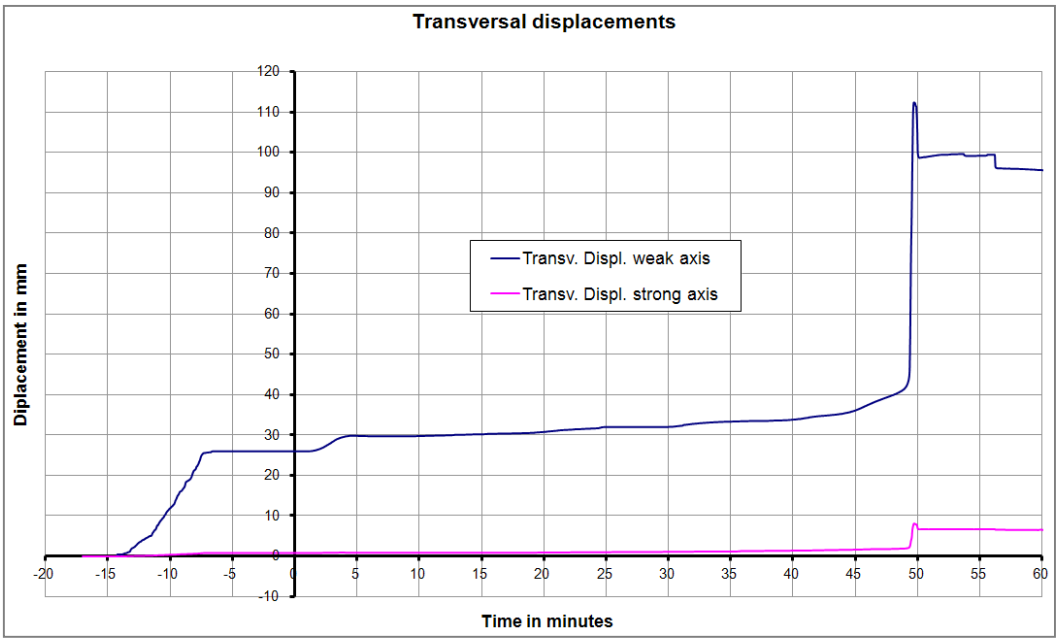

Figure 44 : Transversal displacement in the direction of the strong and weak axis during the test

1.6.2. Experimental Test No 1: hot-rolled column IPE240A

The load applied for the test and the expected failure temperature calculated with SAFIR is given in the table below.

Sizes [mm]	h	t_w	b	t_f	H
	237	5.2	120	8.3	2700

Results	Cold failure load [KN]	Load applied for the test [KN]	Experimental failure temperature [°C]	Failure temperature (SAFIR) [°C] ***Before the test***
	410,3	144.5	**610**	540,7

The location of the resistances and the definition of the control zones are presented on the plan here below. Only 5 zones are used in this test because the web of the column was only 220 mm width and allowed putting only 2 resistances on its width.

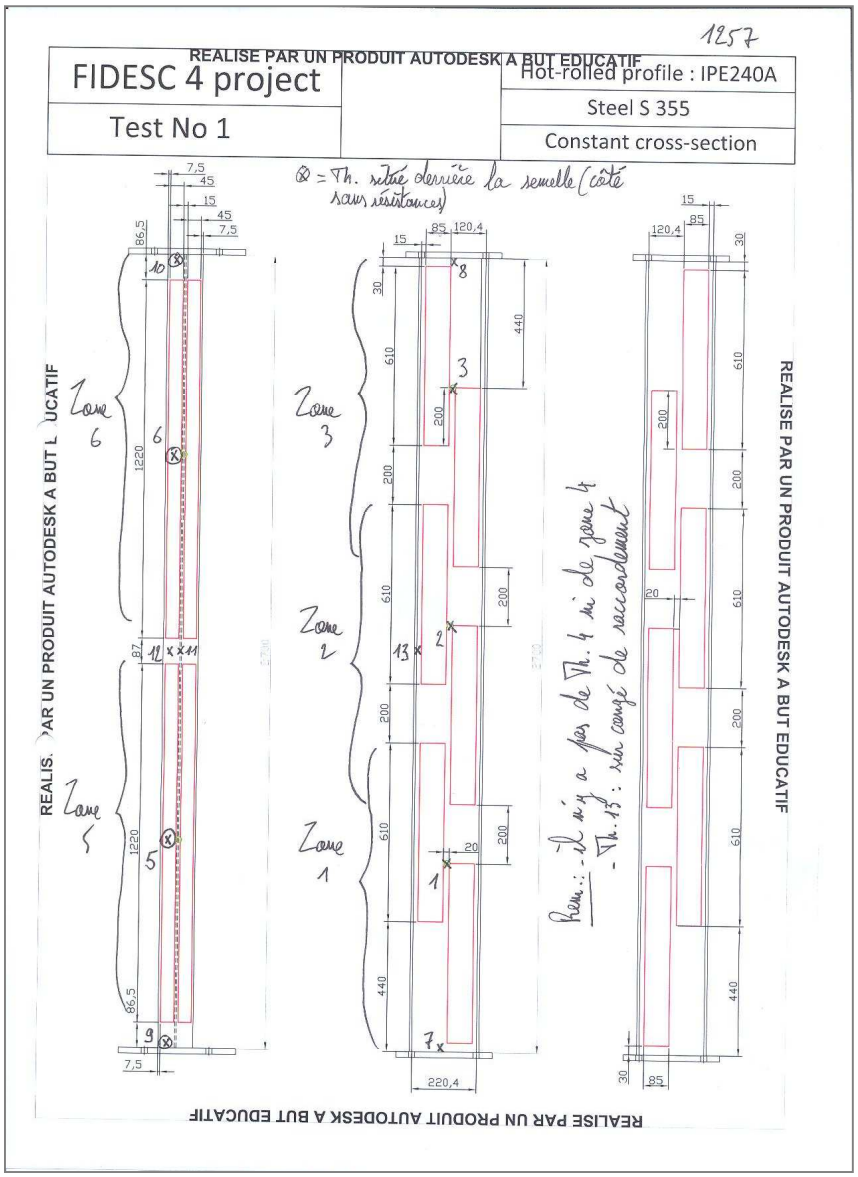

Figure 45 : Definition of the control zones and position of the control thermocouples

The temperature of the control thermocouples as a function of the time is shown in the Figure 46.

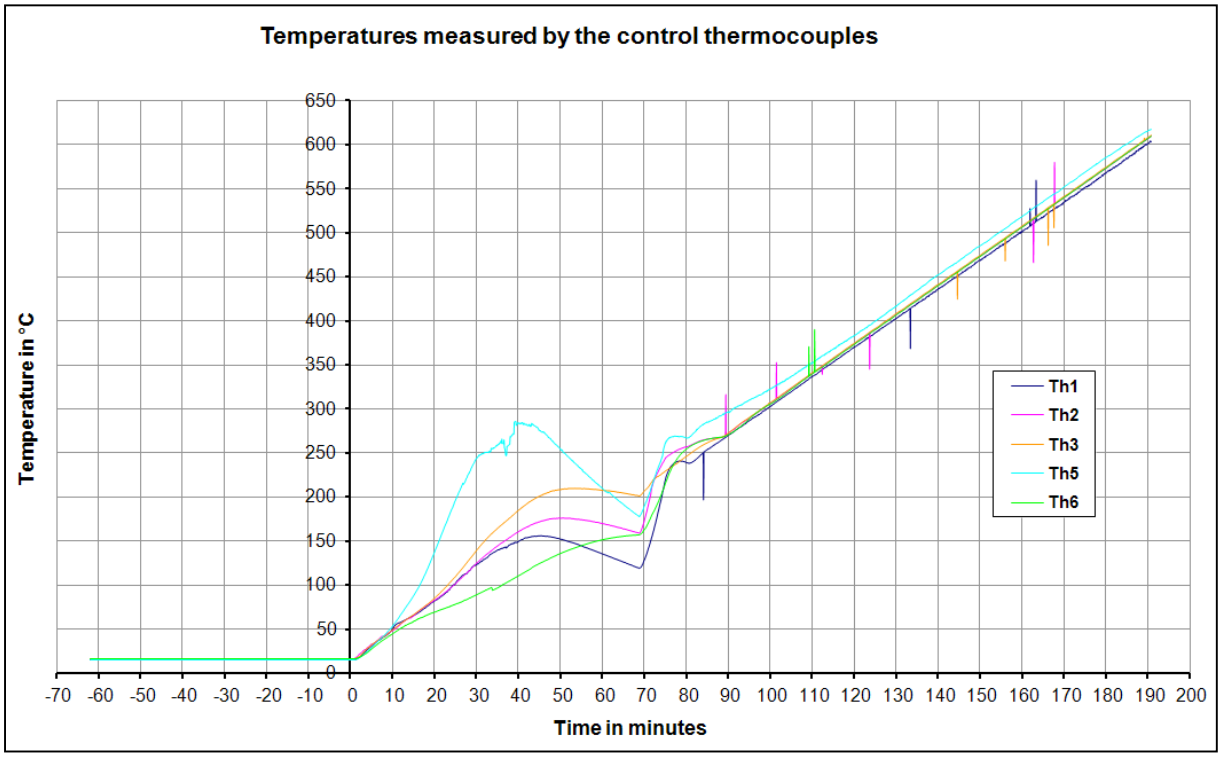

Figure 46 : Temperature recorded by the 5 control thermocouples

We observe that the control temperature curves are very close between each other and the instruction is thus well followed after the 80th minutes. At the beginning of the heating, some differences appear. It is due to the calibration of the different zones and resistances. The heating and loading process was stopped at the minute 190.

By calculating the mean between these 5 temperatures, we can display the evolution of the transversal and axial displacements as a function of the mean temperature of the column.

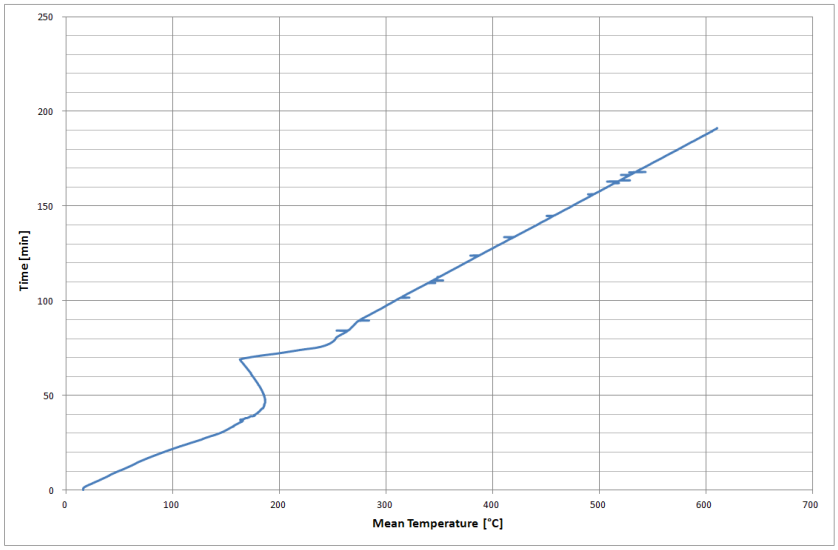

Figure 47 : Time vs. mean temperature

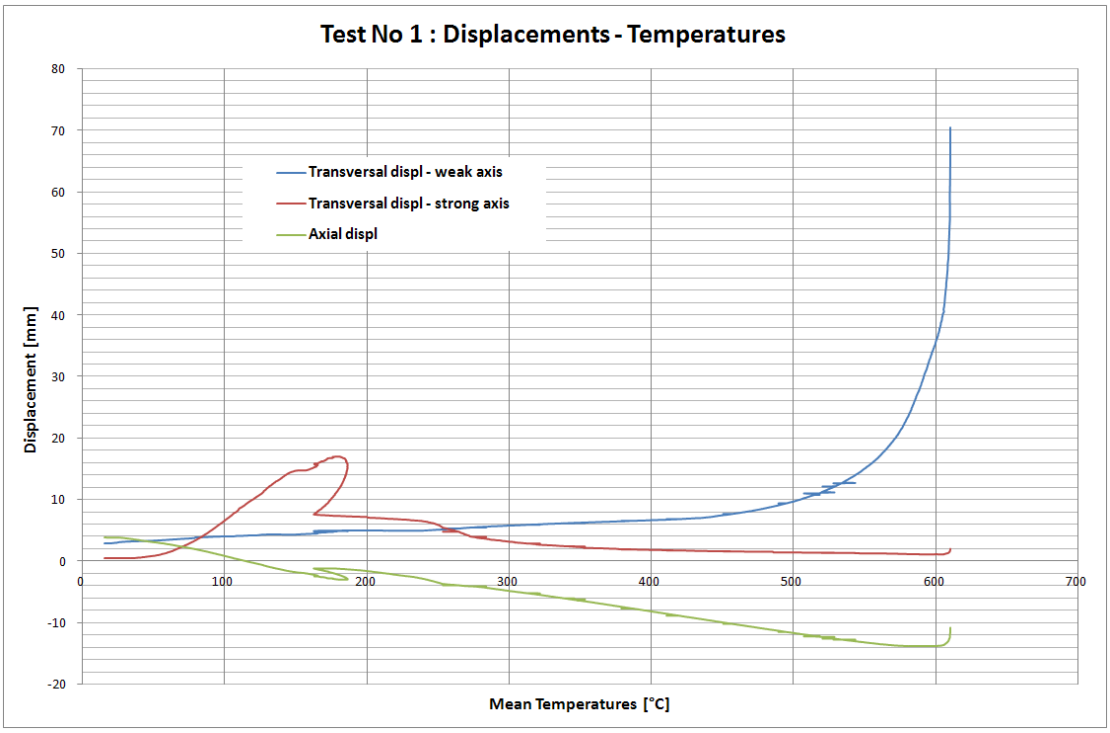

Figure 48 : Test No 1: Displacements – mean temperatures

The real properties are determined by performing materiel tests on samples of the steel of the web and of the flange. For the test No 1, these material tests were performed by University of Prague. The steel grades of the flange and of the web are:

- Flange – upper yield strength: f_y = 408 - 396 MPa → $f_{y,moy}$ = 402 MPa
- Flange – bottom yield strength: f_y = 396 - 391 MPa → $f_{y,moy}$ = 393,5 MPa

- Web – upper yield strength: f_y = 452 - 447 MPa → $f_{y,moy}$ = 449,5 MPa
- Web – bottom yield strength: f_y = 445 - 436 MPa → $f_{y,moy}$ = 441,5 MPa

Figure 49 : Test No 1: Deformed shape after the test

1.6.3. Experimental Test No 2: welded column

The load applied for the test and the expected failure temperature calculated with SAFIR is given in the table.

Sizes [mm]	h	t_w	b	t_f	H
	450	4	150	5	2700

Results	Cold failure load [KN]	Load applied for the test [KN]	Experimental failure temperature [°C]	Failure temperature (SAFIR) [°C] ***Before the test***
	408	122.4	**608**	578

The location of the resistances and the definition of the control zones are presented on the plan here below. In this case, 6 zones are used because the web of the column was 450 mm width and allowed putting 3 resistances on its width.

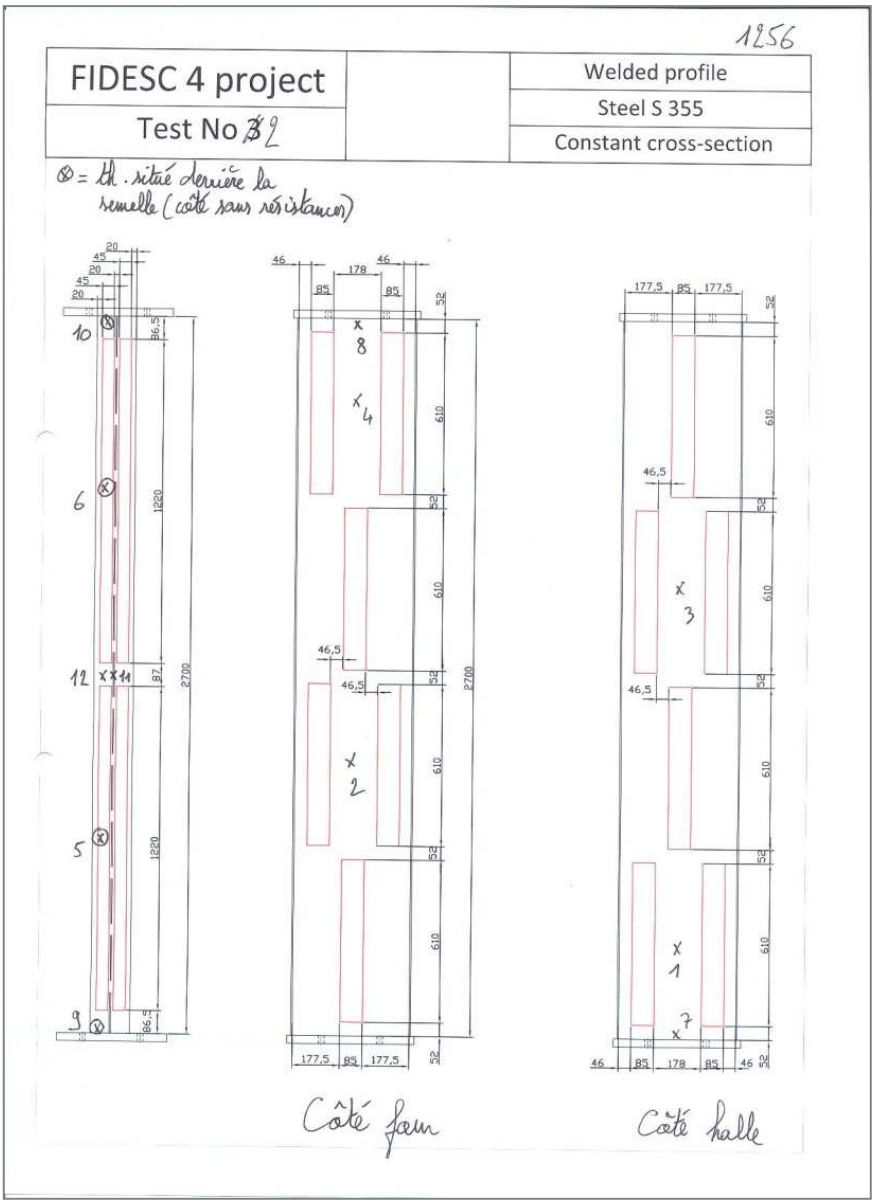

Figure 50 : Definition of the control zones and position of the control thermocouples

The temperature of the control thermocouples as a function of the time is shown in the Figure 50.

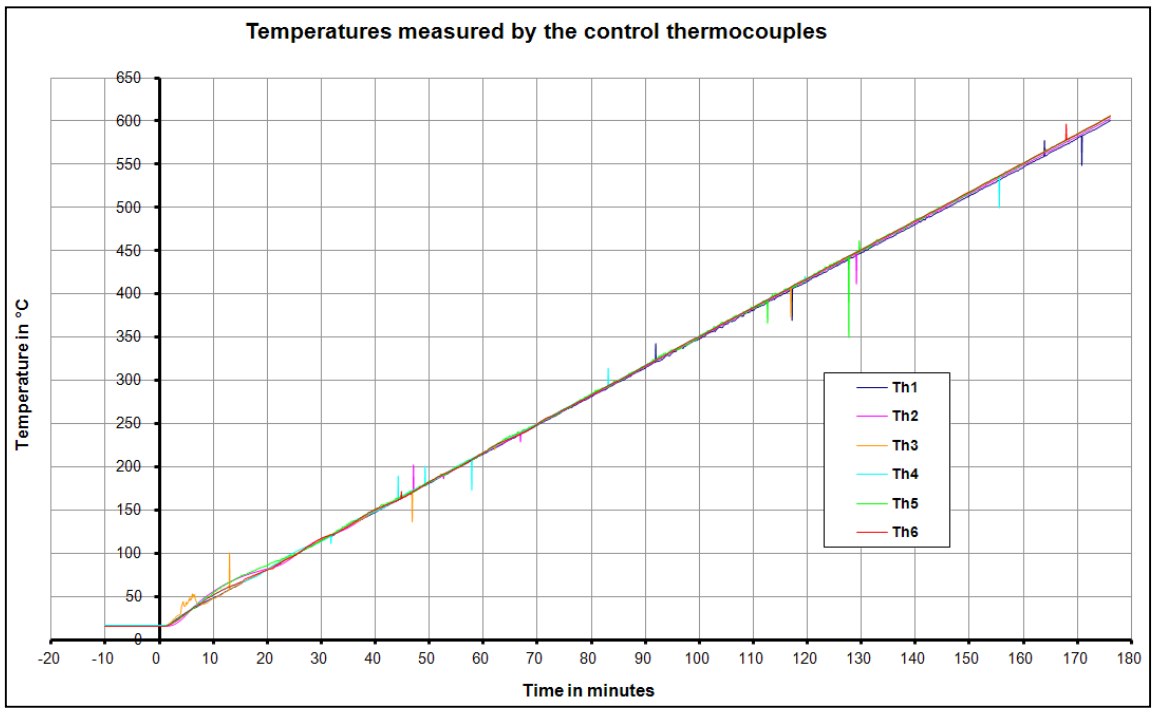

Figure 51 : Temperature recorded by the 6 control thermocouples

We observe that the control temperature curves are very close between each other and the instruction is thus well followed by the six zones. The heating and loading process was stopped at the minute 176.

By calculating the mean between these 6 temperatures, we can display the evolution of the transversal and axial displacements as a function of the mean temperature of the column.

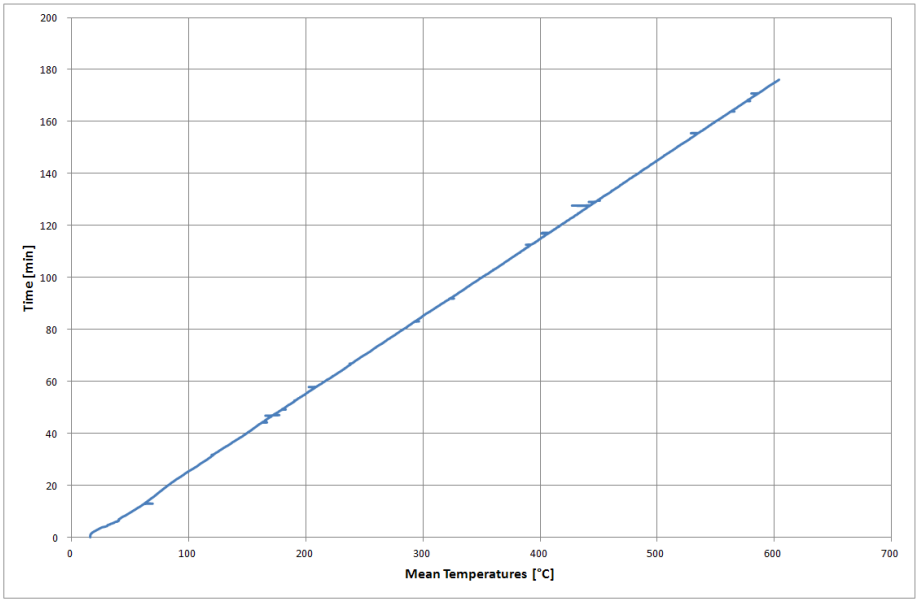

Figure 52 : Time vs. mean temperature

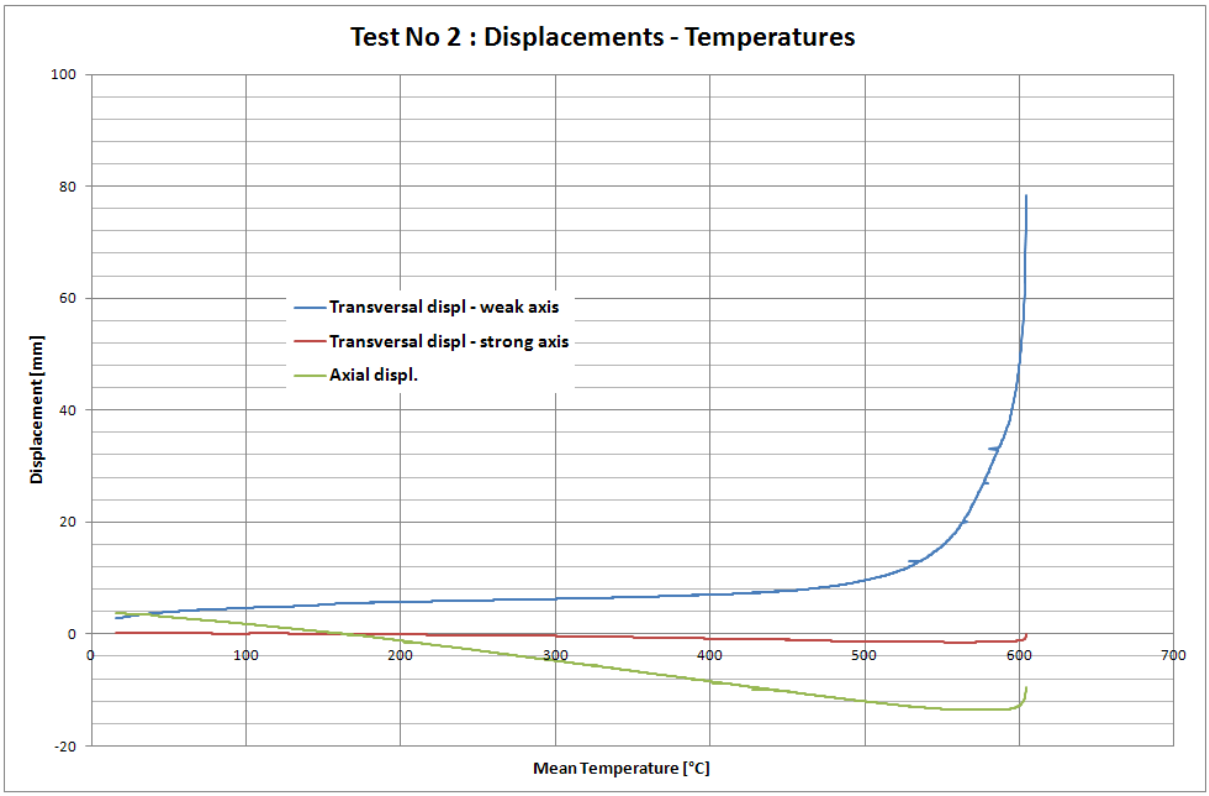

Figure 53 : Test No 2: Displacements – mean temperatures

For the test No 2, the material tests were performed by the manufacturer LINDAB and the certificate was provided with the welded columns. The steel grades of the flange and of the web are:

- Flange: f_y = 404 MPa
- Web – at the lead end of the plate : f_y = 482 MPa
- Web – at the tail end of the plate : f_y = 447 MPa

Figure 54 : Test No 2: Displacements – mean temperatures

1.6.4. Experimental Test No 3: welded column

The load applied for the test and the expected failure temperature calculated with SAFIR is given in the table.

Sizes [mm]	h	t_w	b	t_f	H
	450	4	150	5	2700
Results	Cold failure load [KN]	Load applied for the test [KN]	Experimental failure temperature [°C]	Failure temperature (SAFIR) [°C] ***Before the test***	
	408	204	**452**	420	

The location of the resistances and the definition of the control zones are presented on the plan here below. In this case, 6 zones are used because the web of the column was 450mm width and allowed putting 3 resistances along its width.

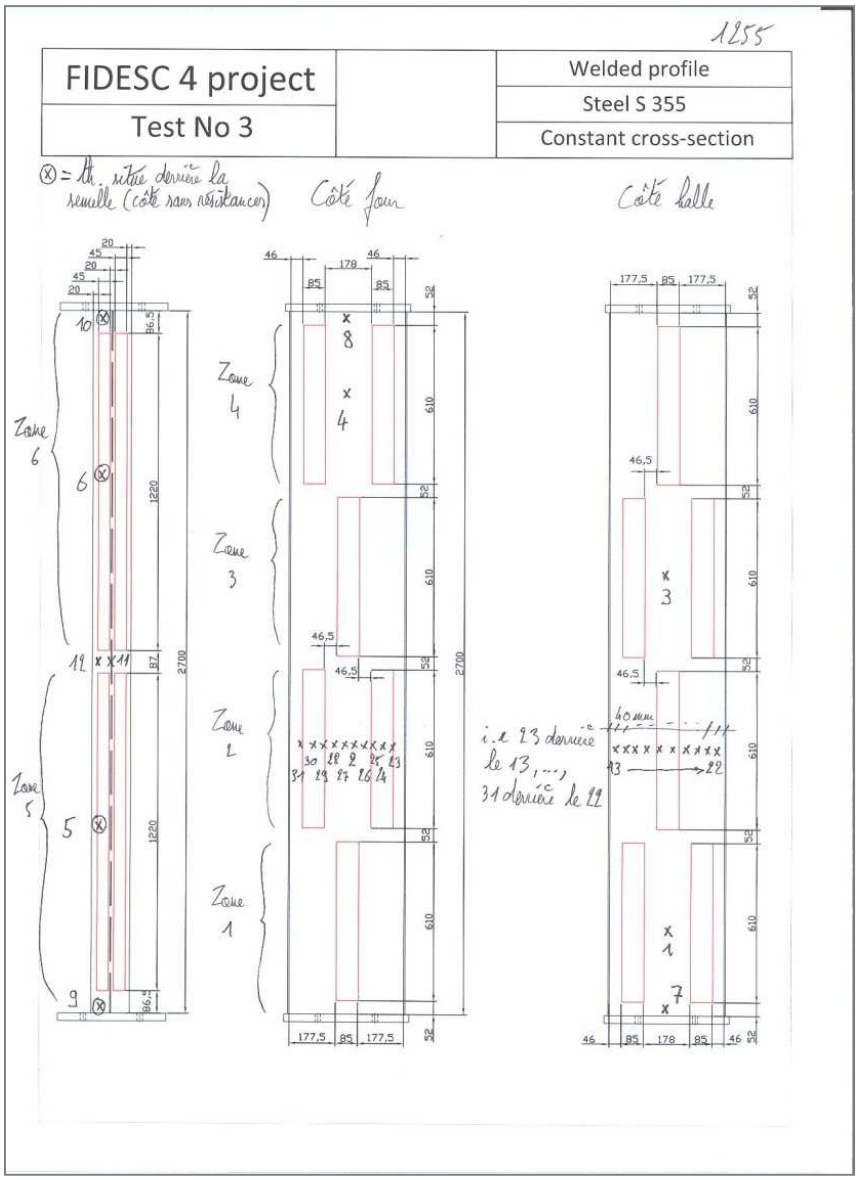

Figure 55 : Definition of the control zones and position of the control thermocouples

The temperature of the control thermocouples as a function of the time is shown in the Figure 54.

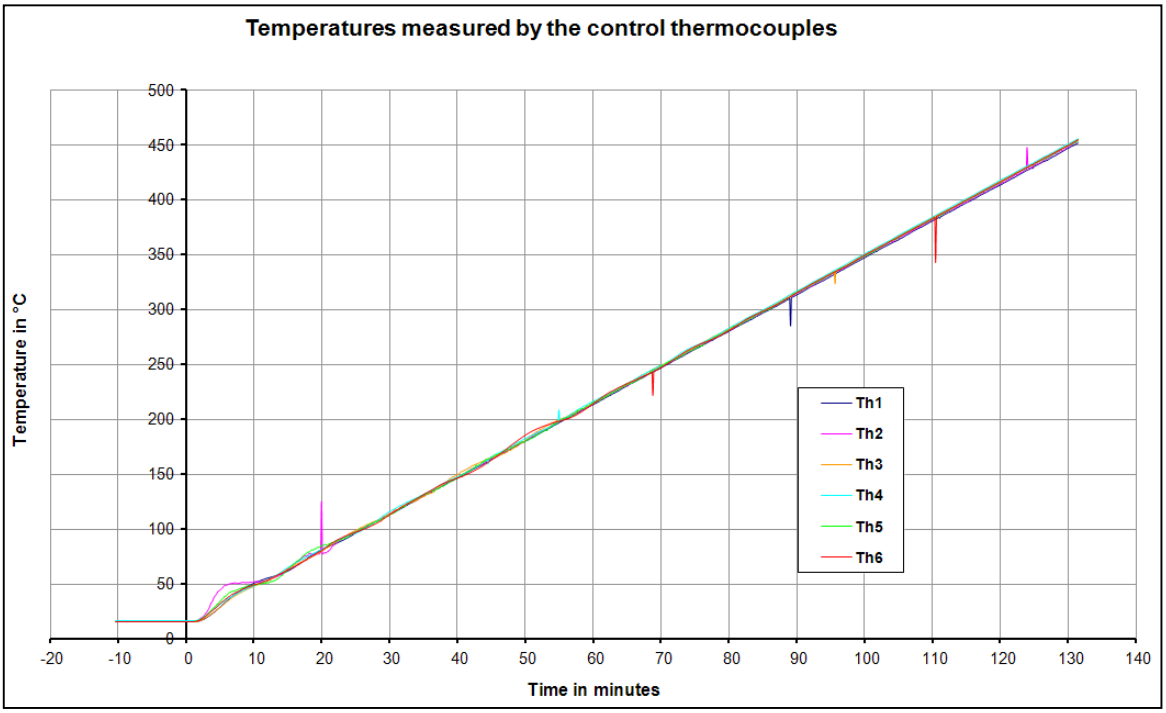

Figure 56 : Temperature recorded by the 6 control thermocouples

We observe that the control temperature curves are very close between each other and the instruction is thus well followed by the six zones. The heating and loading process was stopped at the minute 131.

By calculating the mean between these 6 temperatures, we can display the evolution of the transversal and axial displacements as a function of the mean temperature of the column.

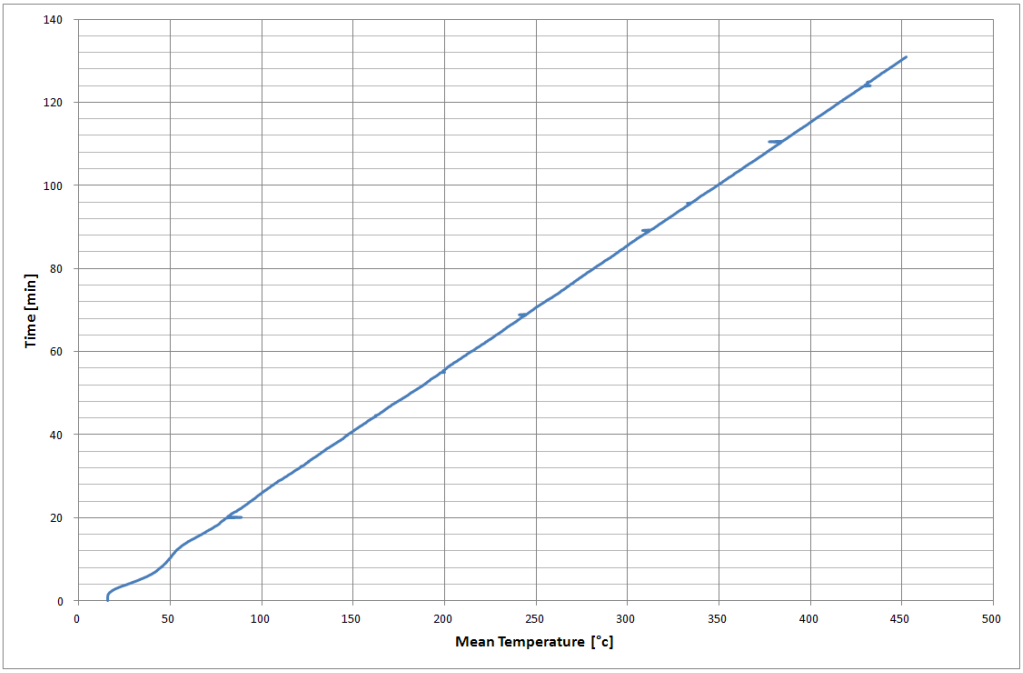

Figure 57 : Time vs. mean temperature

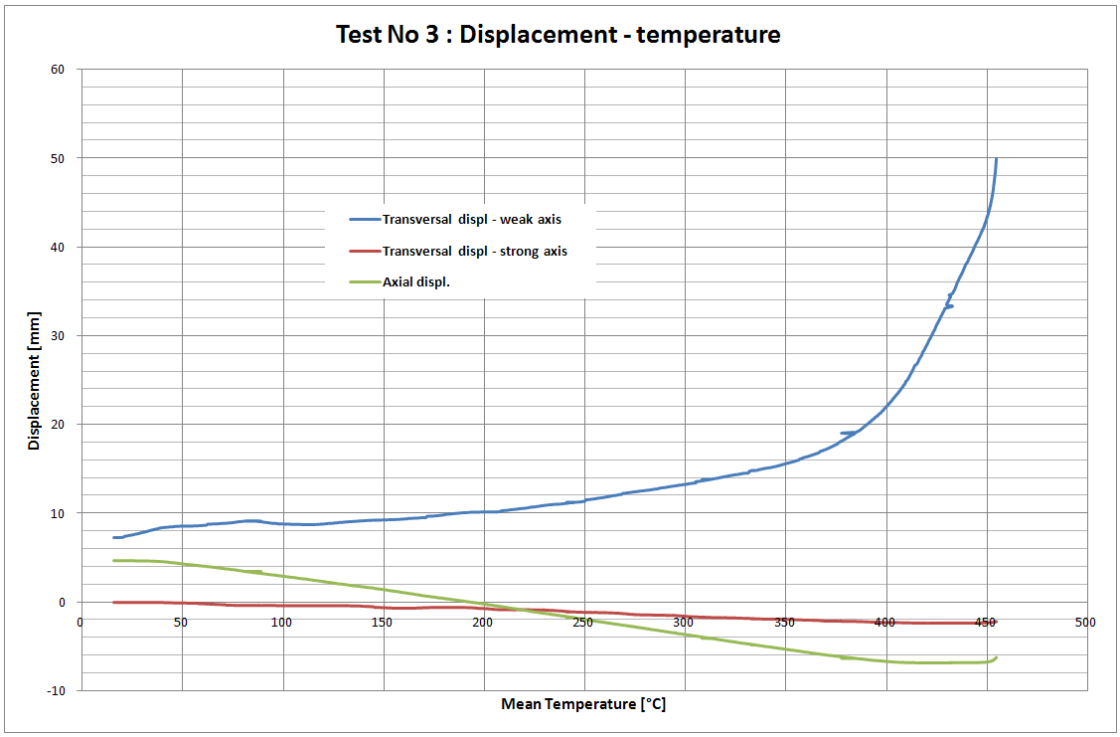

Figure 58 : Test No 3: Displacements – mean temperatures

For the test No 3, the material tests were also performed by the manufacturer LINDAB and the certificates were provided with the welded columns. The steel grades of the flange and of the web are the same than for the test No 2 because the steel of the web and of the flange are a product of the same steel plate:

- Flange: f_y = 404 MPa
- Web –at the lead end of the plate : f_y = 482 MPa
- Web –at the tail end of the plate : f_y = 447 MPa

Figure 59 : Test No 3: Deformed shape of the column after the test

1.6.5. Experimental Test No 4: welded column

The load applied for the test and the expected failure temperature calculated with SAFIR is given in the table.

Sizes [mm]	h	t_w	b	t_f	H
	300 (small base) 500 (large base)	4	150	5	2700

Results	Cold failure load [KN]	Load applied for the test [KN]	Experimental failure temperature [°C]	Failure temperature (SAFIR) [°C] **Before the test**
	696	348	**519.5**	502

The location of the resistances and the definition of the control zones are presented on the plan here below. In this case, 6 zones are used because with a particular disposition of the resistances due to the variable width of the web.

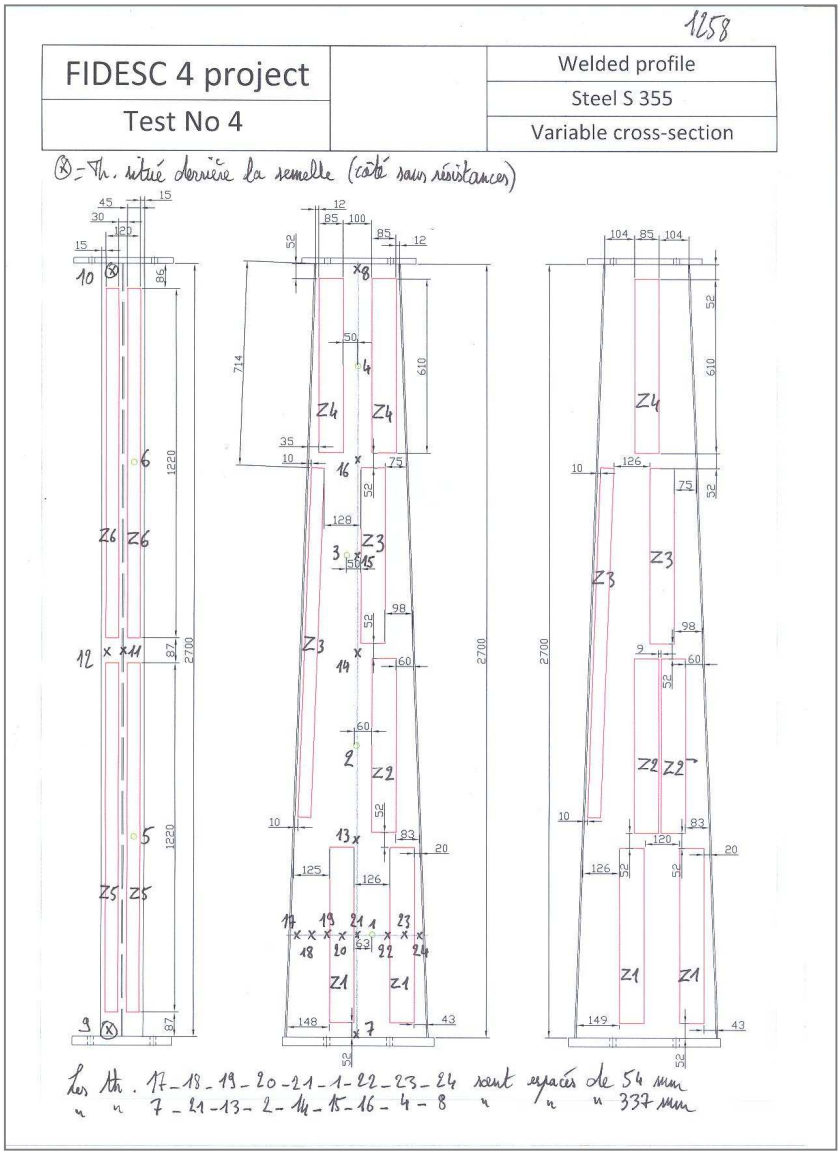

Figure 60 : Definition of the control zones and position of the control thermocouples

The temperature of the control thermocouples as a function of the time is shown in the Figure 58.

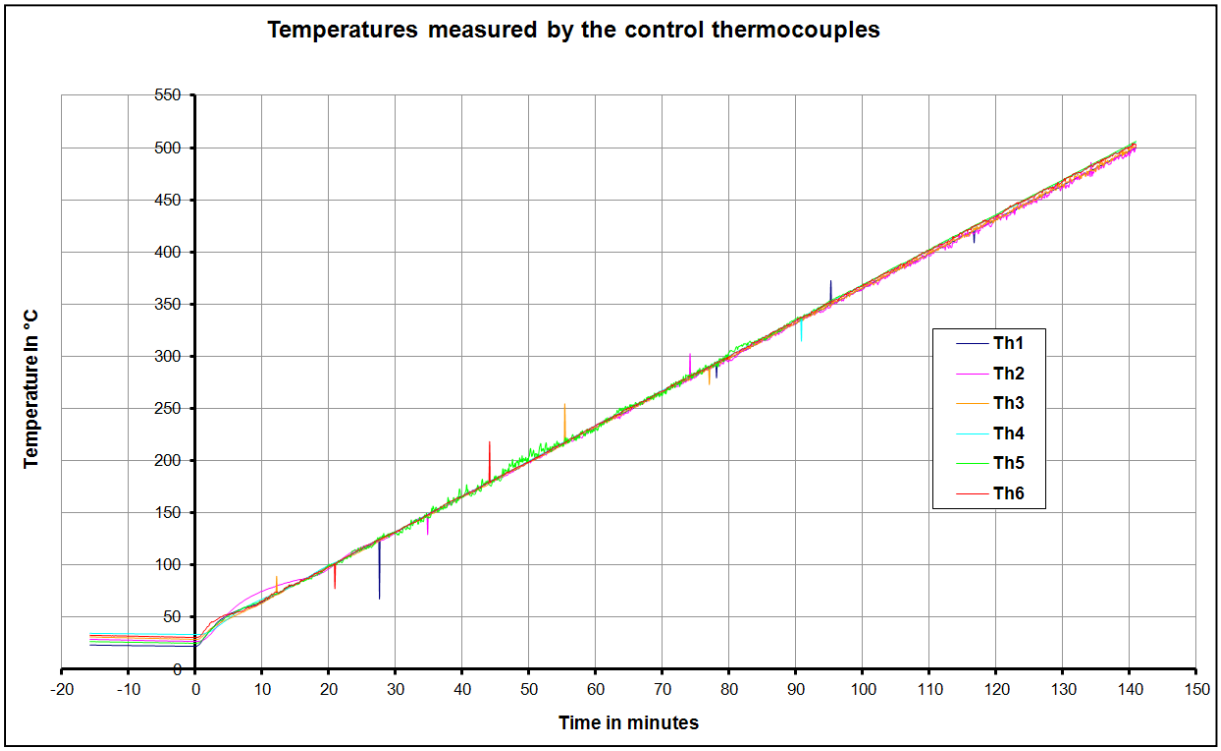

Figure 61 : Temperature recorded by the 6 control thermocouples

We observe that the control temperature curves are very close between each other and the instruction is thus well followed by the six zones. The heating and loading process was stopped at the minute 141.

By calculating the mean between these 6 temperatures, we can display the evolution of the transversal and axial displacements as a function of the mean temperature of the column.

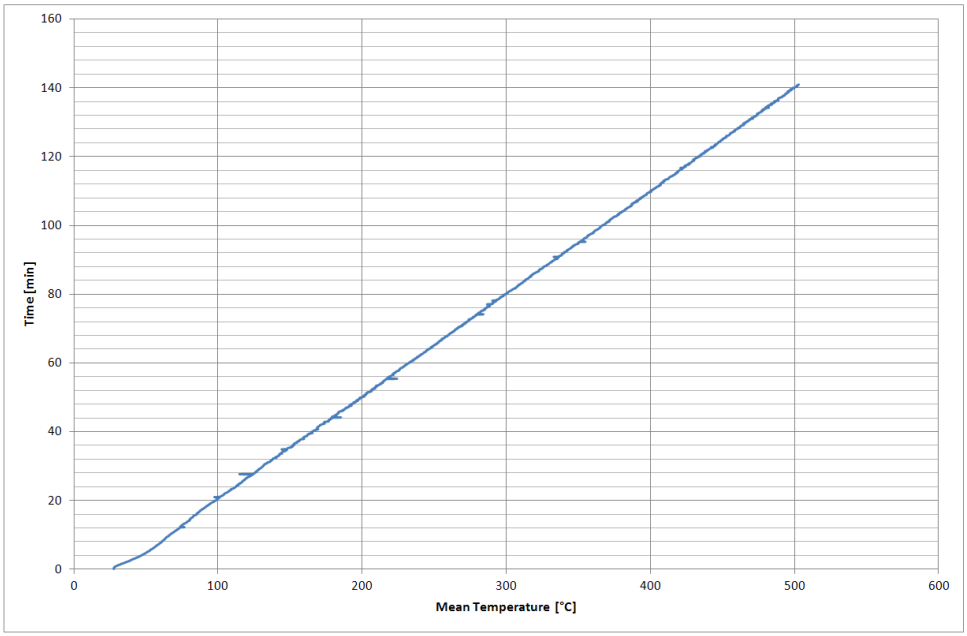

Figure 62 : Time vs. mean temperature

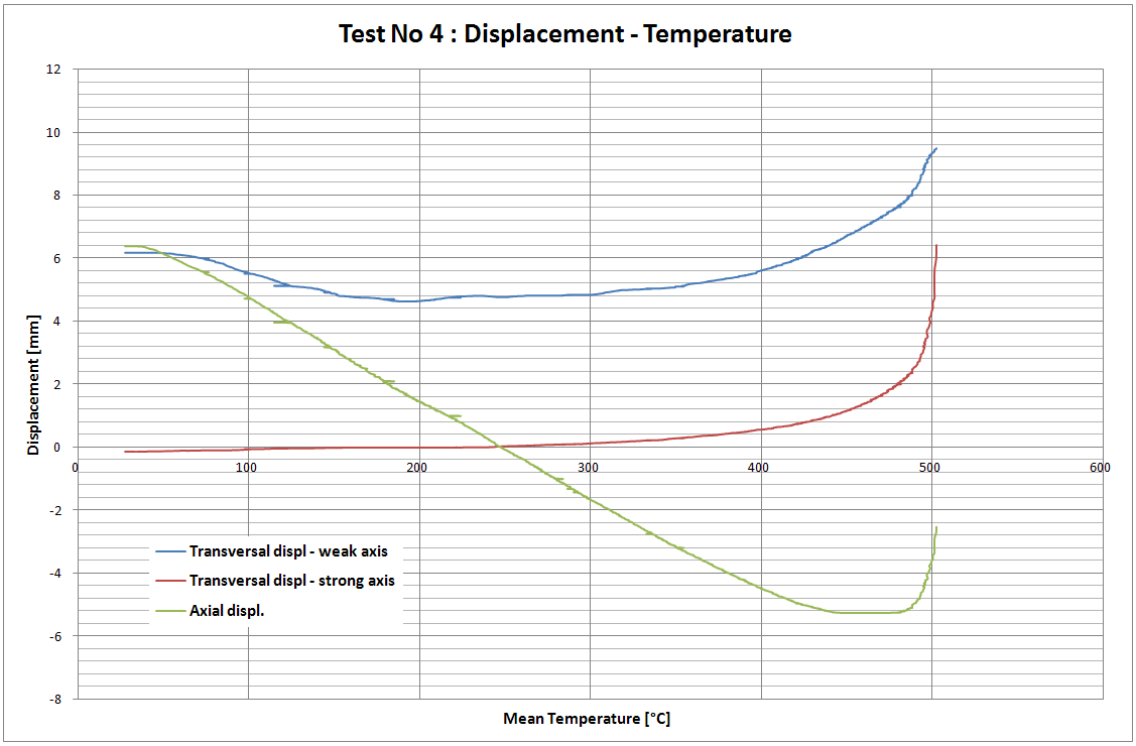

Figure 63 : Test No 4: Displacements – mean temperatures

For the test No 4, we don't have the certificates for the steel of this column and no material tests were performed. We consider that the steel grades of the flange and of the web are the same than for the test No 3 even if the steel of the web and of the flange are a product of a different steel plate.

Figure 64 : Test No 4: Deformed shape of the column after the test

1.6.6. Experimental Test No 5: welded column

The load applied for the test and the expected failure temperature calculated with SAFIR is given in the table here below.

Sizes [mm]	h	t_w	b	t_f	H
	360	4	150	5	2700

Results	Cold failure load [KN]	Load applied for the test [KN]	Experimental failure temperature [°C]	Failure temperature (SAFIR) [°C] **Before the test**
	462.5	231.25	**509**	506

The location of the resistances and the definition of the control zones are presented on the plan here below. In this case, 6 zones are used because the web of the column was 360mm width and allowed putting 3 resistances along its width.

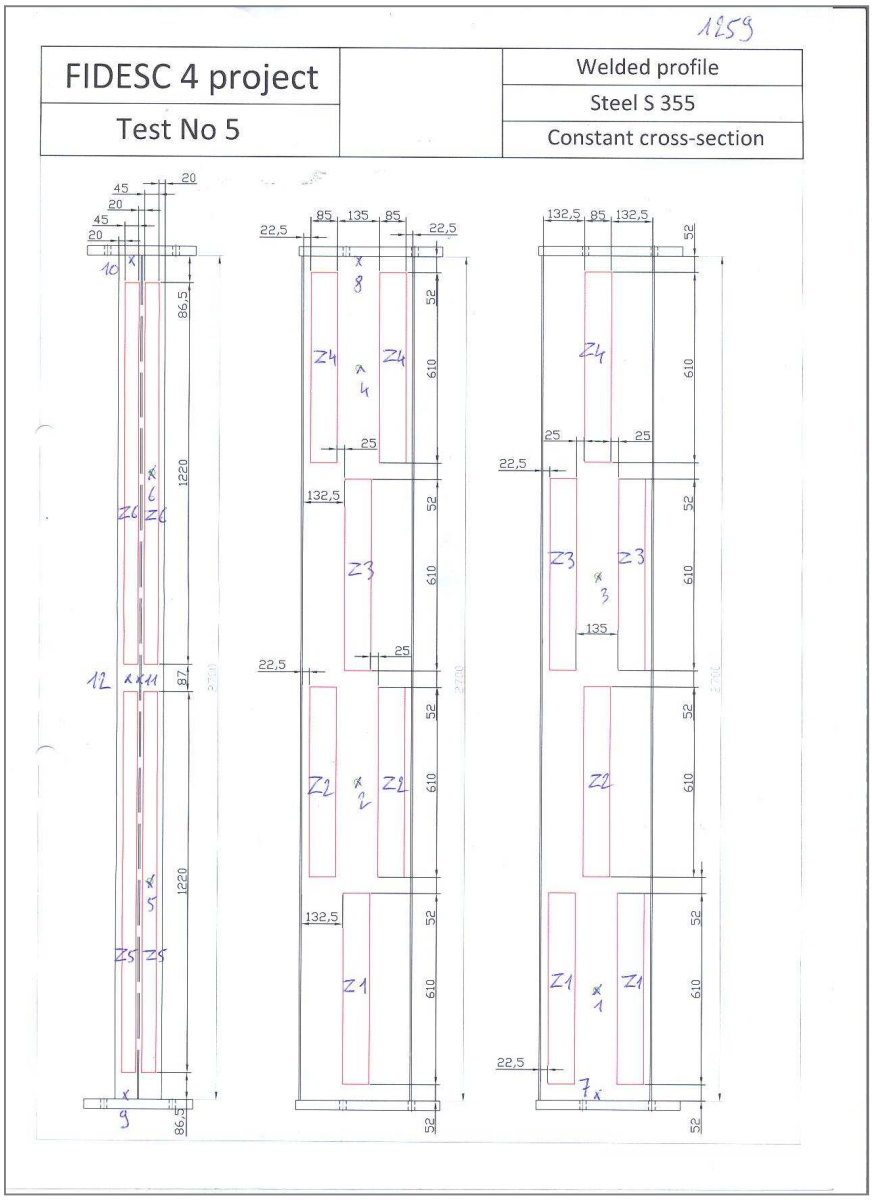

Figure 65 : Definition of the control zones and position of the control thermocouples

The temperature of the control thermocouples as a function of the time is shown in the Figure 62.

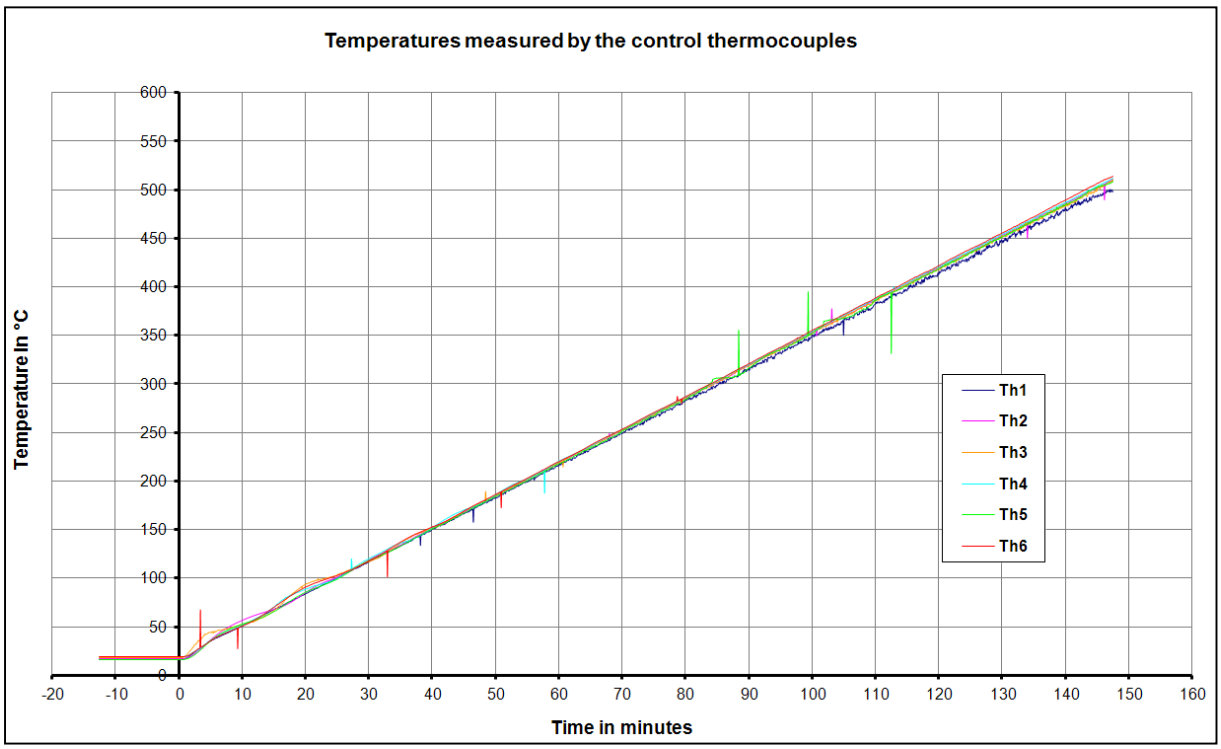

Figure 66 : Temperature recorded by the 6 control thermocouples

We observe that the control temperature curves are very close between each other and the instruction is thus well followed by the six zones. The heating and loading process was stopped at the minute 147.

By calculating the mean between these 6 temperatures, we can display the evolution of the transversal and axial displacements as a function of the mean temperature of the column.

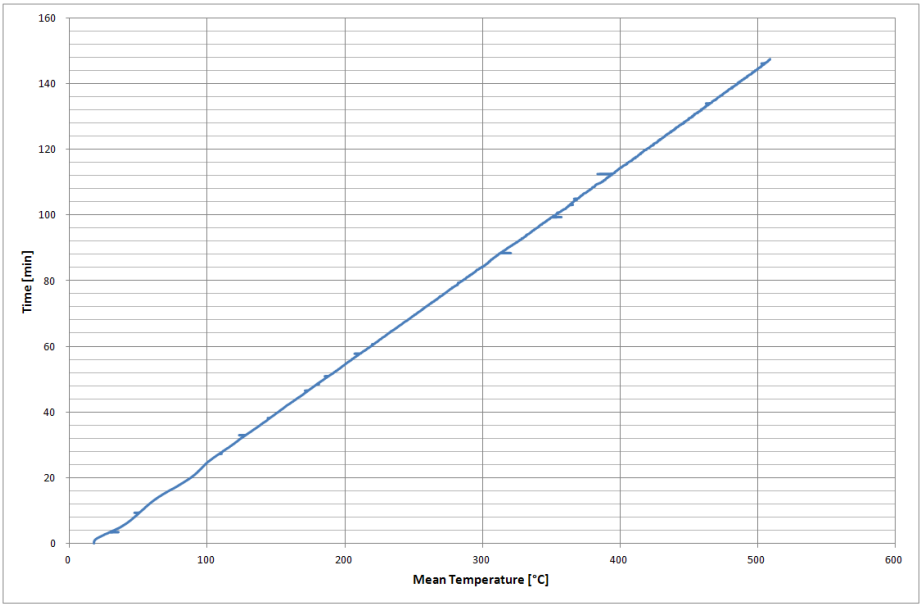

Figure 67 : Time vs. mean temperature

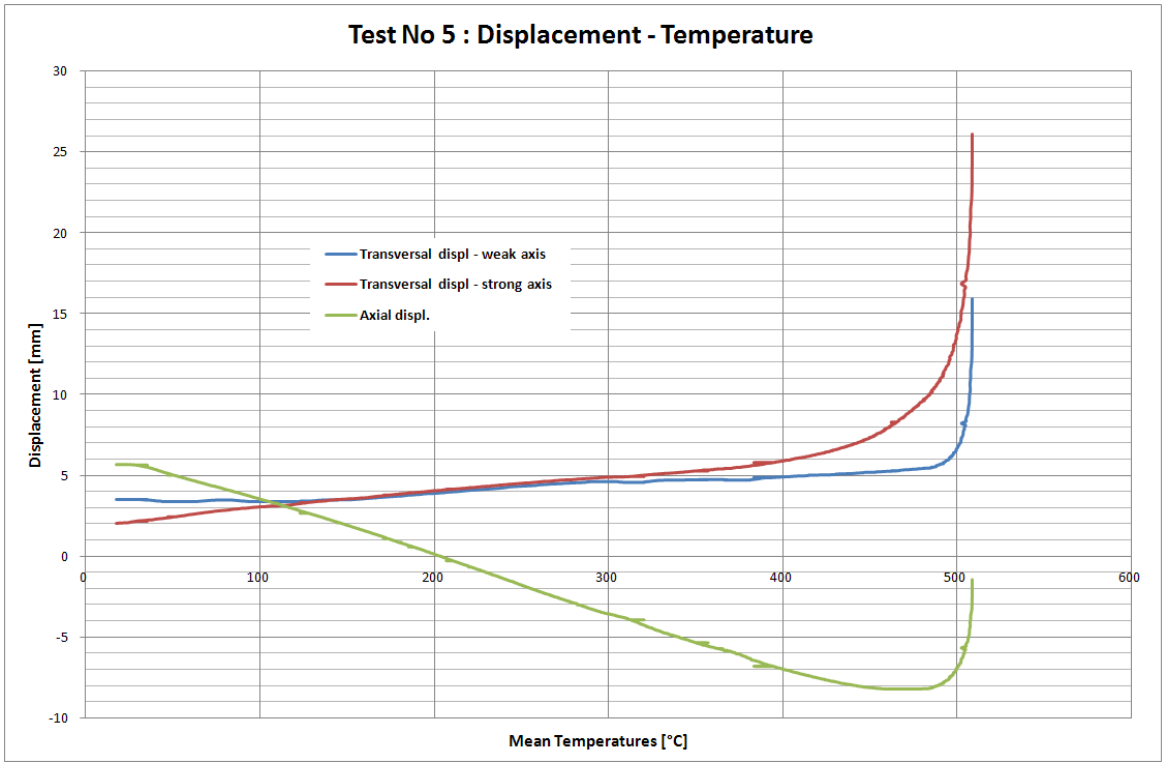

Figure 68 : Test No 5: Displacements – mean temperatures

For the test No 5, we don't have the certificates for the steel of this column and no material tests were performed. We consider that the steel grades of the flange and of the web are the same than for the test No 3 even if the steel of the web and of the flange are a product of a different steel plate.

Figure 69 : Test No 5: Deformed shape of the column after the test

1.6.7. Experimental Test No 6: welded column

The load applied for the test and the expected failure temperature calculated with SAFIR is given in the table.

Sizes [mm]	h	t_w	b	t_f	H
	360	4	150	5	2700
NB: the eccentricity of the load is larger than the test No 5					
Results	Cold failure load [KN]	Load applied for the test [KN]	Experimental failure temperature [°C]	Failure temperature (SAFIR) [°C] ***Before the test***	
	332.8	166.4	**530**	503	

The location of the resistances and the definition of the control zones are presented on the plan here below. In this case, 6 zones are used because the web of the column was 360mm width and allowed putting 3 resistances along its width.

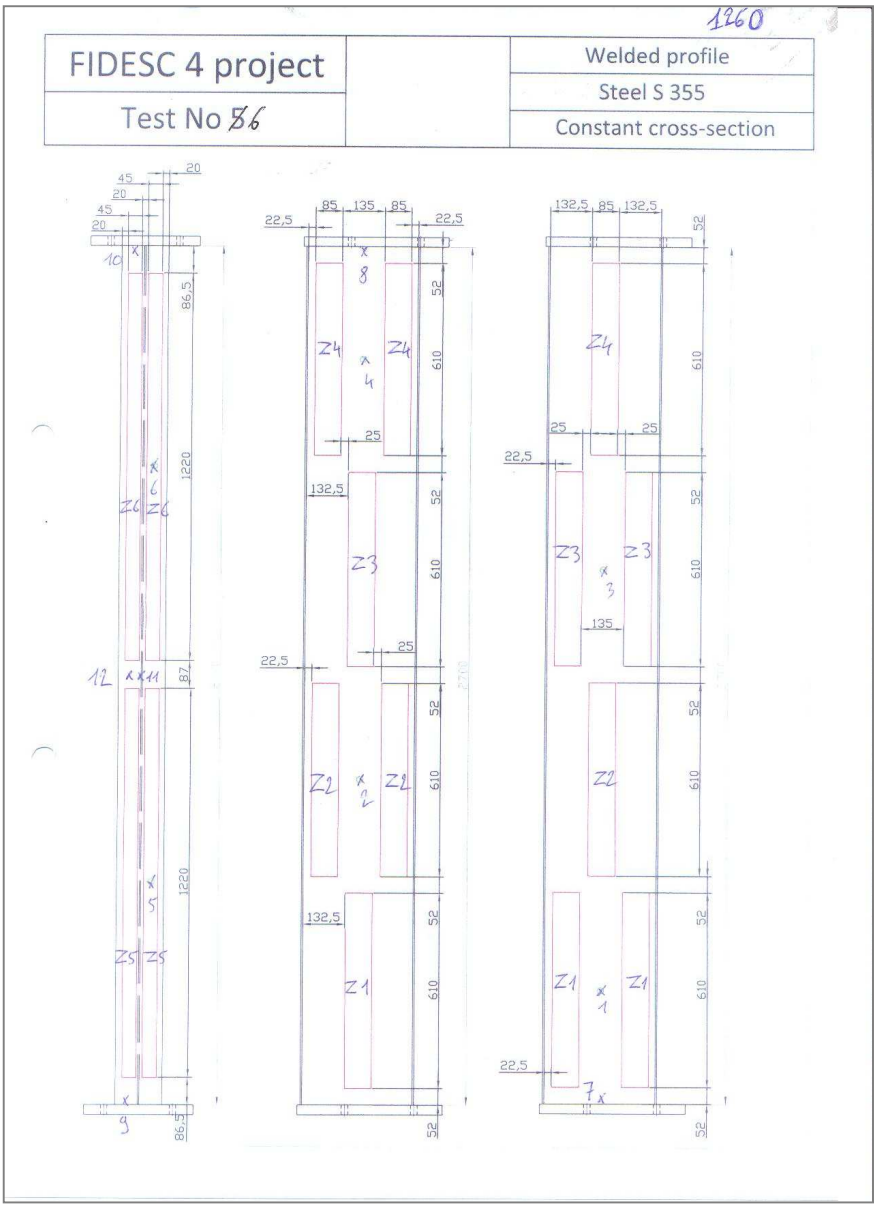

Figure 70 : Definition of the control zones and position of the control thermocouples

The temperature of the control thermocouples as a function of the time is shown in the Figure 66.

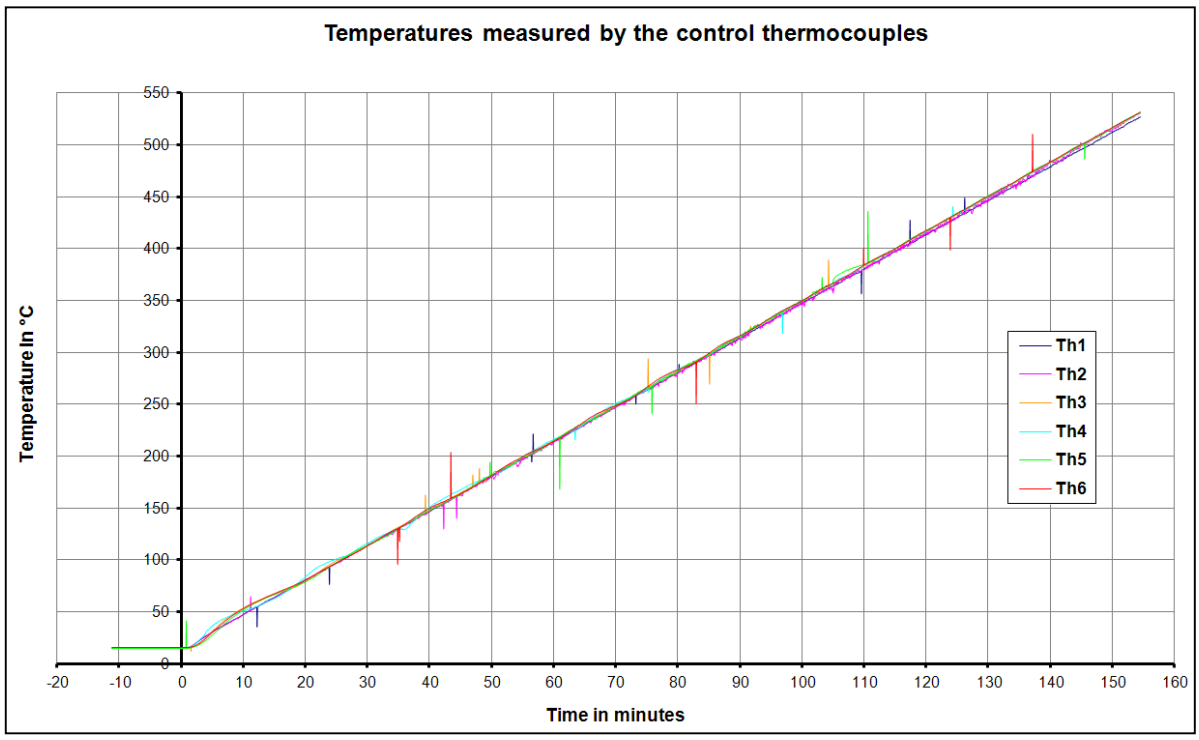

Figure 71 : Temperature recorded by the 6 control thermocouples

We observe that the control temperature curves are very close between each other and the instruction is thus well followed by the six zones. The heating and loading process was stopped at the minute 154.

By calculating the mean between these 6 temperatures, we can display the evolution of the transversal and axial displacements as a function of the mean temperature of the column.

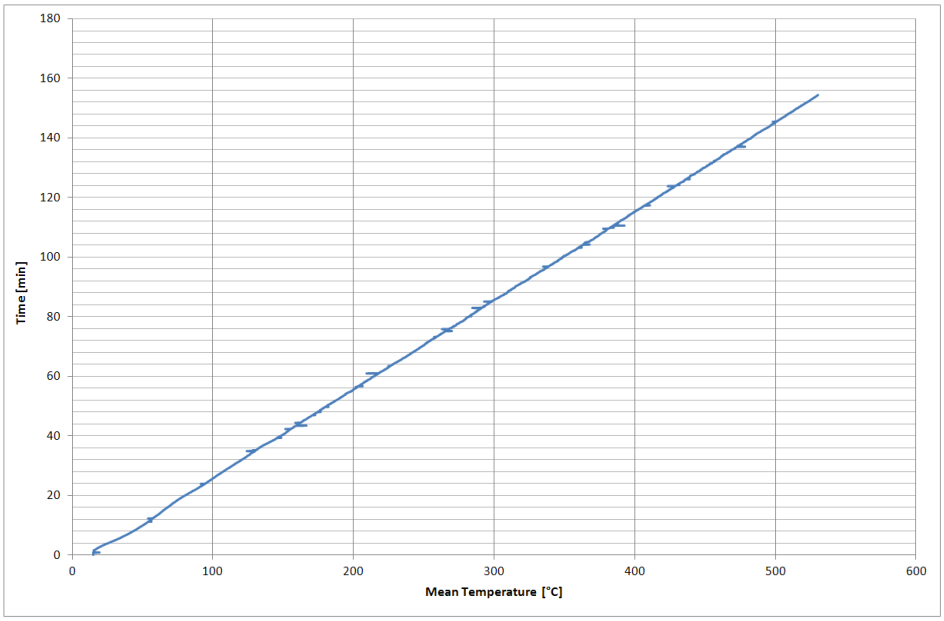

Figure 72 : Time vs. mean temperature

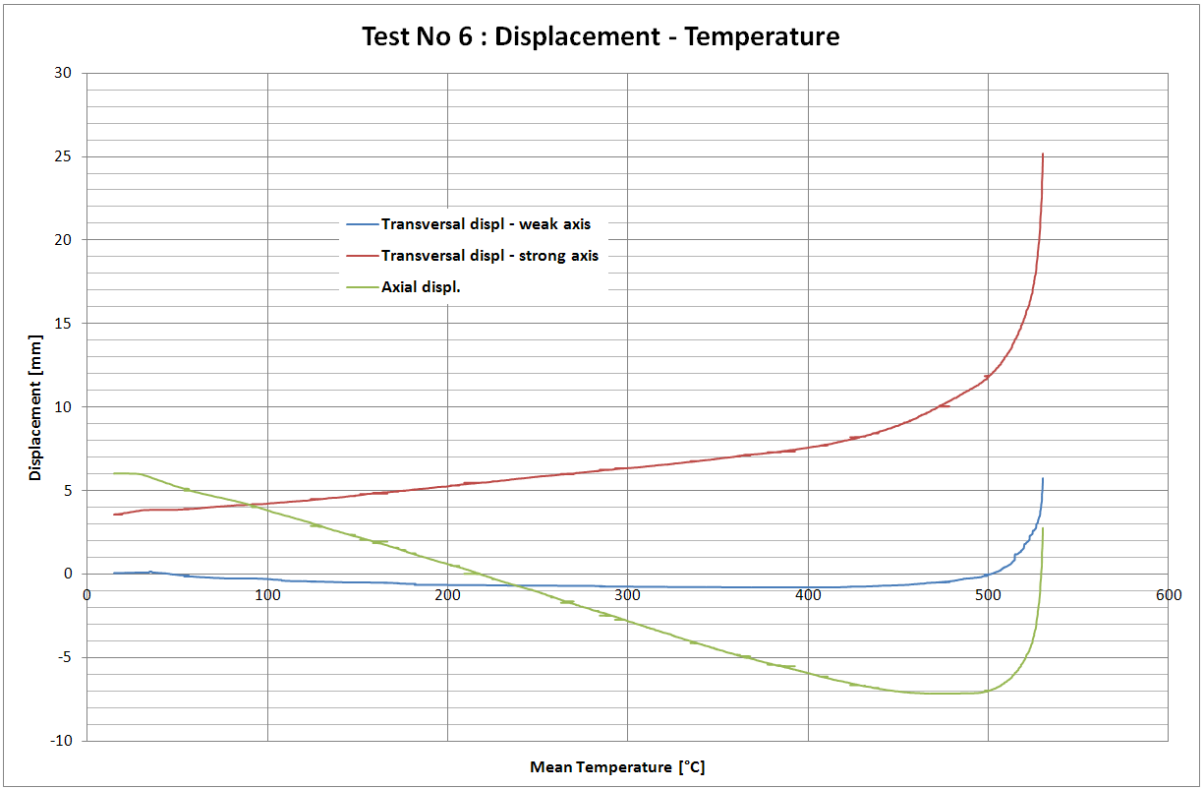

Figure 73 : Test No 6: Displacements – mean temperatures

For the test No 6, the material tests were also performed by the manufacturer LINDAB and the certificates were provided with the welded columns. The steel grades of the flange and of the web are:

- Flange: f_y = 404 MPa
- Web –at the lead end of the plate : f_y = 482 MPa
- Web –at the tail end of the plate : f_y = 447 MPa

Figure 74 : Test No 6: Deformed shape of the column after the test

1.6.8. Experimental Test No 7: hot-rolled column

The load applied for the test and the expected failure temperature calculated with SAFIR is given in the table.

Sizes [mm]	h	t_w	b	t_f	H
	320	8.5	300	11.5	2700

Results	Cold failure load [KN]	Load applied for the test [KN]	Experimental failure temperature [°C]	Failure temperature (SAFIR) [°C] ***Before the test***
	1902	760.8	**622.8**	630.2

The location of the resistances and the definition of the control zones are presented on the plan here below. In this case, 6 zones are used because the web of the column was 320mm width and allowed putting 3 resistances along its width.

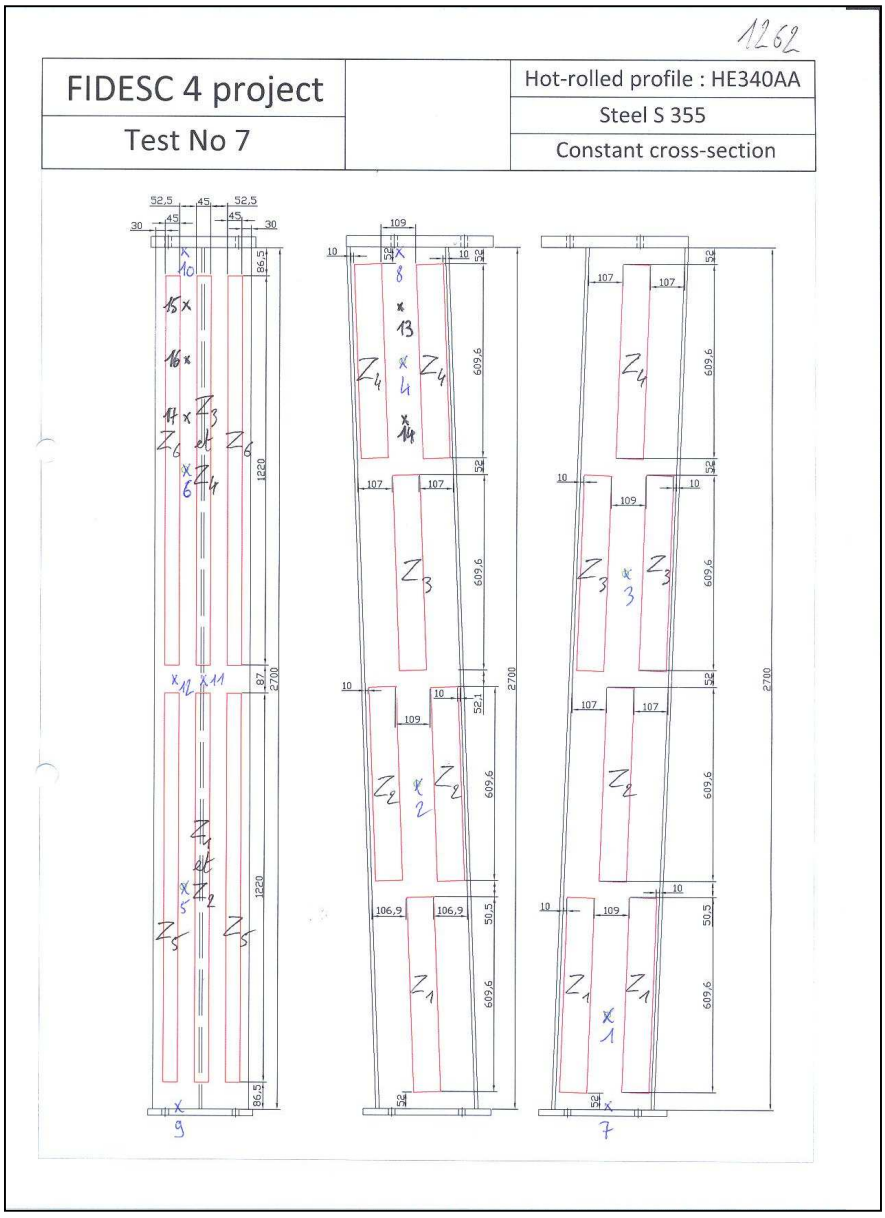

Figure 75 : Definition of the control zones and position of the control thermocouples

The temperature of the control thermocouples as a function of the time is shown in the Figure 66.

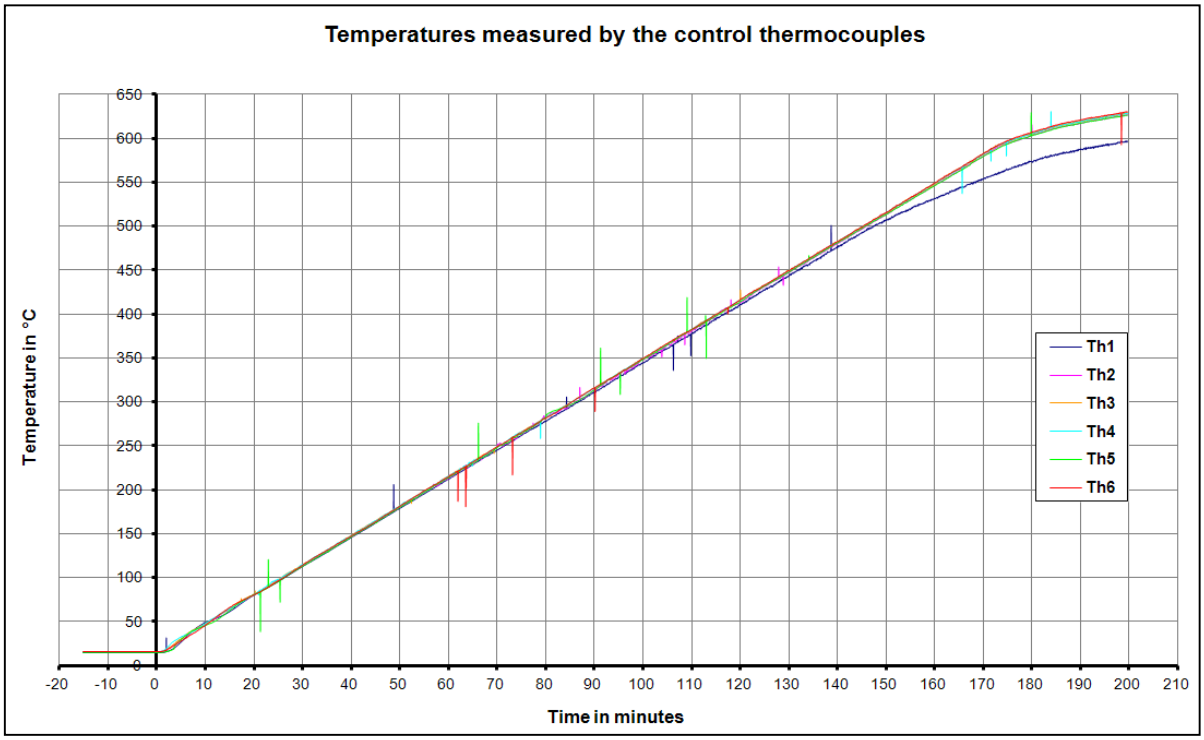

Figure 76 : Temperature recorded by the 6 control thermocouples

We observe that the control temperature curves are very close between each other and the instruction is thus well followed by the six zones up to the minute 145. The control thermocouple of the zone No 1 presents an increasing deviation from the minute 145 to the minute 180 with a maximum value of 30°C. The heating and loading process was stopped at the minute 199.

By calculating the mean between these 6 temperatures, we can display the evolution of the transversal and axial displacements as a function of the mean temperature of the column.

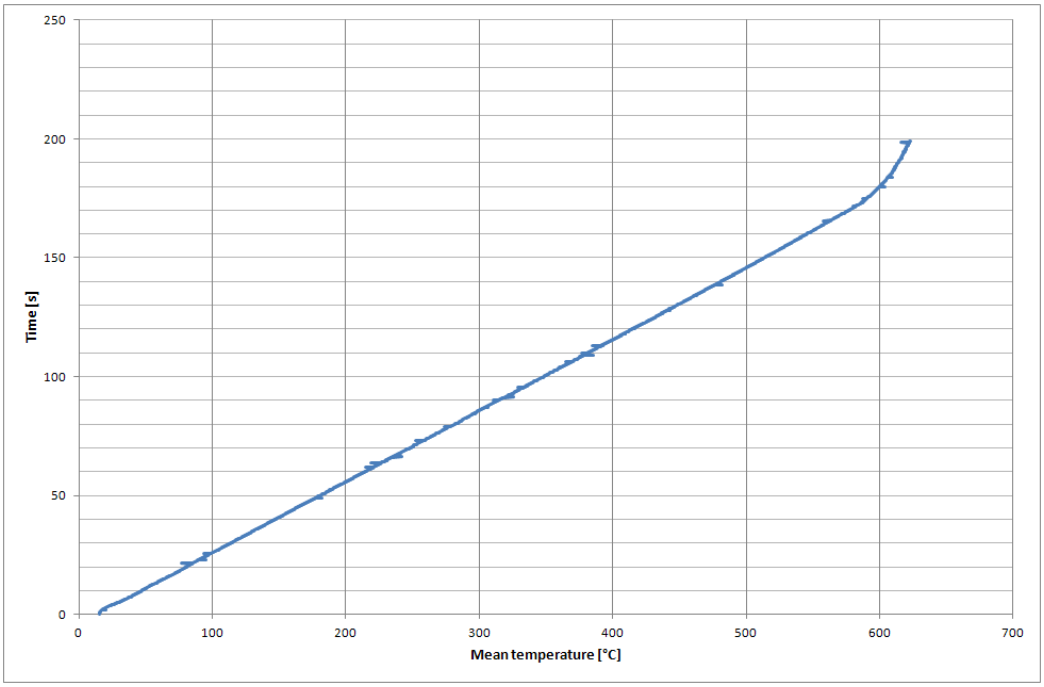

Figure 77 : Time vs. mean temperature

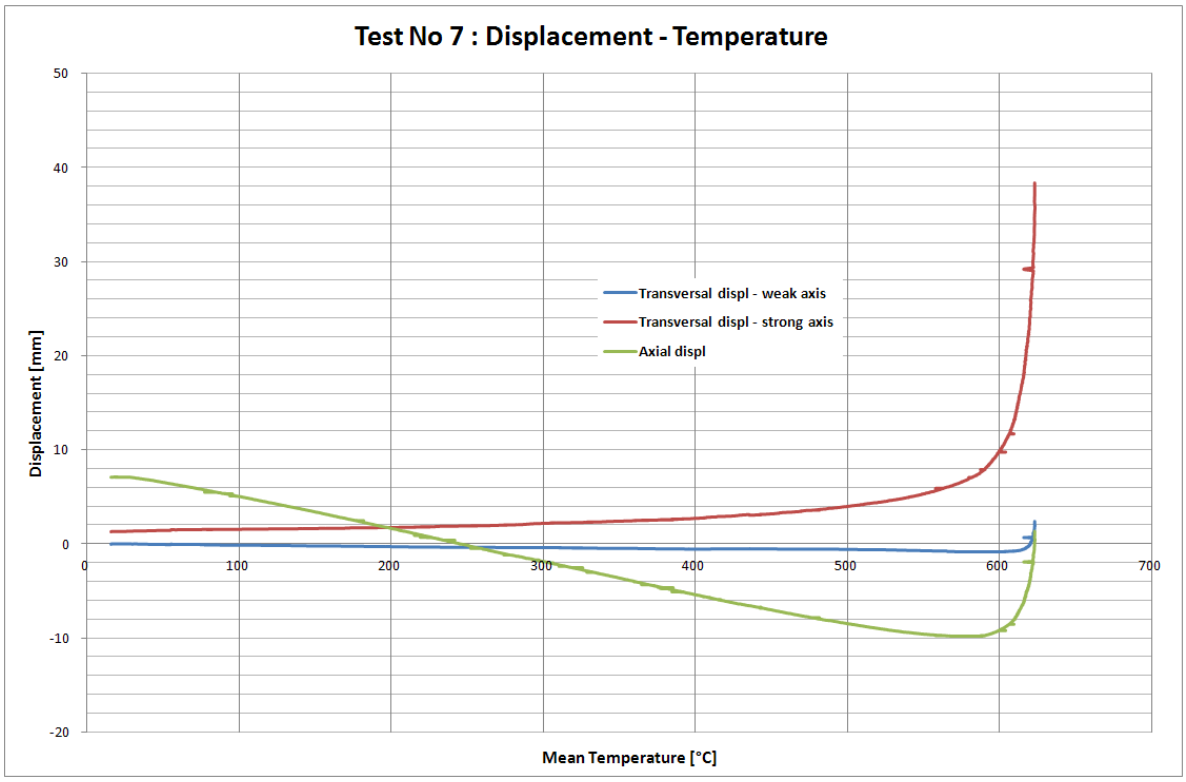

Figure 78 : Test No 7: Displacements – mean temperatures

For the test No 7, the material tests were performed by The University of Prague. The steel grades of the flange and of the web are:

- Flange – upper yield strength: f_y = 538 MPa
- Flange – bottom yield strength: f_y = 523 MPa

- Web – upper yield strength: f_y = 591 - 581 MPa → $f_{y,moy}$ = 585,5 MPa
- Web – bottom yield strength: f_y = 577 - 569 MPa → $f_{y,moy}$ = 573 MPa

Figure 79 : Test No 7: Deformed shape of the column after the test

1.6.9. Experimental Test No 8: welded column

The load applied for the test and the expected failure temperature calculated with SAFIR is given in the table.

Sizes [mm]	h	t_w	b	t_f	H
	350 (small base) 450 (large base)	4	150	5	2700

Results	Cold failure load [KN]	Load applied for the test [KN]	Experimental failure temperature [°C]	Failure temperature (SAFIR) [°C] ***Before the test***
	438	219	**504.5**	510

The location of the resistances and the definition of the control zones are presented on the plan here below. In this case, 6 zones are used because the web of the column was 360mm width and allowed putting 3 resistances along its width.

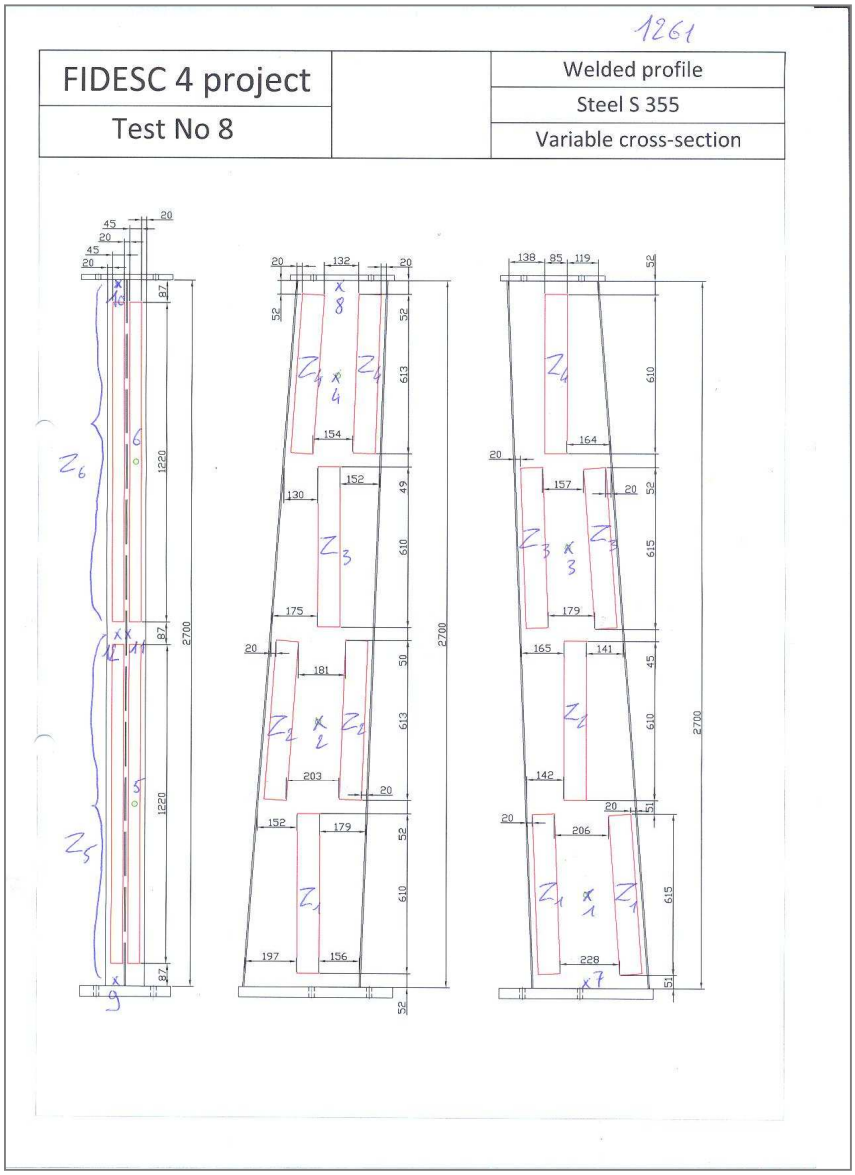

Figure 80 : Definition of the control zones and position of the control thermocouples

The temperature of the control thermocouples as a function of the time is shown in the Figure 70.

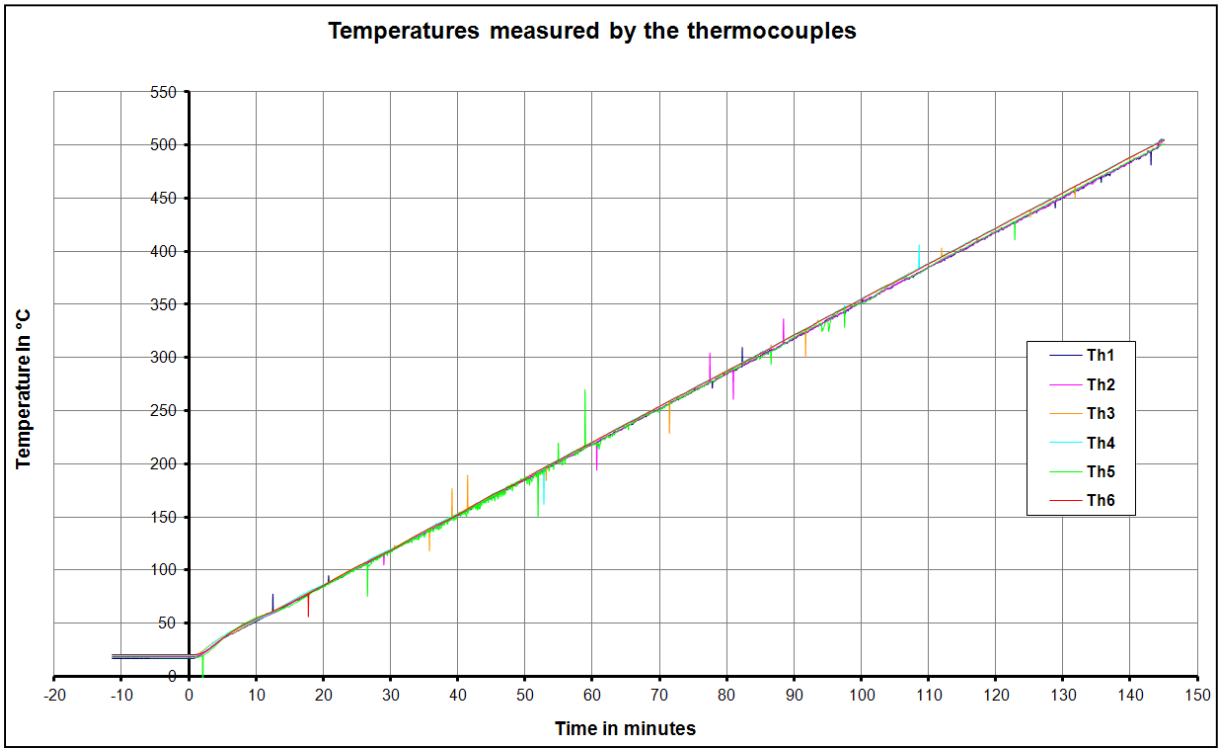

Figure 81 : Temperature recorded by the 6 control thermocouples

We observe that the control temperature curves are very close between each other and the instruction is thus well followed by the six zones. The heating and loading process was stopped at the minute 145.

By calculating the mean between these 6 temperatures, we can display the evolution of the transversal and axial displacements as a function of the mean temperature of the column.

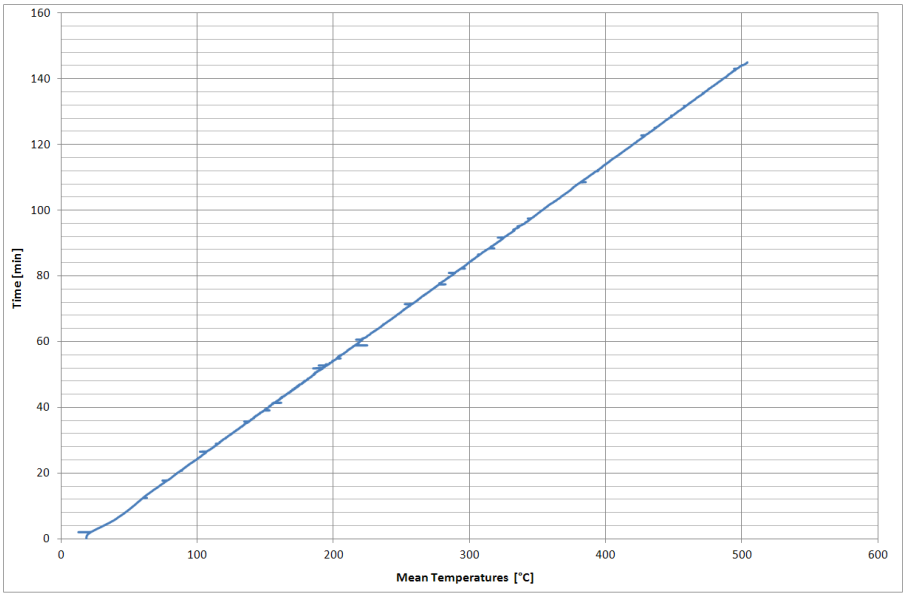

Figure 82 : Time vs. mean temperature

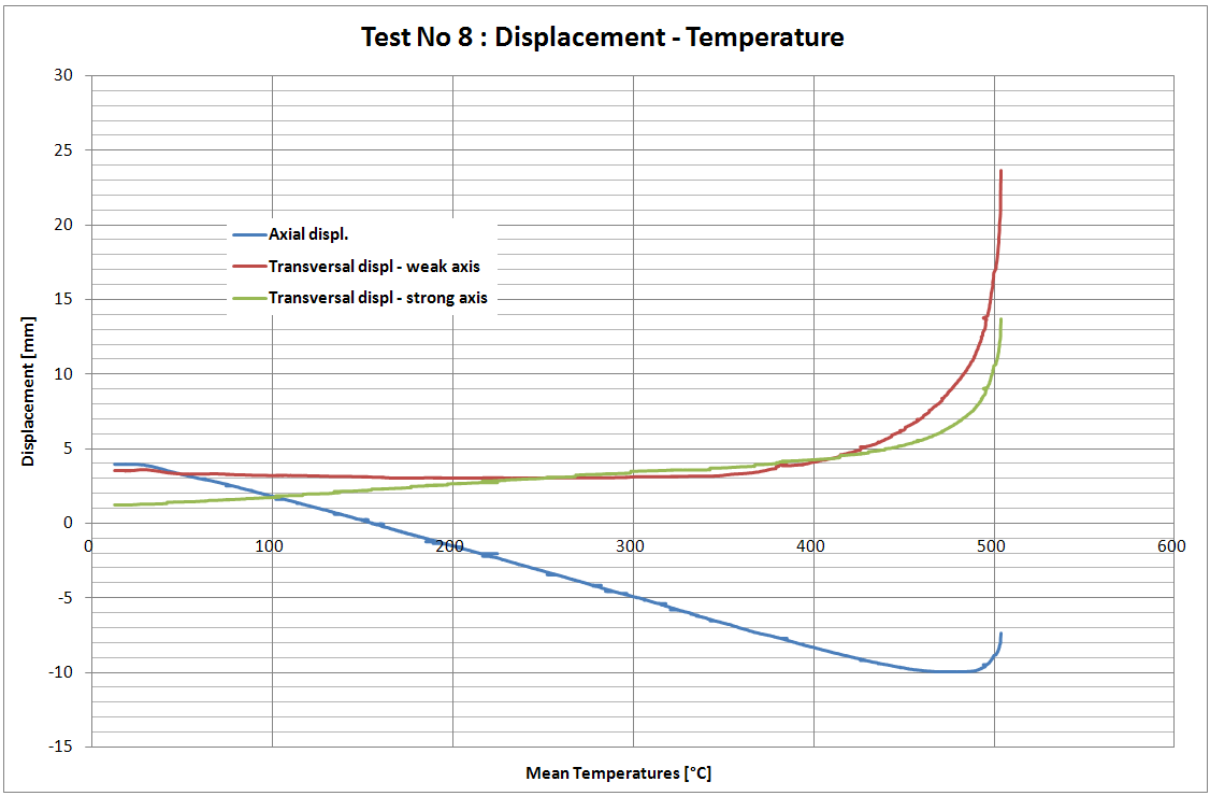

Figure 83 : Test No 8: Displacements – mean temperatures

For the test No 8, the material tests were also performed by the manufacturer LINDAB and the certificate were provided with the welded columns. The steel grades of the flange and of the web are:

- Flange: f_y = 404 MPa
- Web –at the lead end of the plate : f_y = 482 MPa
- Web –at the tail end of the plate : f_y = 447 MPa

Figure 84 : Test No 8: Deformed shape of the column after the test

1.6.10. Comparison between the experimental failure temperatures and the failure temperatures calculated with SAFIR before the experimental tests

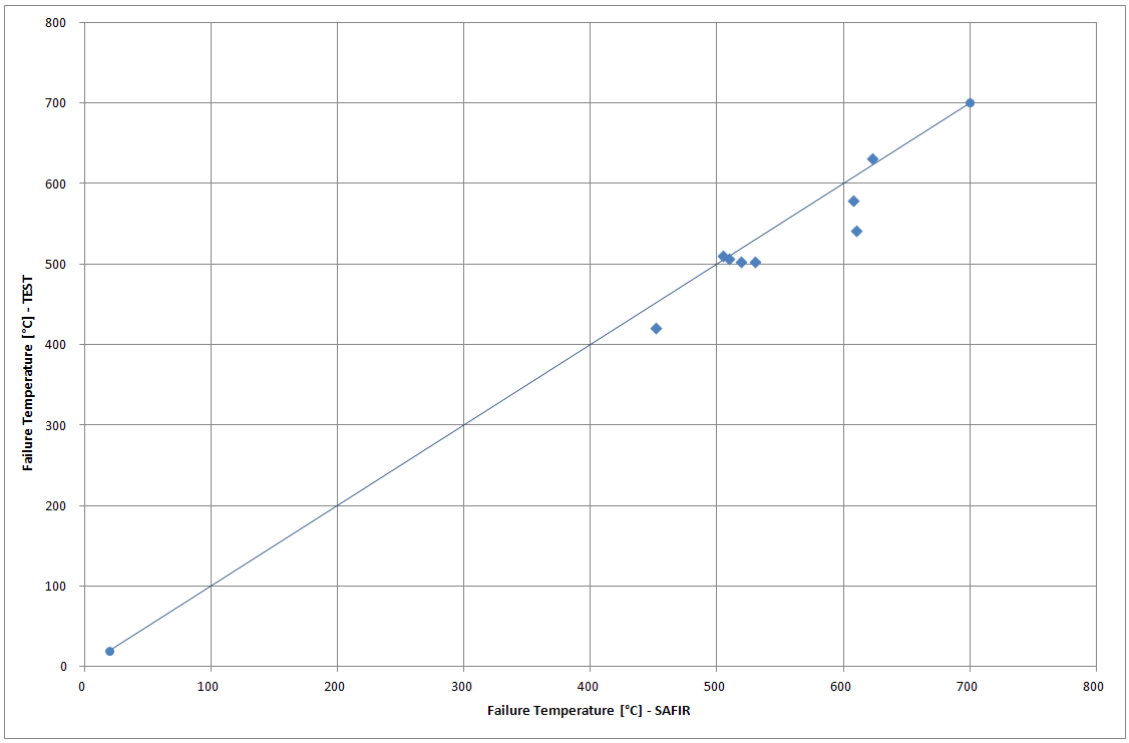

Figure 85 : Comparison between experimental and numerical results

2. Numerical simulations against experimental results

The numerical simulations can be run to catch with the experimental results from the fire tests. The objective is to simulate the tests using the measured properties of the steel of the columns, the measured global and local imperfections, the measured temperature distribution along the column, the measured value of the load and the measured eccentricities of the load applying with the testing frame.

The real properties of the steel of each column were presented in the previous paragraph. We consider in the simulation the maximum value obtained from the material tests. The used values will be reminded for each simulation.

The measuring of the global and local imperfections of the specimens was performed manually, see Paragraph 1.3. Thus, the geometry of the meshing of each column in these simulations takes into account of these real imperfections. We introduce a global imperfection along the weak axis deduced by the general shape of the profile of the imperfection along the web of the columns. Around this deformed shape, we add local sinusoidal imperfections perpendicular to the plan of the web and of the flange along the web and along the flange. The amplitude of this sinusoidal imperfection is the maximum value observed in the profile of imperfections around the global imperfection of the web and flange.

Besides, the temperatures along the profile were recorded during the tests in 5 or 6 zones along the column by means of 5 or 6 control thermocouples. So we can apply the recorded evolution of temperatures along the profile. From these data, we observed that the instruction of heating at a velocity of 200°C/hour was closely followed by all the control zones of the columns for each test. In the simulations, the steel of the column will be heated at a constant velocity of 200°C/hour along the whole column of each test.

The applied loads during the tests were presented in the previous paragraph.

Finally, we have to take into account in these post-simulations the difference between the theorically-planned eccentricities of the load and the eccentricities of the load measured during the tests.

Indeed, two mean types of imprecision may affect the value of the eccentricity of the columns compared to the pinned supports:

- The imprecision's due to the fabrication process
- The imprecision's due to the setting of the column between the pinned supports of the testing frame

The imprecision's due to the fabrication may result from an error of positioning of the column compared to the steel end plates and/or from an error of positioning of the holes into the end plates.

The imprecision's due to the setting of the column into the frame may result from a slack between the holes of the end plates and the holes of the pinned supports and also from the threadbars used to fix the end plates to the pinned supports. Indeed, the holes in the end plates of the column have a diameter of 20mm. The holes in the pinned supports have a diameter of 21mm and the threadbars have a diameter of 16mm. These slack may thus generate an offset from 0 to 4,5mm.

The last characteristic to be taken into account is the length of the column. The length of the columns between the end plates is 2.7m for all the tested columns. But, as the columns are ended by a steel plate at each extremity and as these end plates themselves are fixed to the pinned supports. In fact, the length of the column to consider between the points of application of the load includes the 2,7m length of the column, the thickness of the two end plates (depends on the column) and the two half thicknesses of the pinned supports (2*(265mm/2)) more the thickness of the insulating Promatect (2*35mm).

In order to take into account this feature, we add a vertical line of shell elements with a length equal to the measured over-length along the axis of the column. To introduce the eccentricities of the load we use a horizontal line of shell elements perpendicular to the vertical one and with a length equal to the measured eccentricity of the load. These shell elements have a big thickness of 100mm.

2.1. Test No 1 – IPE240A

a) Real properties of the steel

The maximum steel grades of the flanges and of the web obtained by the material tests are:

	Web	Flange
$F_{y,max,measured}$ [Mpa]	449,5	402

b) Imperfections

The global and initial imperfections deduced from the manual measuring along the web and the flanges of the column are presented in the table. We impose a global imperfection in the direction of the weak axis only, with a half sinusoidal shape. The amplitude of this global imperfection is deduced from the profile of imperfection measured along the web. Around this global imperfection, some local imperfections are imposed to the web and to the flanges along the column. They have a sinusoidal shape in the direction perpendicular to the plan of the flange for the flanges and perpendicular to the web for the webs respectively.

Amplitude of the global imperfection in the direction of the weak axis [mm]	Amplitude of the local imperfection of the web [mm]	Amplitude of the local imperfection of the flange [mm]
1,5	0,2	0,3

c) Real eccentricities of the load

The eccentricities between the axis of the pinned supports and the axis of the column were measured once the column was equipped and placed into the testing frame.

Eccentricity at the bottom basis [mm]	Eccentricity at the top basis [mm]
5	5

d) Over-length of the column

- Bottom end : 132,5 + 35 + 20/2 = 177,5 mm
- Upper end : 132,5 + 35 + 20/2 = 177,5 mm

e) Results of the post-test simulations: Failure temperature – Displacements – Failure mode

Applied load for the test [KN]	Failure Temperature – SAFIR [°C]	Failure Temperature – TEST [°C]
122,4	572,1	610

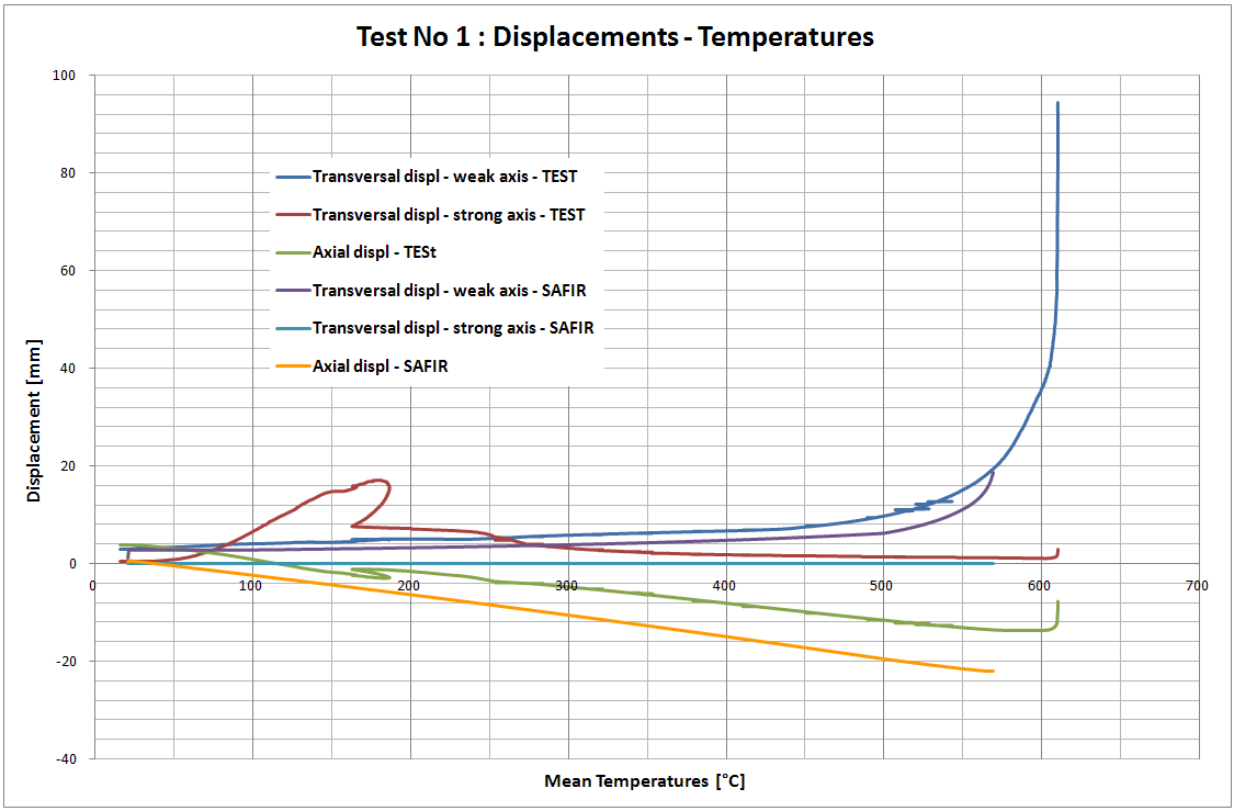

Figure 86 : Test No 1 – Comparison between the displacements obtained numerically and experimentally

The transversal displacement in the direction of the weak axis is recorded at the mid-height of the column and at the mid-width of the web. The transversal displacement in the direction of the strong axis is recorded at the mid-height of the column and at the mid-width of the flange. The vertical displacement is recorded for the central node of the node line of application of the force.

The failure mode obtained numerically is a global buckling along the weak axis. The failure mode obtained experimentally was the same mode.

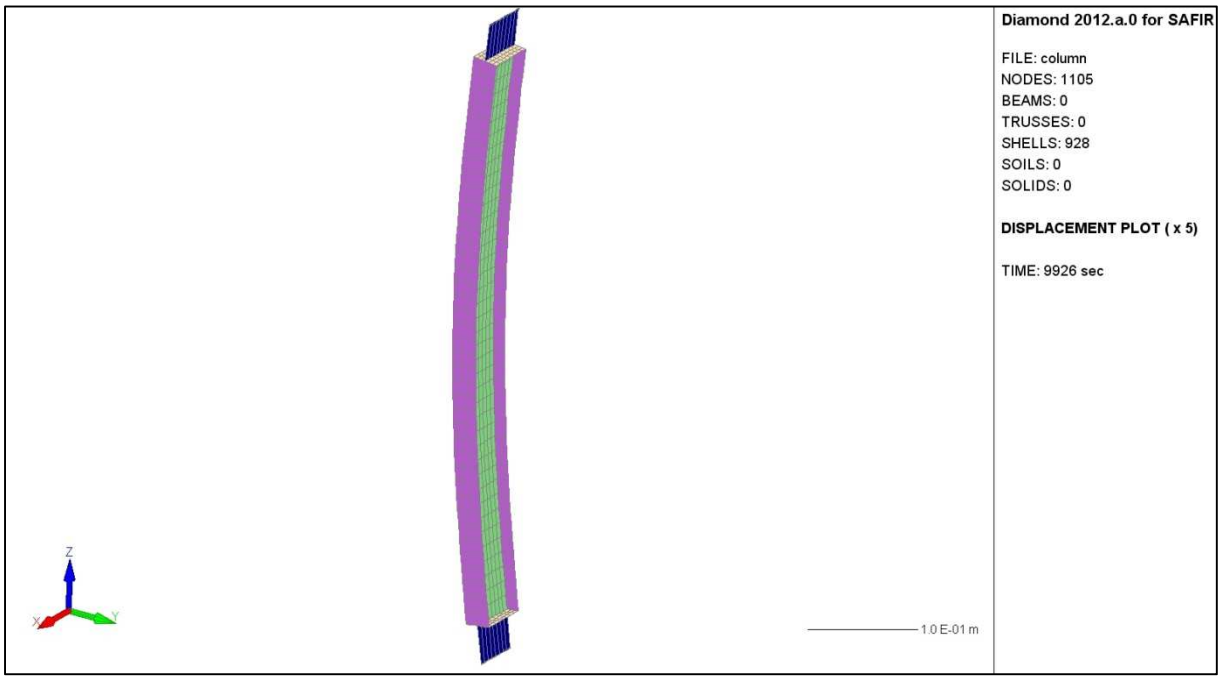

Figure 87 : Test No 1 – Failure mode (SAFIR)

2.2. Test No 2

a) Real properties of the steel

The maximum steel grade of the flanges and of the web obtained by the material tests is:

	Web	Flange
$F_{y,max,measured}$ [Mpa]	482	404

b) Imperfections

Amplitude of the global imperfection in the direction of the weak axis [mm]	Amplitude of the local imperfection of the web [mm]	Amplitude of the local imperfection of the flange [mm]
2,7	3,2	2,4

c) Real eccentricities of the load

The eccentricities between the axis of the pinned support and the axis of the column were measured once the column was equipped and placed into the testing frame.

Eccentricity at the bottom basis [mm]	Eccentricity at the top basis [mm]
5	5

f) Over-length of the column

- Bottom end : 132,5 + 35 + 30/2 = 182,5 mm
- Bottom end : 132,5 + 35 + 30/2 = 182,5 mm

d) Results of the post-test simulations: Failure temperature – Displacements – Failure mode

Applied load for the test [KN]	Failure Temperature – SAFIR [°C]	Failure Temperature – TEST [°C]
122,4	594,7	608

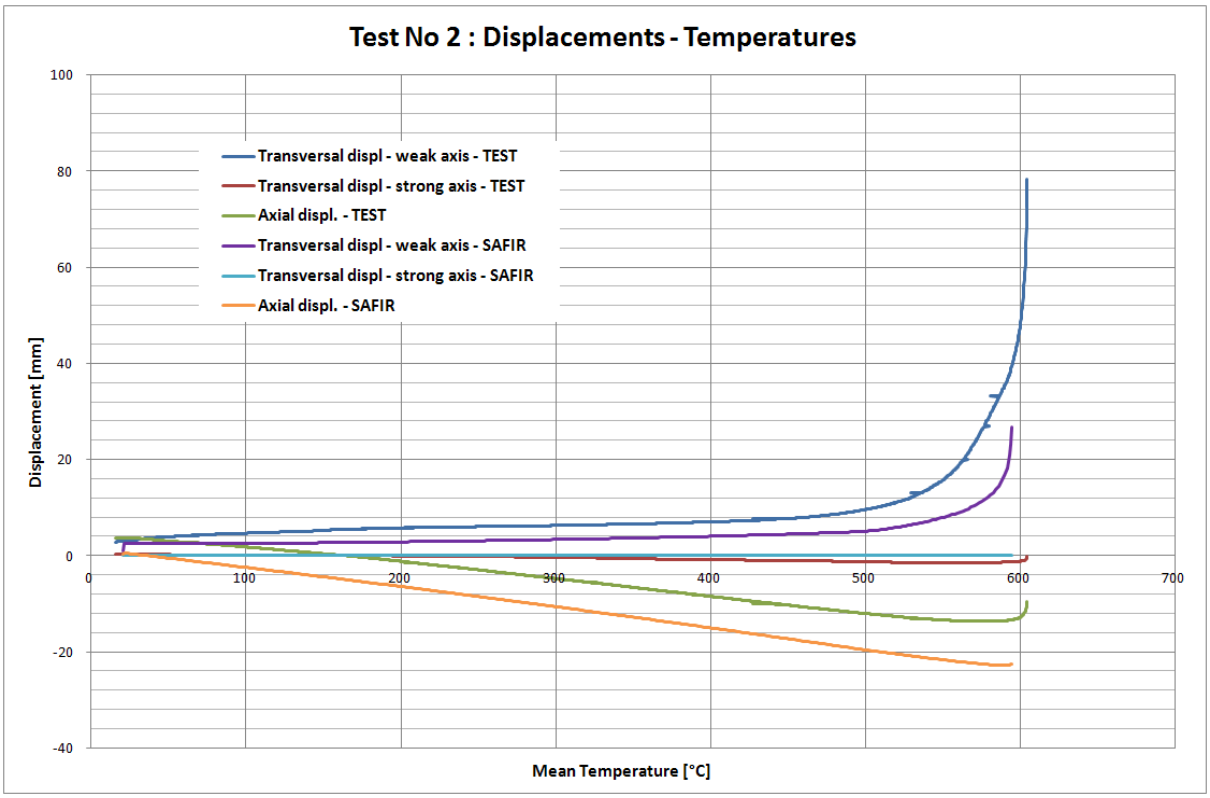

Figure 88 : Test No 2 – Comparison between the displacements obtained numerically and experimentally

The failure mode obtained numerically is a global buckling along the weak axis with a local buckling of the flange at mid-high of the column. The failure mode obtained experimentally was the same mode.

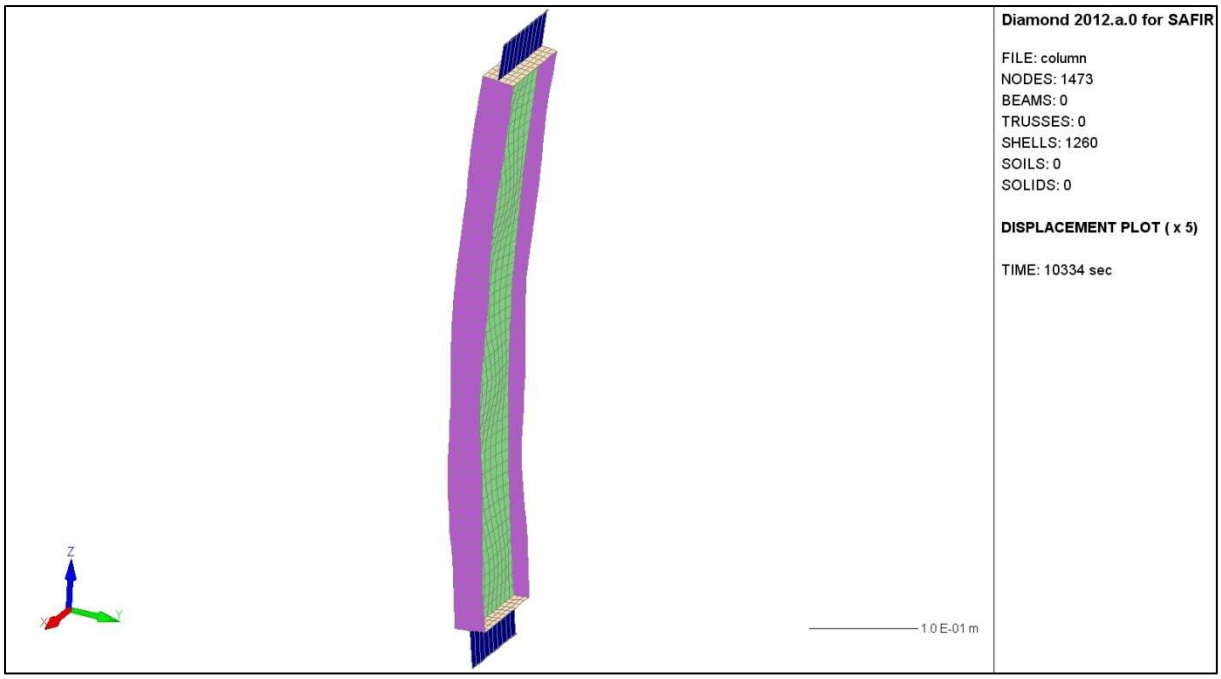

Figure 89 : Test No 2 – Failure mode (SAFIR)

2.3. Test No 3

a) Real properties of the steel

The maximum steel grade of the flanges and of the web obtained by the material tests is:

	Web	Flange
$F_{y,max,measured}$ [Mpa]	482	404

b) Imperfections

Amplitude of the global imperfection in the direction of the weak axis [mm]	Amplitude of the local imperfection of the web [mm]	Amplitude of the local imperfection of the flange [mm]
5,4	2,7	4,7

c) Real eccentricities of the load

The eccentricities between the axis of the pinned support and the axis of the column were measured once the column was equipped and placed into the testing frame.

Eccentricity at the bottom basis [mm]	Eccentricity at the top basis [mm]
4	13

d) Over-length of the column

- Bottom end : 132,5 + 35 + 30/2 = 182,5 mm
- Bottom end : 132,5 + 35 + 30/2 = 182,5 mm

e) Results of the post-test simulations: Failure temperature – Displacements – Failure mode

Applied load for the test [KN]	Failure Temperature – SAFIR [°C]	Failure Temperature – TEST [°C]
204	459	452

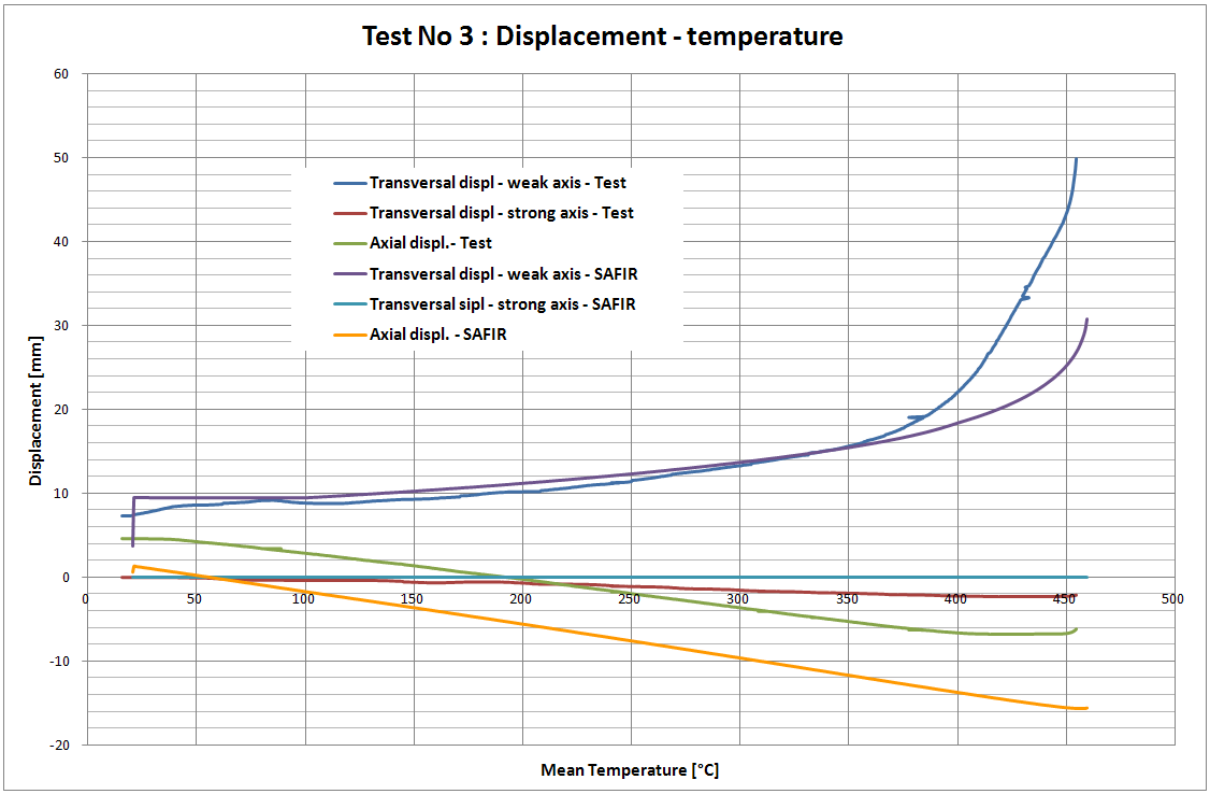

Figure 90 : Test No 3 – Comparison between the displacements obtained numerically and experimentally

The failure mode obtained numerically is a global buckling along the weak axis with a local buckling of the flange at mid-high of the column. The failure mode obtained experimentally was the same mode.

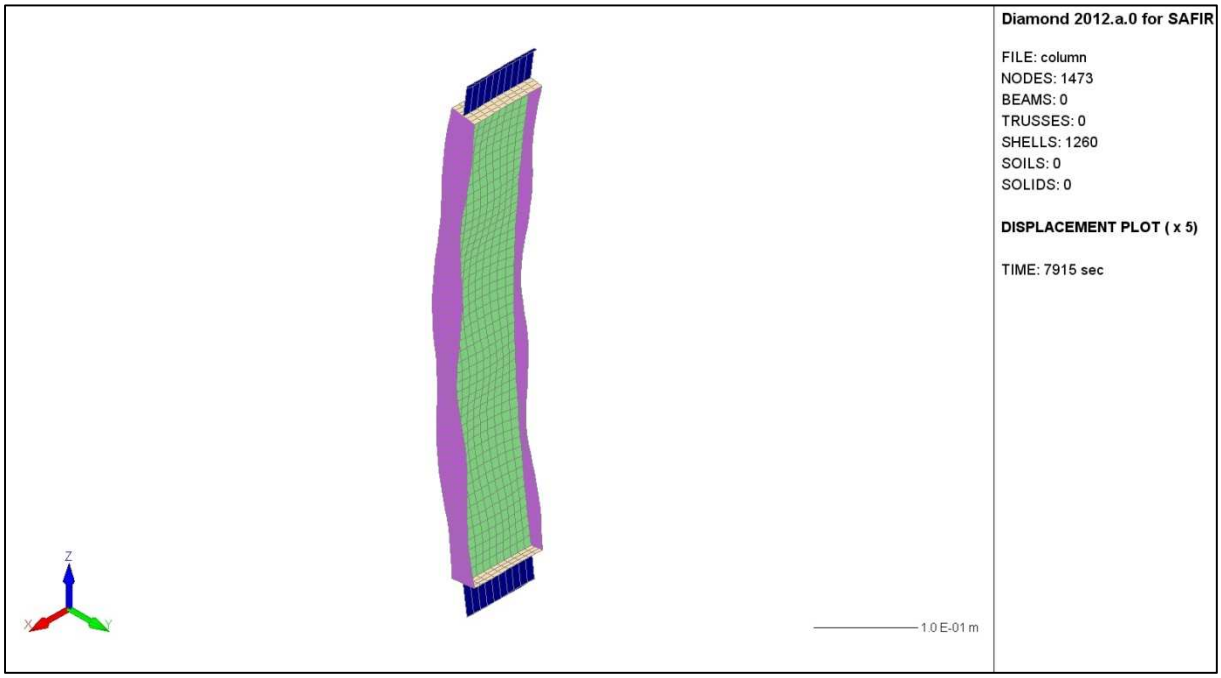

Figure 91 : Test No 3 – Failure mode (SAFIR)

2.4. Test No 4

a) Real properties of the steel

For this column, we don't have the real properties of the steel neither the certificates. Thus, we consider the following values based upon the material tests done for the column No 3.

	Web	Flange
F_y [Mpa]	464,5	404

b) Imperfections

Amplitude of the global imperfection in the direction of the weak axis [mm]	Amplitude of the local imperfection of the web [mm]	Amplitude of the local imperfection of the flange [mm]
1,8	4,5	1,5

c) Real eccentricities of the load

The eccentricities between the axis of the pinned support and the axis of the column were measured once the column was equipped and placed into the testing frame.

Eccentricity at the bottom basis [mm]	Eccentricity at the top basis [mm]
5	3,5

d) Over-length of the column

- Bottom end : 132,5 + 35 + 30/2 = 182,5 mm
- Bottom end : 132,5 + 35 + 20/2 = 177,5 mm

e) Results of the post-test simulations: Failure temperature – Displacements – Failure mode

Applied load for the test [KN]	Failure Temperature – SAFIR [°C]	Failure Temperature – TEST [°C]
348	535	519,5

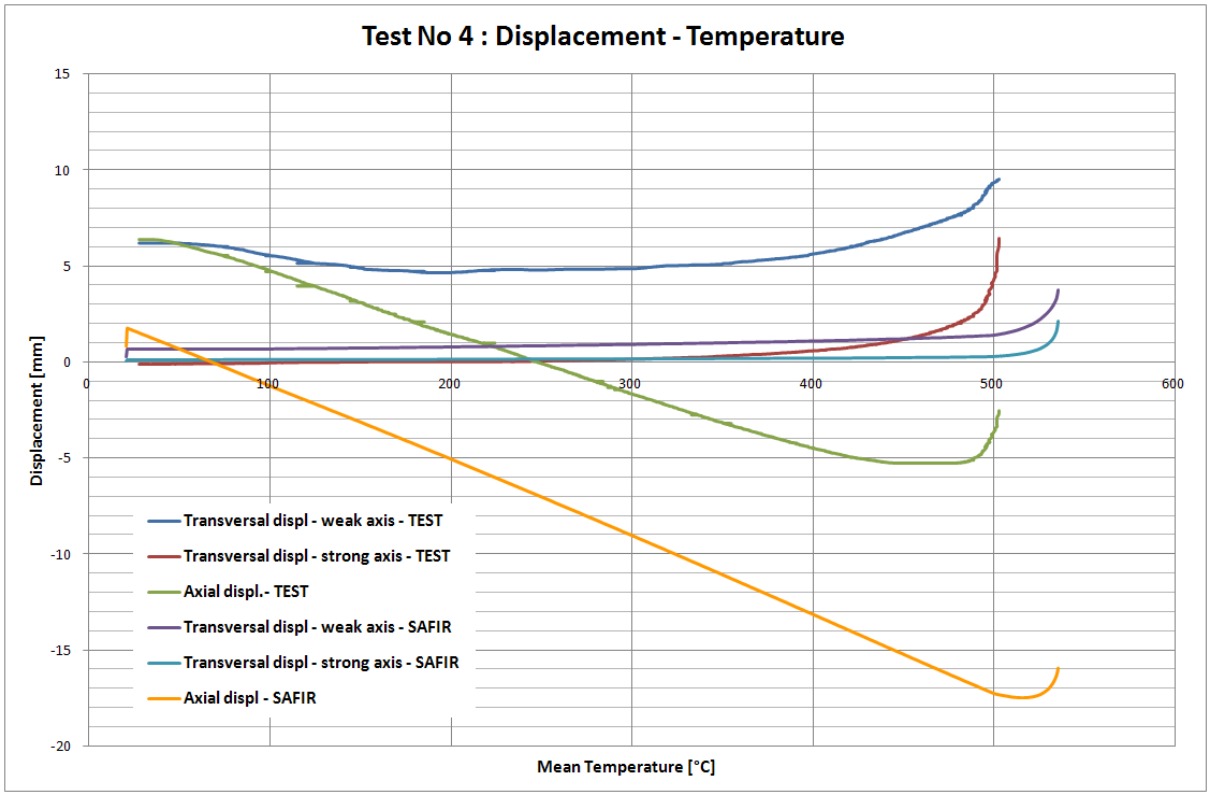

Figure 92 : Test No 4 – Comparison between the displacements obtained numerically and experimentally

The failure mode obtained numerically is a global buckling along the weak axis with a local buckling of the flange at mid-high of the column. The failure mode obtained experimentally was the same mode.

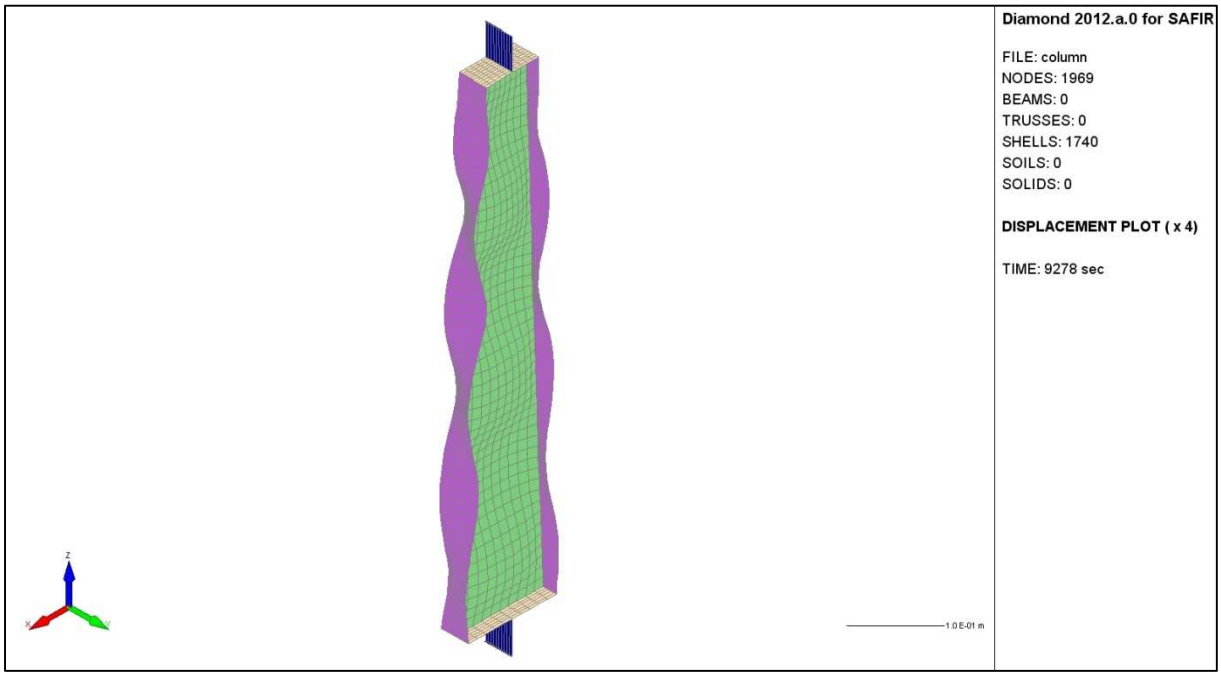

Figure 93 : Test No 4 – Failure mode (SAFIR)

2.5. Test No 5

a) Real properties of the steel

For this column, we don't have the real properties of the steel neither the certificates. Thus, we consider the following values based upon the material tests done for the column No 3.

	Web	Flange
F_y [Mpa]	464,5	404

b) Imperfections

Amplitude of the global imperfection in the direction of the weak axis [mm]	Amplitude of the local imperfection of the web [mm]	Amplitude of the local imperfection of the flange [mm]
2,2	3,4	1,6

c) Real eccentricities of the load

The eccentricities between the axis of the pinned support and the axis of the column were measured once the column was equipped and placed into the testing frame.

Eccentricity at the bottom basis [mm]	Eccentricity at the top basis [mm]
71	71

d) Over-length of the column

- Bottom end : 132,5 + 35 + 30/2 = 182,5 mm
- Bottom end : 132,5 + 35 + 30/2 = 182,5 mm

e) Results of the post-test simulations: Failure temperature – Displacements – Failure mode

Applied load for the test [KN]	Failure Temperature – SAFIR [°C]	Failure Temperature – TEST [°C]
231,25	526	510

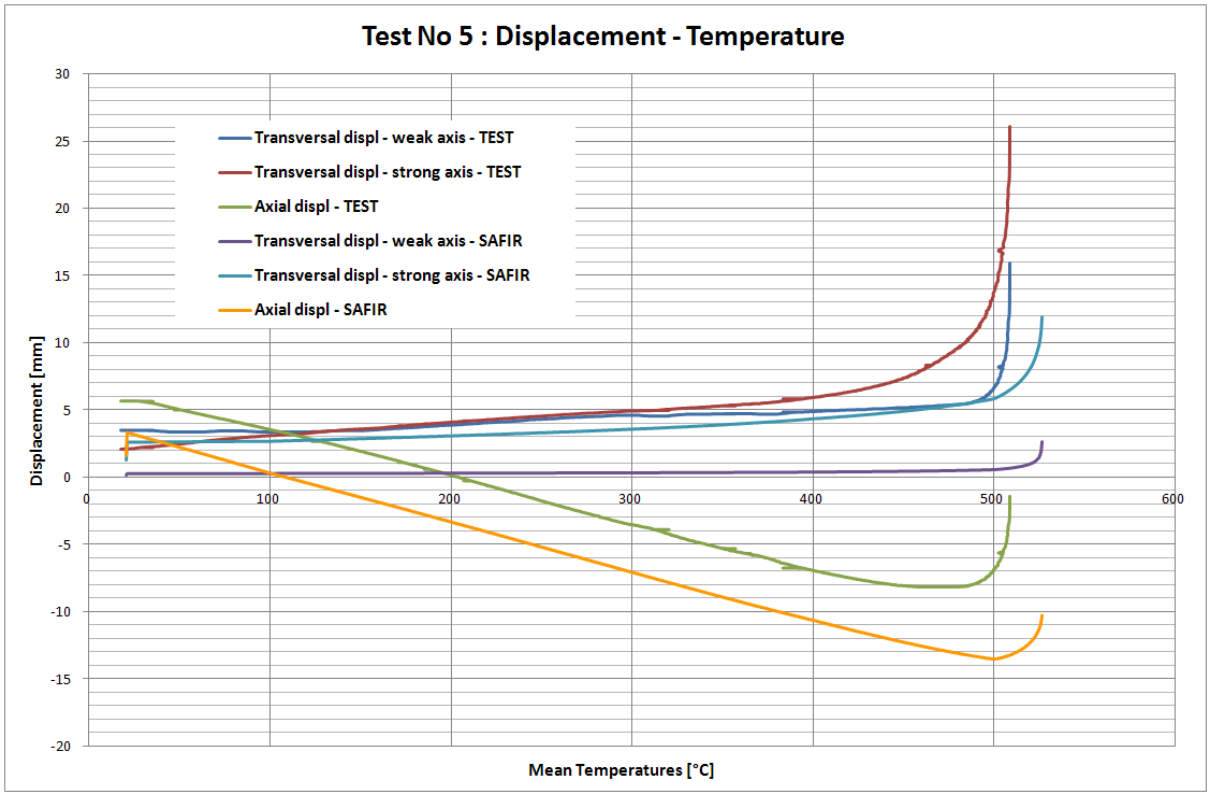

Figure 94 : Test No 5 – Comparison between the displacements obtained numerically and experimentally

The failure mode obtained numerically is a global buckling along the weak axis with a local buckling of the flange at mid-high of the column. The failure mode obtained experimentally was the same mode.

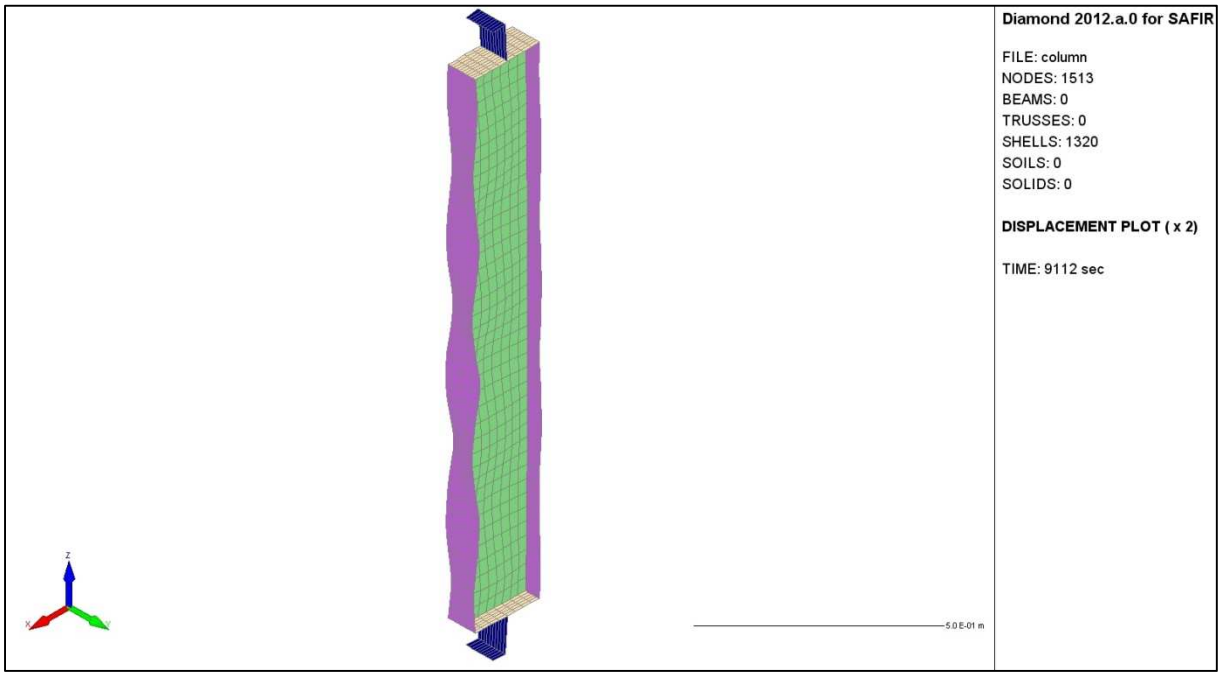

Figure 95 : Test No 5 – Failure mode (SAFIR)

2.6. Test No 6

a) Real properties of the steel

The maximum steel grade of the flanges and of the web obtained by the material tests is:

	Web	Flange
$F_{y,max,measured}$ [Mpa]	482	404

b) Imperfections

Amplitude of the global imperfection in the direction of the weak axis [mm]	Amplitude of the local imperfection of the web [mm]	Amplitude of the local imperfection of the flange [mm]
1	2,2	1,2

c) Real eccentricities of the load

The eccentricities between the axis of the pinned support and the axis of the column were measured once the column was equipped and placed into the testing frame.

Eccentricity at the bottom basis [mm]	Eccentricity at the top basis [mm]
172	175

d) Over-length of the column

- Bottom end : 132,5 + 35 + 40/2 = 187,5 mm
- Bottom end : 132,5 + 35 + 40/2 = 187,5 mm

e) Results of the post-test simulations: Failure temperature – Displacements – Failure mode

Applied load for the test [KN]	Failure Temperature – SAFIR [°C]	Failure Temperature – TEST [°C]
166,4	531,5	530

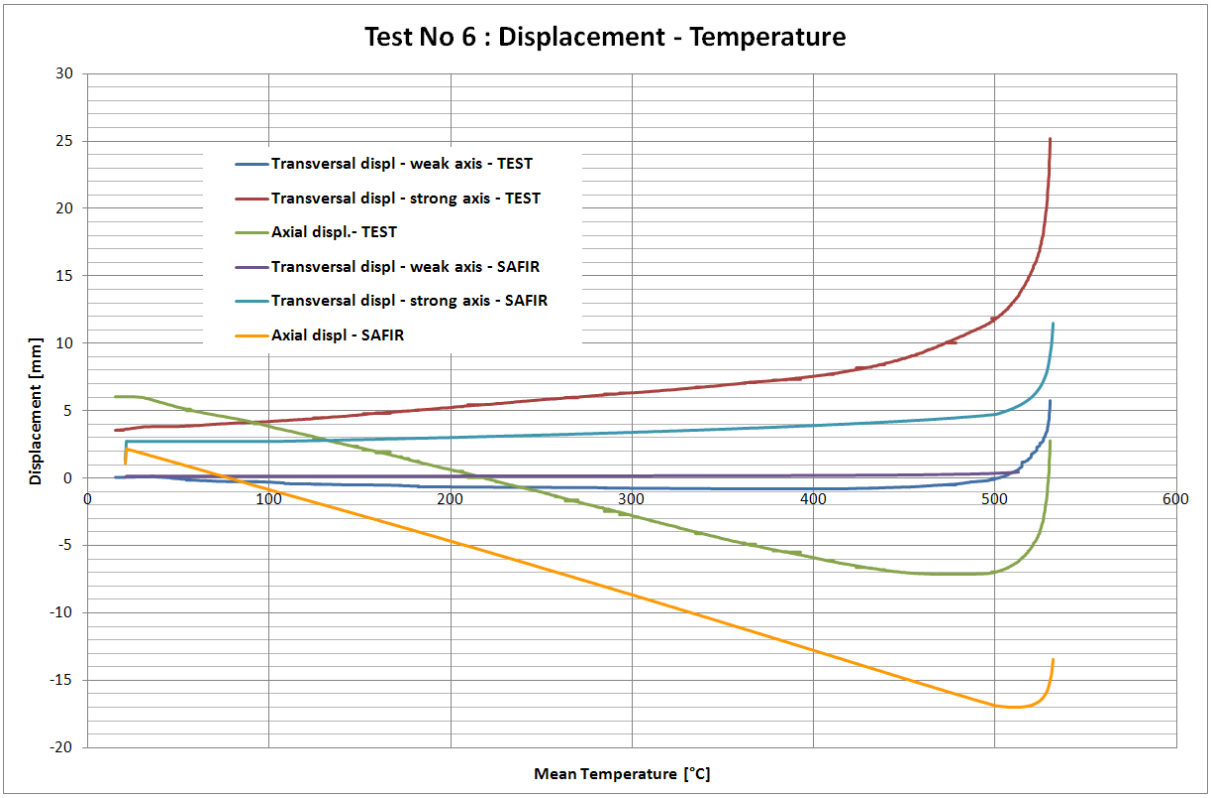

Figure 96 : Test No 6 – Comparison between the displacements obtained numerically and experimentally

The failure mode obtained numerically is a global buckling along the weak axis with a local buckling of the flange at mid-high of the column. The failure mode obtained experimentally was the same mode.

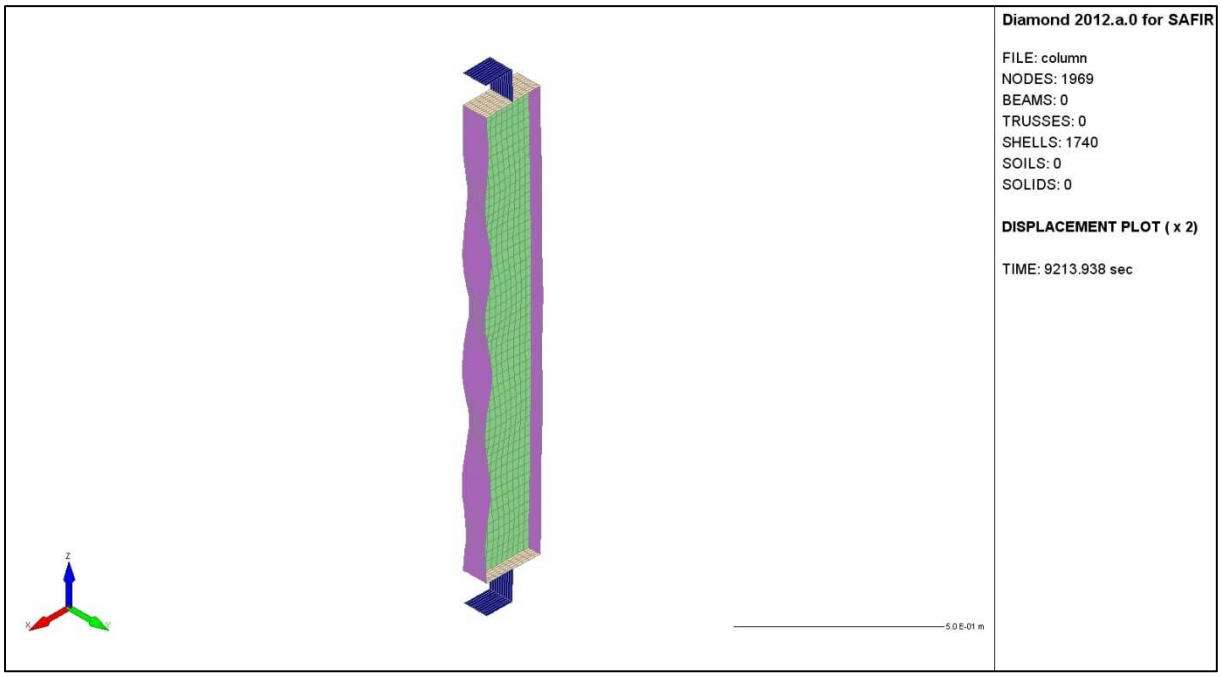

Figure 97 : Test No 6 – Failure mode (SAFIR)

2.7. Test No 7 – HE240AA

a) Real properties of the steel

The maximum steel grade of the flanges and of the web obtained by the material tests is:

	Web	Flange
$F_{y,max,measured}$ [Mpa]	585,5	538

b) Imperfections

Amplitude of the global imperfection in the direction of the weak axis [mm]	Amplitude of the local imperfection of the web [mm]	Amplitude of the local imperfection of the flange [mm]
1,5	0,5	0,6

c) Real eccentricities of the load

The eccentricities between the axis of the pinned support and the axis of the column were measured once the column was equipped and placed into the testing frame.

Eccentricity at the bottom basis [mm]	Eccentricity at the top basis [mm]
5	98

d) Over-length of the column

- Bottom end : 132,5 + 35 + 20/2 = 177,5 mm
- Bottom end : 132,5 + 35 + 35/2 = 185 mm

e) Results of the post-test simulations: Failure temperature – Displacements – Failure mode

Applied load for the test [KN]	Failure Temperature – SAFIR [°C]	Failure Temperature – TEST [°C]
760,8	631	622,8

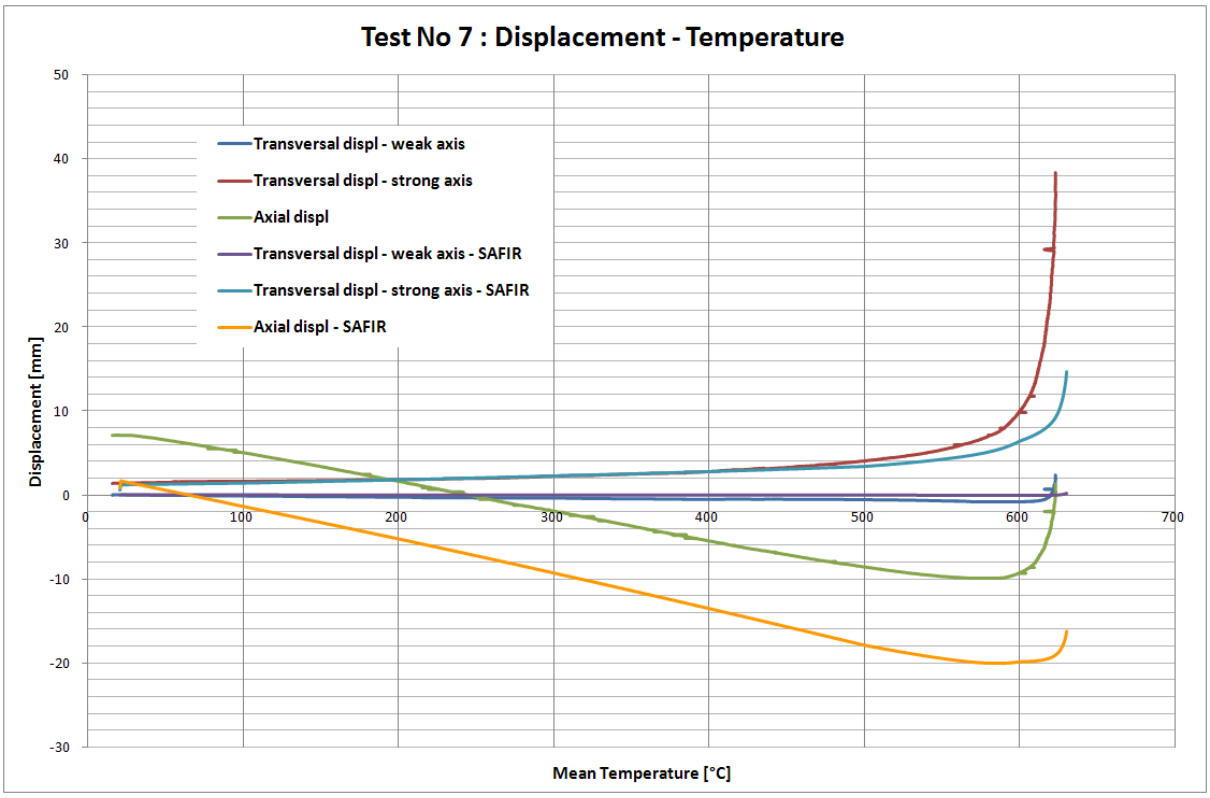

Figure 98 : Test No 7 – Comparison between the displacements obtained numerically and experimentally

The failure mode obtained numerically is a global buckling along the weak axis with a local buckling of the flange at mid-high of the column. The failure mode obtained experimentally was the same mode.

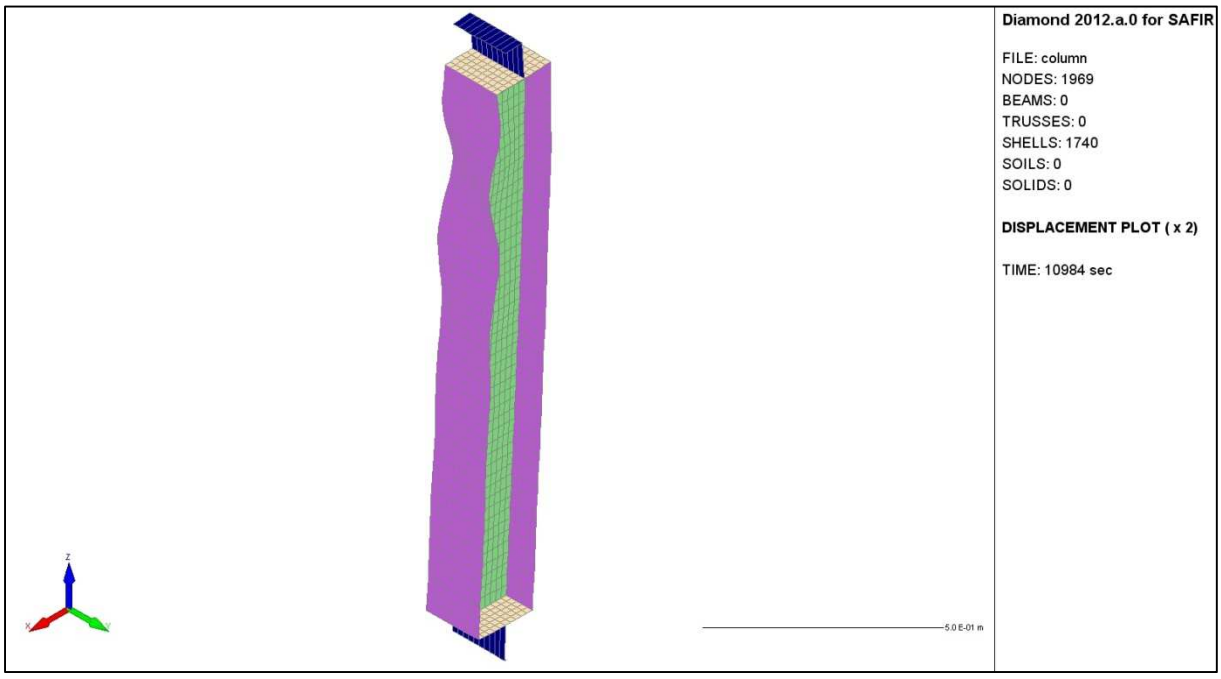

Figure 99 : Test No 7 – Failure mode (SAFIR)

2.8. Test No 8

a) Real properties of the steel

The maximum steel grade of the flanges and of the web obtained by the material tests is:

	Web	Flange
$F_{y,max,measured}$ [Mpa]	482	404

b) Imperfections

Amplitude of the global imperfection in the direction of the weak axis [mm]	Amplitude of the local imperfection of the web [mm]	Amplitude of the local imperfection of the flange [mm]
1	2,8	1,5

c) Real eccentricities of the load

The eccentricities between the axis of the pinned support and the axis of the column were measured once the column was equipped and placed into the testing frame.

Eccentricity at the bottom basis [mm]	Eccentricity at the top basis [mm]
143,5	2,5

d) Over-length of the column

- Bottom end : 132,5 + 35 + 40/2 = 187,5 mm
- Bottom end : 132,5 + 35 + 20/2 = 177,5 mm

e) Results of the post-test simulations: Failure temperature – Displacements – Failure mode

Applied load for the test [KN]	Failure Temperature – SAFIR [°C]	Failure Temperature – TEST [°C]
219	537	504,5

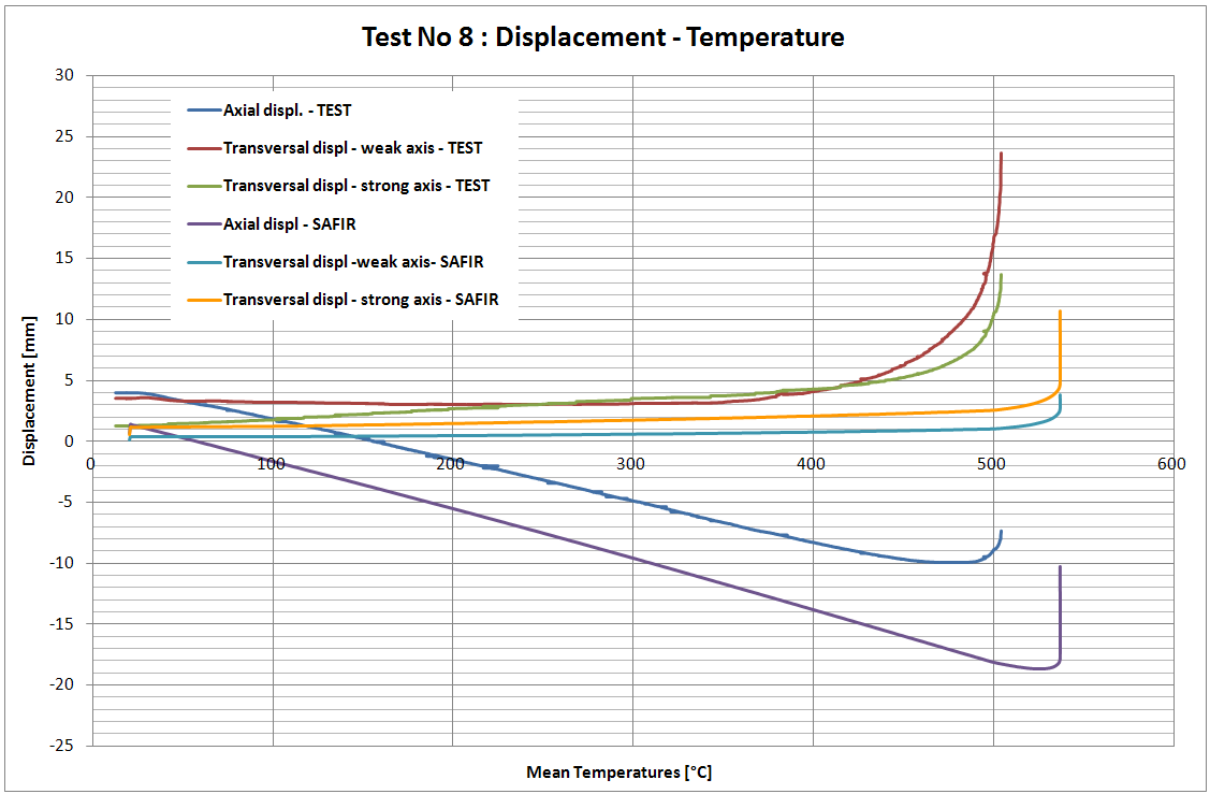

Figure 100 : Test No 8 – Comparison between the displacements obtained numerically and experimentally

The failure mode obtained numerically is a global buckling along the weak axis with a local buckling of the flange at mid-high of the column. The failure mode obtained experimentally was the same mode.

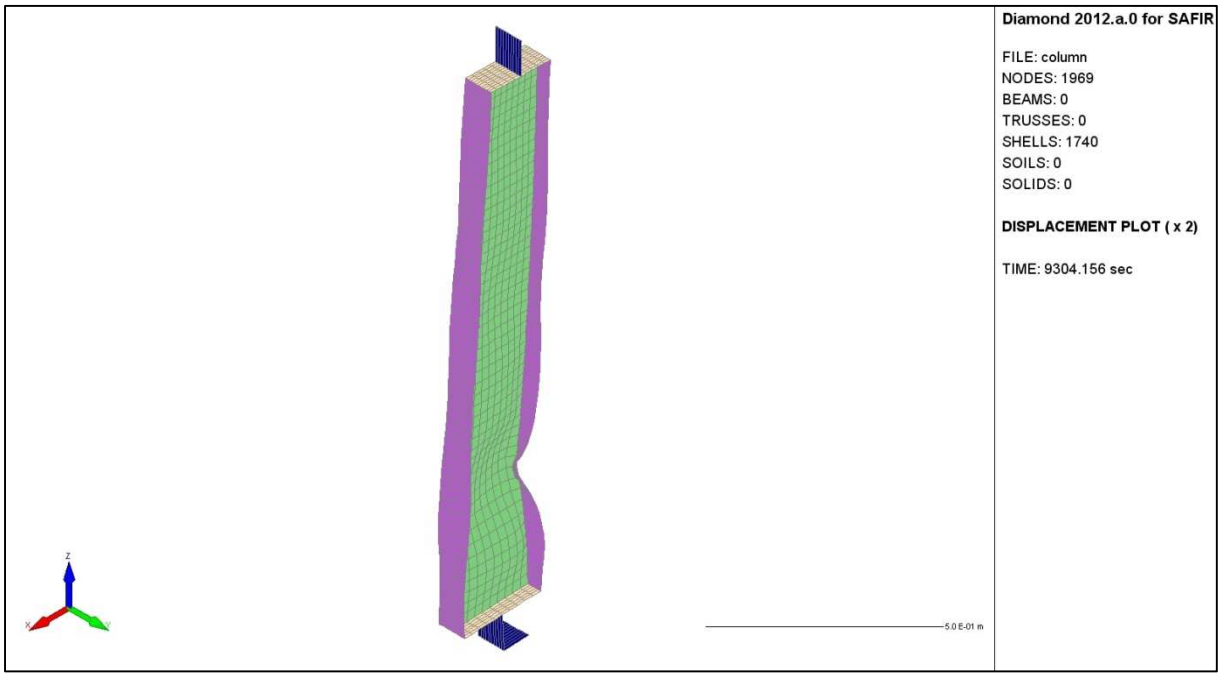

Figure 101 : Test No 8 – Failure mode (SAFIR)

2.9. Comparison